The Role of 5' *hox13* Genes in *Danio rerio* (Zebrafish) Caudal Fin Ray/Joint Development and Regeneration

Hailey Quigley

Thesis submitted to the University of Ottawa
in partial Fulfillment of the requirements for the
Master of Science

Department of Biology
Faculty of Science
University of Ottawa

Abstract

Zebrafish are part of the teleost infraclass (bony fish) of the ray-finned fish. Like other teleosts, zebrafish possess the ability to regenerate most tissues, including their fins. Zebrafish fins contain segmented bony fin rays that longitudinally span the fin. The segments of fin ray are separated by fibrous joints at regularly spaced intervals providing segmentation and flexibility for the fin. Based on gene expression and changes in cell morphology, joint cell differentiation during development and regeneration proceeds through three stages: presumptive joint, joint-forming, and mature joint cells. Our lab has shown that new joint formation correlates with the upregulation of 5' *hoxa* gene, *hoxa13a.* The *hox* genes encode transcription factors important for patterning in development. In mice, phenotypes resulting from loss- and gain-of-function mutations in *Hox* genes have revealed that the spatiotemporal expression of these genes is critical for the correct morphogenesis of the limb, a homologous structure to the fin. The first experiments in this thesis use the NTR/MTZ mechanism to partially ablate *hoxa13a*-expressing cells in the joints and blastema of the regenerating caudal fin. Partial ablation of the *hoxa13a*-expressing cells results in shorter bone segments following regeneration of the fin. This experiment draws the conclusion that *hoxa13a*-expressing cells are involved in the regulation of segment length. To examine the function of the 5' *hoxa/d* genes in zebrafish, our lab created CRISPR/Cas9 mutations that inactivate *hoxa13a, hoxa13b*, and *hoxd13a.* The triple mutants created through serial breeding, show fin-specific defects in the formation and patterning of joints, as well as general defects in the morphology of the ray and in the actinotrichia, collagenous fibres found at the distal edge of the fin. Overall, our data suggest that *hox13* genes are necessary for joint formation and proper fin ray growth. With further phenotypic and genotypic analyses our lab proposes that the dosage of *hox13* alleles is responsible for anomalies in fin ray formation found in *hox13* mutants.

Acknowledgements

I would like to begin by thanking my supervisor, Dr. Marie-Andrée Akimenko, for the endless amount of support and guidance throughout the entirety of my program. In addition, I would like to thank Dr. Akimenko for the knowledge and passion she shares with not only myself but every student under her supervision. Next, I would like to thank my supervisory committee Dr. Marc Ekker and Dr. Shelley Hepworth for additional guidance and constructive input throughout my master's program. In addition, thank you to Dr. Shelley Hepworth and Dr. Odette Laneuville for taking time out of their busy schedules and agreeing to be my examiners and read this very long thesis. I also would like to send a special thanks to Jing Zhang and Dr. Qingming Qu, for teaching me various laboratory techniques and equipment. Moreover, I would like to thank Dr. Qu for creating the CRISPR-Cas9 mutants used in my study. A special thanks also goes out to some past and present members of the Akimenko lab, Dr. Robert Lalonde, Hannah Nichols, Shea Keil, Joshua Ivare, Mustafa Hamid, Reeham Kadhom, and Bidemi Keshinro for their input, their encouragement, and most importantly for keeping me sane over the past three years. Finally, thank you to my friends and family who have given me endless amounts of support during my educational endeavours.

Table of Contents

List of Figures

List of Tables

List of Abbreviations

2A	Self-cleaving peptide
and	*actinodin*
BMP	Bone Morphogenetic Protein
Bmp2b	Gene coding for bone morphogenetic protein 2
Col2 antibody	Collagen Type Two antibody
CRISPR-Cas9	clustered regularly interspaced short palindromic repeats associated protein 9
Cx43	*connexin43*
DAPI	4',6-diamidino-2-phenylindole
DMSO	Dimethyl sulfoxide
DNA	deoxyribonucleic acid
DNP	dinitrophenol
dpa	days post amputation
dpf	days post fertilization
EGFP	Enhanced green fluorescent protein
evx1	*even-skipped homeobox 1*
FF	fin fold
FGF	Fibroblast growth factor
FISH	fluorescence *in situ* hybridization
hoxa13a	*homeobox a13 a*
hoxa13b	*homeobox a13 b*
hoxd13a	*homeobox d13 a*
hpa	hours post-amputation
hpf	hours post-fertilization
IHC	immunohistochemistry
ISH	*in situ* hybridization
m-inta11	*mouse derived hoxa11 intron regulatory element*
MO	morpholino
MTZ	metronidazole
NFP	nifurpirinol
NTP	nucleoside triphosphate
NTR	nitroreductase
pthlha	*parathyroid hormone-like hormone a*
RNA	ribonucleic acid
runx2a	*runt-related transcription factor 2 orthologue a*
sp7	Gene coding for Sp7
Tg	transgene
TUNEL	Terminal deoxynucleotidyl transferase dUTP nick end labeling
UTP	uridine triphosphate
UV	ultraviolet
Wnt	*wingless-related integration site*
wpf	weeks post fertilization
WT	wildtype
YFP	yellow fluorescent protein

Nomenclature Conventions

Zebrafish

Gene: *hoxa13a*
Protein: Hoxa13a

Mouse

Gene: *Hoxa13*
Protein: HOXA13

Human

Gene: *HOXA13*
Protein: HOXA13

Study Specific Nomenclature

Triple *hox* deletion mutant: Combined *homeobox a13 a, homeobox a13 b, homeobox d cluster* deletion zebrafish.

Triple *hox13* deletion mutant: Combined *homeobox a13 a, homeobox a13 b, homeobox d13 a* zebrafish gene deletion.

m-inta11: Mouse intron of *Homeobox A11* gene; contains an enhancer bound by HoxA13 and HoxD13.

Glossary

Actinotrichia:	Bundles of rigid elastoidin fibers comprised of actinodin and collagen. These fibers are forming within the pectoral fin fold and the median fin fold during embryonic development. They are used as support for the fin fold and as a scaffold for migration of mesenchymal cells within the fin fold. They are restricted to the distal end of the fin ray in adult fish.
Apical Ectodermal Ridge:	Cell signalling centre comprised of ectodermal tissue. Found at the distal edge of the limb/fin bud along the anterior/ posterior axis where it promotes cell proliferation and patterning of the proximal/distal axis of the future limb or fin.
Fin Fold:	Two layers of ectodermal cells created when the apical ectodermal ridge (AER) tissue of the embryonic fins folds on itself and elongates during fin development at approximately 36 hours post fertilization. The fin fold is supported by two rows of actinotrichia fibrils.
Bifurcation:	Splitting of a single fin ray into sister rays.
Blastema:	Mass of dedifferentiated mesenchymal cells that forms underneath the wound epidermis at two days post fin amputation, distal to each amputated fin ray. Composed of two regions, the proximal and the distal blastema. Cells of the distal most blastema do not proliferate, while cells in the more proximal blastema strongly proliferate (known as the proliferation zone). During the regenerative outgrowth phase, starting at approximately 3 dpa, cells of the proximal blastema control the direction of outgrowth; when exiting the proximal blastema, cells differentiate.
Breeding Tubercles:	Secondary sexual characteristic that develops around 2.5 months post fertilization. They are multicellular epidermal structures that often support a conical keratin cap. The breeding tubercles (BT) found on the surface of some of the pectoral fin rays of the male zebrafish are used during mating to coerce the female into releasing eggs.
Distal Radials:	Bone nodules of the paired fins, dorsal and anal fins forming by endochondral ossification and located within the body of the zebrafish. Comprise the second portion of the endoskeleton articulating to both the proximal radials and base of the fin rays.

Endochondral Ossification:	Process by which a cartilage template is first formed, and later replaced by bone cells that produce bone proteins and minerals creating bony tissue.
Endoskeleton:	Skeletal portion of the fin found within the body. Made of endochondral bones that have a cartilaginous origin and are necessary for connecting to the base of the fin rays. Consists of proximal and distal radials.
Exoskeleton:	Supports the external portion of the fin, protrudes from the body and is comprised of lepidotrichia, and actinotrichia that are located at the distal tips of the fin.
Fibrous Joints:	Joints between bone segments of the hemiray, providing flexibility for the fin. Fibrous joints lack a joint capsule and bone segments are held together via collagenous fibrils.
Hemiray:	Concave intramembranous segmented bone comprising half of the lepidotrichia.
Homeobox:	DNA sequence, around 180 base pairs long, coding for the homeodomain of transcription factors. The homeodomain is a DNA binding domain.
Intramembranous Ossification:	Process by which the bone of the fin rays, lepidotrichia, are formed. A bone matrix is released by the osteoblasts located beneath the epithelial cells and this matrix calcifies; there is no cartilage formation as in endochondral ossification.
Lepidotrichia:	Skeleton of the fin rays. Bone is formed via intramembranous ossification and comprised of two concave hemirays segmented at regularly spaced intervals by fibrous joints. Encase soft intra-ray tissue.
Proximal Radials:	Bones forming by endochondral ossification located within the body of the zebrafish. Comprise the first portion of the endoskeleton articulating to the distal radials and anchoring the fins to the body of the fish.

Chapter 1: Introduction.

1.1 Zebrafish as a Model for Regeneration Studies

Zebrafish, *Danio rerio,* are part of the teleost infraclass (bony fish) of the ray-finned fish. Similar to other teleosts, zebrafish possess the ability to regenerate most tissues, including their fins after injury or amputation. Studying the regenerative capabilities of zebrafish provides insight into the molecular mechanisms used during these complex processes in a well-established model organism. Specifically, studying bone formation in the zebrafish fin, can elucidate molecular mechanisms involved in bone and joint formation of higher vertebrates. The zebrafish possess two paired fins; the pectoral and pelvic fins, and three unpaired fins: the dorsal, anal (often referred to as ventral) and caudal fins. The most commonly used fin for regenerative studies is the caudal fin. In addition to being the most accessible, the caudal fin of the zebrafish is also used for its simpler anatomy, short regeneration time and relative symmetry. The zebrafish also makes an ideal study organism due to its ability to be genetically and molecularly manipulated. Researchers have access to the complete zebrafish genome as well as well-established protocols for transgenesis, genome editing including knockout, and genetic post-manipulation screening (Pfefferli and Jazwinska, 2015; Wehner and Weidinger, 2015). Zebrafish fin rays are comprised of intramembranous bone. The intramembranous bone of the fin ray is separated by fibrous joints in which the anatomy and composition remains relatively unknown (reviewed in: Smeeton et al., 2016). Currently, limited information is available about the structure and molecular mechanisms behind the formation of intramembranous bone.

1.2 Zebrafish Fin Anatomy

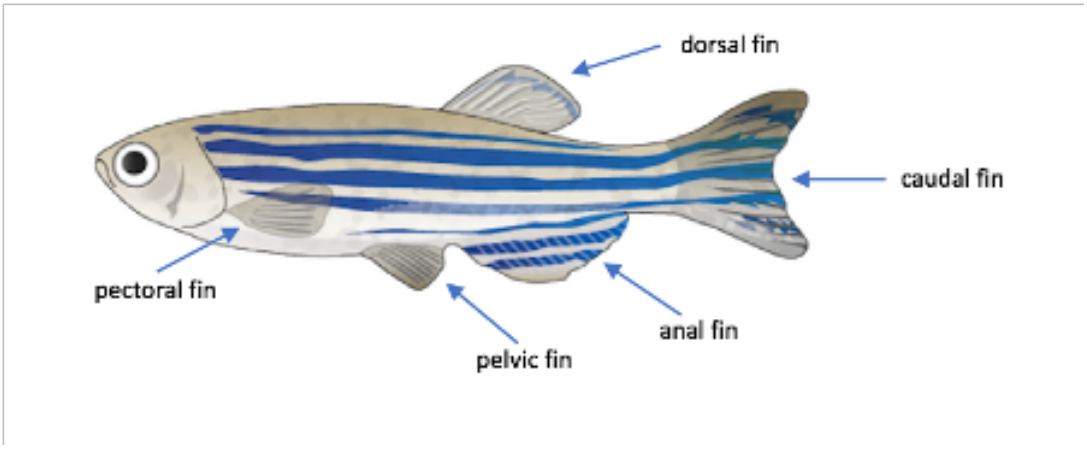

Figure 1. Schematic of adult zebrafish fins. Schematic shows the two paired fins: pectoral and pelvic as well as the three unpaired fins: dorsal, anal, and caudal. Schematic created by Togo Picture Gallery and obtained from Database Centre for Life Sciences (DCLS) CC BY 3.0 (https://creative commons.org/licenses/by/3.0/deed.en)

The zebrafish possess two paired fins; the pectoral and pelvic, and three unpaired fins; the dorsal, anal (ventral), and caudal (figure 1). All of the fins are composed of an endoskeleton, more or less abundant depending on the type of fin, and an exoskeleton. The external adult zebrafish fins are supported by their exoskeleton, which protrudes from the body and is comprised of lepidotrichia, often referred to as fin rays, and actinotrichia that are located at the distal tips of the fin (Akimenko et al., 2003). These fin rays are articulated to the endoskeleton (Akimenko et al., 2003). The endoskeleton is made of endochondral bones that have a cartilaginous origin and are necessary for connecting to the base of the fin rays. The endoskeleton is usually set within the body and not visible without dissection. Moreover, unlike the exoskeleton, amputation of the endoskeleton is not followed by regeneration in adult fish (Akimenko et al., 2003, Yoshida et al., 2020).

1.2.1 The Exoskeleton

The exoskeleton of the fins has many similar qualities throughout the different types of fins. In the caudal fin, there are 16-18 bony rays that span the length of the fin (figure 2), the pectoral fin is generally comprised of 10-14, the pelvic 7, the dorsal 8-10, and ventral 13-15 (Grandel & Schulte-Merker, 1998; Bird & Mabee, 2003; Siomava & Diogo, 2017). With exception of the lateral lepidotrichia in the unpaired fins, and the leading edge lateral fin ray as well as five smaller fin rays on the posterior edge in the paired fins, each ray will bifurcate into sister rays toward the distal end of the fin (Pfefferli & Jaźwińska, 2015). Lepidotrichia are comprised of two segmented biconcave hemirays; each segment of hemiray is separated by fibrous joints (figure 2) (Borday et al., 2001). The lepidotrichia are created by intramembranous ossification where the bone matrix is deposited by osteoblasts found beneath the epidermal cells. During intramembranous ossification, mesenchyme cells differentiate into osteoblasts, which then deposit the bone matrix; there is no cartilage formation as in endochondral bone (Abzhanov et al., 2007; Akimenko et al., 2003; Mackie, Tatarczuch, & Mirams, 2011). In addition, the mature hemiray is surrounded in layers of osteoblasts necessary for bone formation and repair (Akimenko et al., 2003; Poss et al., 2003; Pfefferli and Jazwinska, 2015). The two adjacent fin rays encase innervated and vascularized mesenchymal tissue known as the soft interray tissue (figure 2) (Borday et al., 2001; Gemberling, Bailey, Hyde, & Poss, 2013). Specifically, this mesenchymal tissue contains, blood vessels, nerve tissue, fibroblasts-like cells, and pigment cells. In zebrafish, actinotrichia are also part of the exoskeleton. Actinotrichia are rigid fibers organized in bundles found at the distal tips of each fin ray where they provide support for the distal edge. Actinotrichia are comprised of two elements, actinodin and collagen. Together these two elements form rigid fibre of elastoidin (Duran, et al., 2011; Becerra et al., 1996; Montes et al., 1982). During

development and regeneration actinotrichia can be used as a scaffold for mesenchymal cells including osteoblast precursors to migrate to their respective locations along the fin (Duran, et al., 2011; Becerra et al., 1996; Montes et al., 1982). All of these elements combined comprise the exoskeleton of the fin.

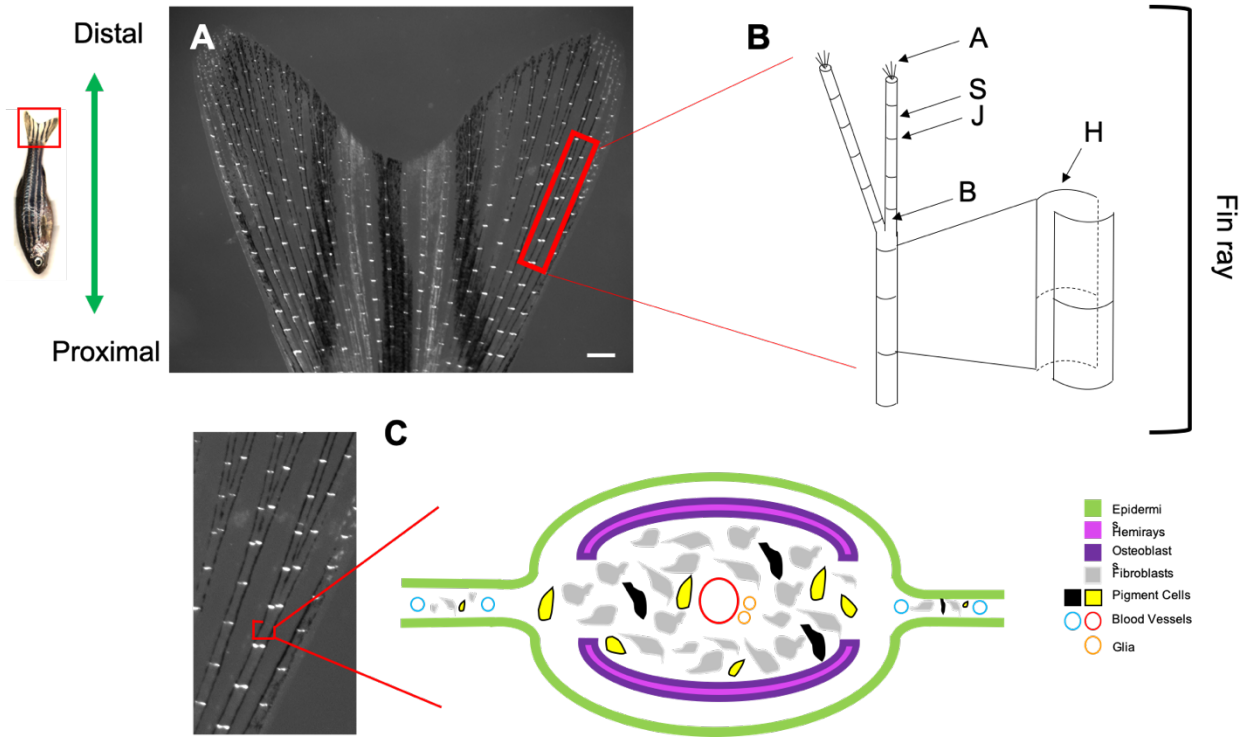

Figure 2. Schematic representation of zebrafish lepidotrichia. A) Whole mount, bright field image of an intact caudal fin. B) Illustration of a lepidotrichia composed of two concave hemirays; A, actinotrichia; S, bone segment; J, joint; B, bifurcation point; H, hemiray. C) Transverse cross-sectional illustration of the interior of the lepidotrichia/inter-ray and mesenchymal tissues within. Scale bar = 200µm.

1.2.2 The Endoskeleton

The endoskeleton of the paired fins has been the most extensively studied since the pectoral fin is a homologous structure to the limbs found in mammals. The endoskeleton of the paired fins includes bony elements that connect the base of the fin rays to the girdle. The endoskeleton of the pectoral fin anchors the fin rays to the body, the first three to four lepidotrichia articulate in a one-

to-one manner with the distal radials while further medially, several lepidotrichia articulate to one distal radial (Akimenko et al., 2003; Grandel & Schulte, 1998). The pectoral endoskeleton is comprised of four proximal radials articulated to six-eight distal radials aligned along the anteroposterior axis of the fin. On the pectoral fin, there are 10-14 fin rays, most of which will articulate with the distal radials (figure 3) (reviewed in: Hamada et al., 2019). The endoskeleton of the unpaired fins is comprised of modified elements of the vertebral column (Bird & Mabee, 2003; Bensimon-Brito et al., 2012; Wiley et al., 2015). The caudal fin endoskeleton is comprised of preurals, with neural spines protruding dorsally and haemal arches protruding ventrally (Bird & Mabee, 2003; Bensimon-Brito et al., 2012; Wiley et al., 2015). The final element of the vertebral column, the urostyle, has a ural neural arch protruding dorsally and a parhypural protruding ventrally. Articulated to the urostyle are five hypurals which articulate with the base of the fin rays (figure 4) (Bird & Mabee, 2003; Bensimon-Brito et al., 2012; Wiley et al., 2015). The dorsal fin rays are articulated to distal radials which in turn articulate to 7-9 proximal radials that extend into the intramuscular space of the neural arches (figure 4). Similarly, the ventral fin rays articulate to distal radials which in turn articulate to 12-14 proximal radials that extend into the intramuscular space of the haemal arches (figure 4) (Bird & Mabee, 2003).

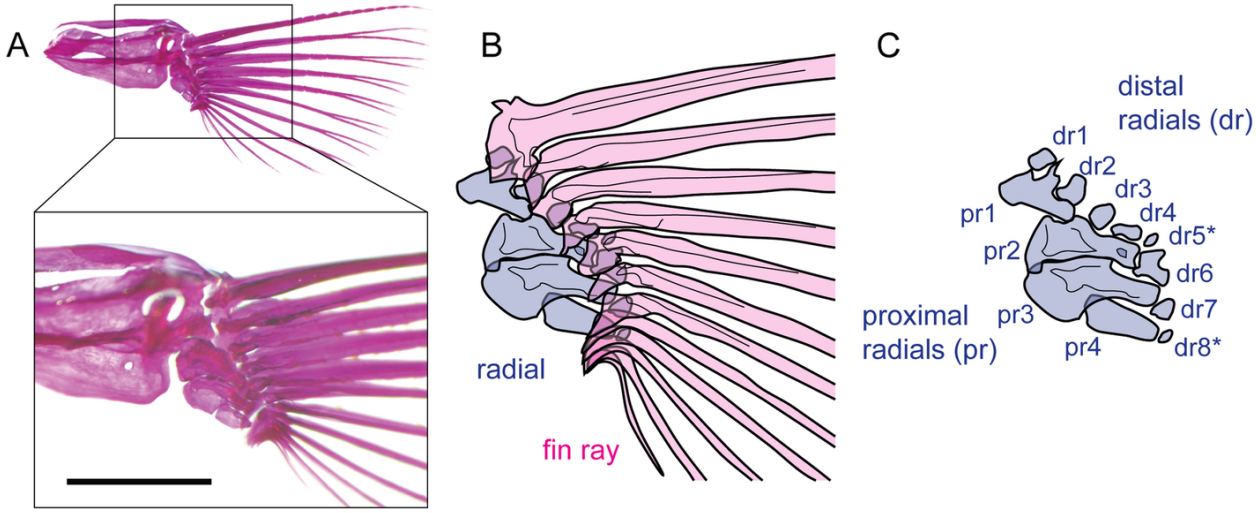

Figure 3. Zebrafish pectoral fin skeleton. A) Bone staining of zebrafish pectoral fin endoskeleton and exoskeleton; enlarged image focused on the endoskeleton and base of the fin rays. B) Schematic illustrating articulation of radials with the fin rays. C) Schematic of the proximal and distal radials. Adapted with permissions from BMC Part of Springer Nature, Open Access Articles: January 23, 2021.Adapted from Hamada et al., 2019.

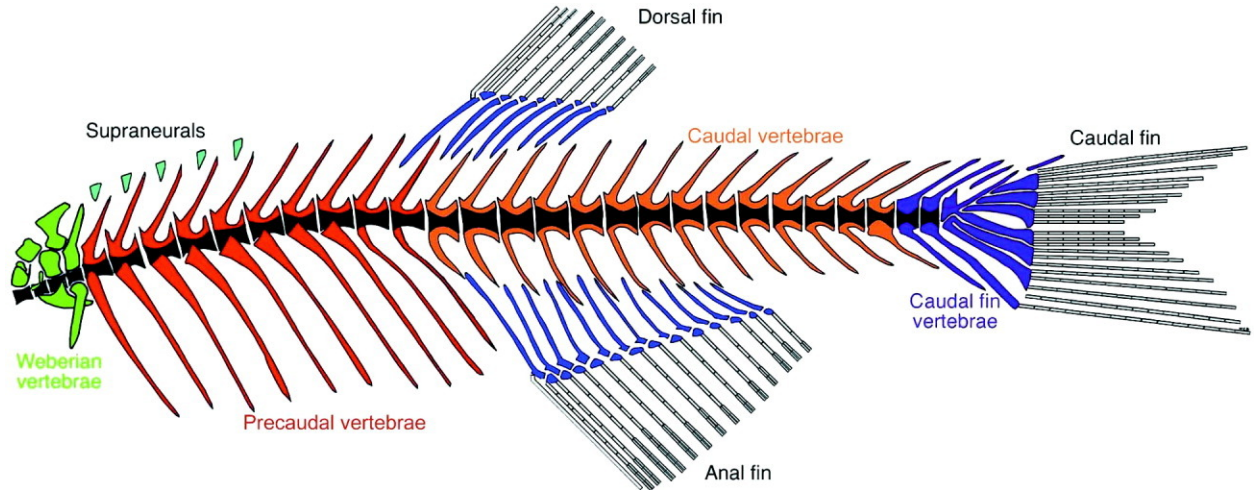

Figure 4. Zebrafish endoskeleton and exoskeleton (without actinotrichia) of the dorsal, anal, and caudal fin (blue). Radials of the dorsal and anal fin labelled in blue articulating to the caudal vertebrae, distal radials also labelled in blue articulating radials to the fin rays. Caudal fin hypurals shown in blue articulated to the urostyle also blue, articulated to the caudal fin vertebrae (blue and black). Adapted from Bird & Mabee, 2003; with permission from Copy Copyright Clearance Center's RightsLink®, January 23, 2021.

1.3 Overview of Caudal Fin Regeneration

Zebrafish fin rays undergo epimorphic regeneration which entails perfect replacement of the lost exoskeleton. An important step in this process is the formation of a blastema. First cell dedifferentiation occurs forming the blastema, rapid proliferation follows, and then once again the cells differentiate reforming the lost exoskeleton as well as all tissues within the fin ray. Regeneration begins with formation of the wound epithelium one to three hours (in an optimal housing environment, 28.5ºC, 10h light and 14h dark) following injury. Epithelial cells migrate to the amputation plane forming a single cell layer to cover the wound. Over the course of twelve to eighteen hours, migration of epithelial cells from the stump will continue creating an accumulation of cells constituting the wound epithelium (Akimenko et al., 2003; Poss et al., 2003; Pfefferli and Jazwinska, 2015; Wehner and Weidinger, 2015).

Following formation of the wound epithelium, a nascent blastema begins to form at 24 hours post-amputation (hpa). Mature cells from the first few segments proximal to the amputation plane dedifferentiate and migrate towards the amputation plane. At the amputation plane, these cells become a large mass of dedifferentiated mesenchymal cells creating the blastema (Akimenko et al., 2003; Poss et al., 2003; Pfefferli and Jazwinska, 2015; Wehner and Weidinger, 2015). The blastema is composed of two regions, the proximal and the distal blastema. The distal blastema is responsible for cell proliferation and epidermal patterning. The distal blastema is where cell proliferation occurs allowing for outgrowth of the fin rays (Grotek, Wehner, & Weidinger, 2013; Münch, González-Rajal, & de la Pompa, 2013). The proximal portion controls the redifferentiation of dedifferentiated cells (Grotek, Wehner, & Weidinger, 2013; Münch, González-Rajal, & de la Pompa, 2013). These two processes are monitored through Notch, Fgf, as well as Wnt signaling. When any of these signaling pathways are inhibited, a decrease in blastema cell proliferation, is

observed leading to absence of the regenerate (Stewart, Gomez, Armstrong, Henner, & Stankunas, 2014; Wehner et al., 2014). At approximately 72 hpa the blastema will be fully formed and contributing to regenerate outgrowth.

Regenerate outgrowth begins when proximal cells in the blastema enter the differentiation zone. In the differentiation zone, mesenchymal cells lose their proliferative state and begin to redifferentiate into specific cell types. In particular, blastema cells lining the basal epithelial layer will differentiate into osteoblasts (figure 5C) (Knopf et al., 2011). Overall regeneration of the fin rays proceeds through three stages: formation of the wound epithelium, formation of the blastema, and regenerative outgrowth. As part of the exoskeleton actinotrichia also regenerate and most likely provide a scaffold for migration (see section 1.4).

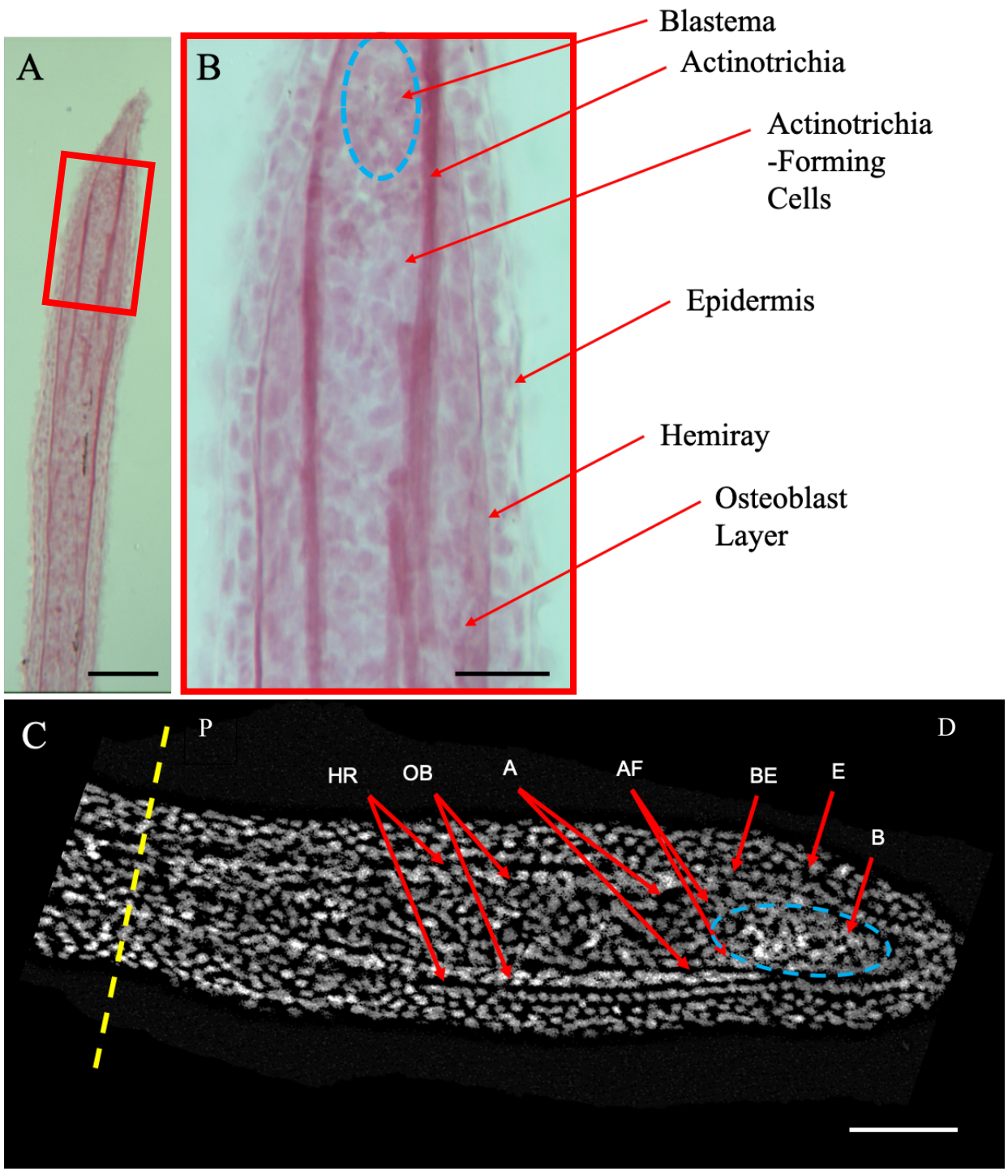

Figure 5. Longitudinal cryosection through a fin ray of a regenerate at four-days post-amputation (dpa) stained with picrosirius red (A & B) and DAPI (C). A) longitudinal cryosection of a fin regenerate at 4dpa with picrosirius red staining (10x). B) Magnified image of (A). C) Longitudinal cryosection of a 4dpa fin regenerate with DAPI staining of the nuclei. Yellow dashed line represents amputation plane. White P and D represent proximal and distal directions, respectively. HR, hemiray; OB, osteoblast layers; A, actinotrichia; AF, actinotrichia forming cells;

BE, basal epithelial layer; E, epidermis; B, blastema. Scale bar in (A) & (C) = 100 μm. Scale bar in (B) = 50 μm. Images A and B taken by Jing Zhang.

1.4 Actinotrichia in Fin Development and Regeneration

As previously mentioned, actinotrichia are fibres organized in bundles that provide a scaffold for cells to migrate along while forming the fin or fin regenerate. Many studies involved in, the developmental role of actinotrichia are performed on the pectoral fin bud. The fin bud begins to form at 24 hpf as an outgrowth of the lateral plate mesoderm (Kimmel et al., 1995). Within the fin bud there are several signaling centers such as the apical ectodermal ridge (AER). The AER is found at the distal edge of the fin bud along the anterior/ posterior axis where it promotes cell proliferation and patterning of the proximal distal axis (Grandel and Schulte-Merker, 1998; Kawakami et al., 2006). During development, the AER will fold on itself giving rise to the apical fin fold (FF). In between the two layers of ectodermal cells forming the FF, actinotrichia organized in two parallel rows provide support and a scaffold for mesenchymal cells migrating into the FF (figure 6) (Wood and Thorogood, 1984; Geraudie and Meunier, 1980; Grandel and Schulte-Merker, 1998). Actinotrichia themselves, are made by actinotrichia-forming mesenchymal cells. In the later stages of development, at approximately three weeks post-fertilization (wpf), lepidotrichia begin to form in the proximal to distal direction within the elongating FF and progressively restrict actinotrichia to the distal edges of the rays (Geraudie and Meunier, 1980). Actinotrichia are also located in the embryonic median FF forming around the posterior end part of the embryo and that will, later, develop into the unpaired fins (Lalonde and Akimenko, 2018). During fin regeneration in adult fish, actinotrichia fibres support the distal edge of the regenerate. Actinotrichia are composed of elastoidin which is comprised of collagen and non-collagenous protein, actinodin (Wood, 1982; Wood and Thorogood, 1984; Zhang et al., 2010). There are four *actinodin* genes identified in zebrafish that translate into the actinodin protein: *and1, and2, and3,*

and *and4* (Zhang, et al., 2010). Our lab previously performed a transient gene knockdown using morpholino (MO) against *and1* and *and2* (*and1/2)* in zebrafish embryos. This created an absence of actinotrichia and caused disruptions of the migration of cells within the fin fold during early stages of fin development (Zhang et al., 2010). However, the effect of MO knockdowns is transient, therefore this prevented the analysis of the effects of the absence of actinotrichia fibres in the adult fins. In an effort to further analyse the role of the actinotrichia in adult fins our lab has recently developed mutant fish using the CRISPR/Cas9 genome editing technology that are *and1/2* null. As in morphants, the double mutants show an absence of actinotrichia and disruptions of the migration of cells in the FF during embryonic development. In addition, the fin rays of the adult *and1/2* null mutants possess abnormal fin rays: irregular shape, shortened bone segments, and fewer fin rays.

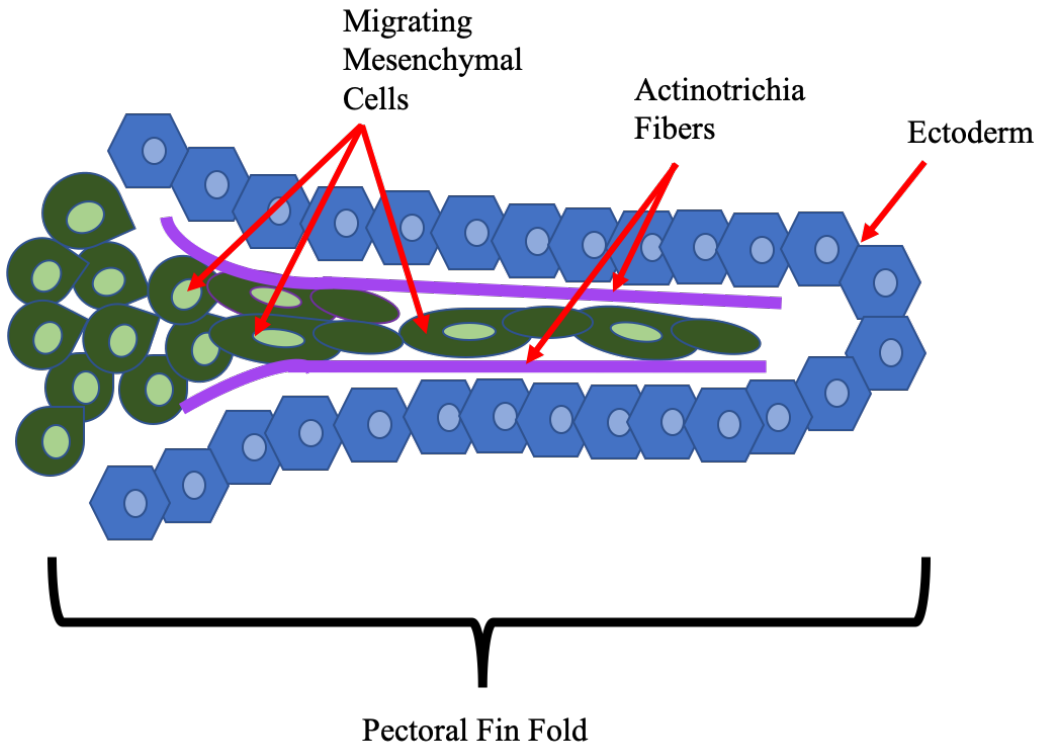

Figure 6. Actinotrichia in the pectoral FF and caudal in regenerate. Schematic representation of actinotrichia in the pectoral FF with migrating mesenchymal cells.

Similar to fin development, actinotrichia are important for support and cell migration in the fin regenerate (figure 5A). Within the fin ray, actinotrichia are first to regenerate and therefore can serve as a support for the pre-osteoblasts to migrate along. During regeneration, *and1* expression is located in the actinotrichia-forming cells, comprised of a subset of the basal epithelial layer and the mesenchymal cells on the interior of the osteoblast cell layer; additionally there is high expression in the blastema (Zhang et al., 2010; Duran et al., 2011; Konig et al., 2017). Within the subepithelial space of the regenerate, actinotrichia are assembled in longitudinal bundles toward the distal end. Specifically, actinotrichia at the distal end of the fin ray occupy the area between the epithelial and mesenchymal cells (figure 5B). Proximally there are pre-osteoblast / osteoblasts located between the epithelial layers and the actinotrichia (figure 5B). Therefore, the actinotrichia are located among mesenchymal cells, on one side osteoblasts, on the other side actinotrichia-forming cells. Actinotrichia are constantly remodelled as the fin ray grows, they are synthesized by addition of actinotrichial material at the distal end of the fibre (towards the distal part of the regenerate) while, at the proximal end, the fibre is degraded (Marí-Beffa et al., 1989). Actinotrichia's role in cell migration and fin fold support may contribute to the proper patterning and formation of intramembranous bone, as evidenced from the fin defects observed in the *and1/2* double mutants.

1.5. Bone Formation After Amputation

Studies on caudal fin regeneration have shown that following amputation, the mature osteoblasts that are located near the amputation plane will begin dedifferentiation (Knopf et al., 2011). Following dedifferentiation, they will proliferate and migrate towards the wound site. In the forming blastema, the dedifferentiated osteoblasts will remain fate restricted, toward the lateral edges of the blastema with additional mesenchymal cells remaining medial (Akimenko et al., 2003; Mackie et al, 2011). In the distal portion of the regenerate, the osteoblasts will secrete bone matrix

between themselves and the basement membrane of the epithelium. They progressively mature in more proximal regions of the regenerate, as the hemiray begins to take form osteoblasts will encapsulate the developing hemiray (figure 7) (Akimenko et al., 2003; Mackie et al, 2011).

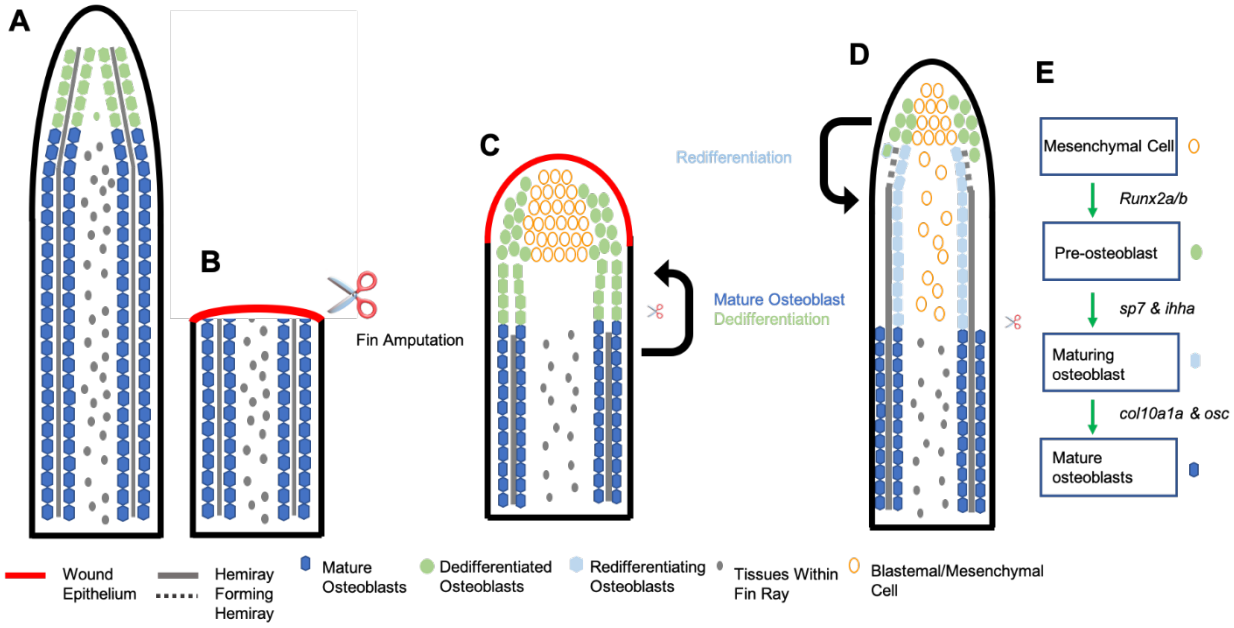

Figure 7. Schematic representation of osteoblast dedifferentiation and redifferentiation during fin regeneration. A) Intact longitudinal section of an intact fin ray. B) First stage following fin amputation, formation of the wound epithelium. C) Mature osteoblast migrating toward the amputation plane and dedifferentiating, creation of the blastema. D) Redifferentiation of the dedifferentiated fate restricted osteoblasts. E) Osteoblast commitment markers expressed at each stage of redifferentiation.

The dedifferentiated osteoblasts downregulate expression of intermediate and late osteoblast markers but continue to express *run-related transcription factor 2* (*runx2)*, a pre-osteoblast marker (Figure 8). The *runx2*$^{+}$ cells are restricted to the lateral sides of the blastema under the epidermis (Figure 7C) (Knopf et al., 2011). The more distal subpopulation of the *runx2*$^{+}$ cells remain highly proliferative. Stewart et al., (2014) suggested that this proliferative state is controlled by Wnt/β-catenin. Wnt/β-catenin contributes a continuous supply of *runx2*$^{+}$ cells to the

blastema during regeneration of the fin. As the fin grows, the source of Wnt is moved from *runx2*, *bmp2b* is upregulated, which in turn activates the BMP signaling pathway (figure 8) (Stewart et al., 2014). BMP signaling from the basal epithelial layer is associated with the maturation of *runx2*$^{+}$ expressing pre-osteoblasts into osteoblasts through the upregulation of osteoblast commitment factor, *osterix* (*sp7)* (figure 8) (McMillan et al., 2018; Smith et al. 2006; Laforest et al., 1998). In the intermediate stages of maturation, these maturing osteoblasts will express *collagen, type X, alpha* (*col10a1a*), a component of the bone matrix (Avaron et al., 2006). Following expression of *sp7, osteocalcin* or *bone γ-carboxyglutamic acid-containing protein* (*osc*, *bglap*), osteoblast maturation factors are expressed as cells synthesize and release bone matrix into the subepidermal space forming intramembranous bones of the hemiray (figure 8) (Gavaia et al., 2006).

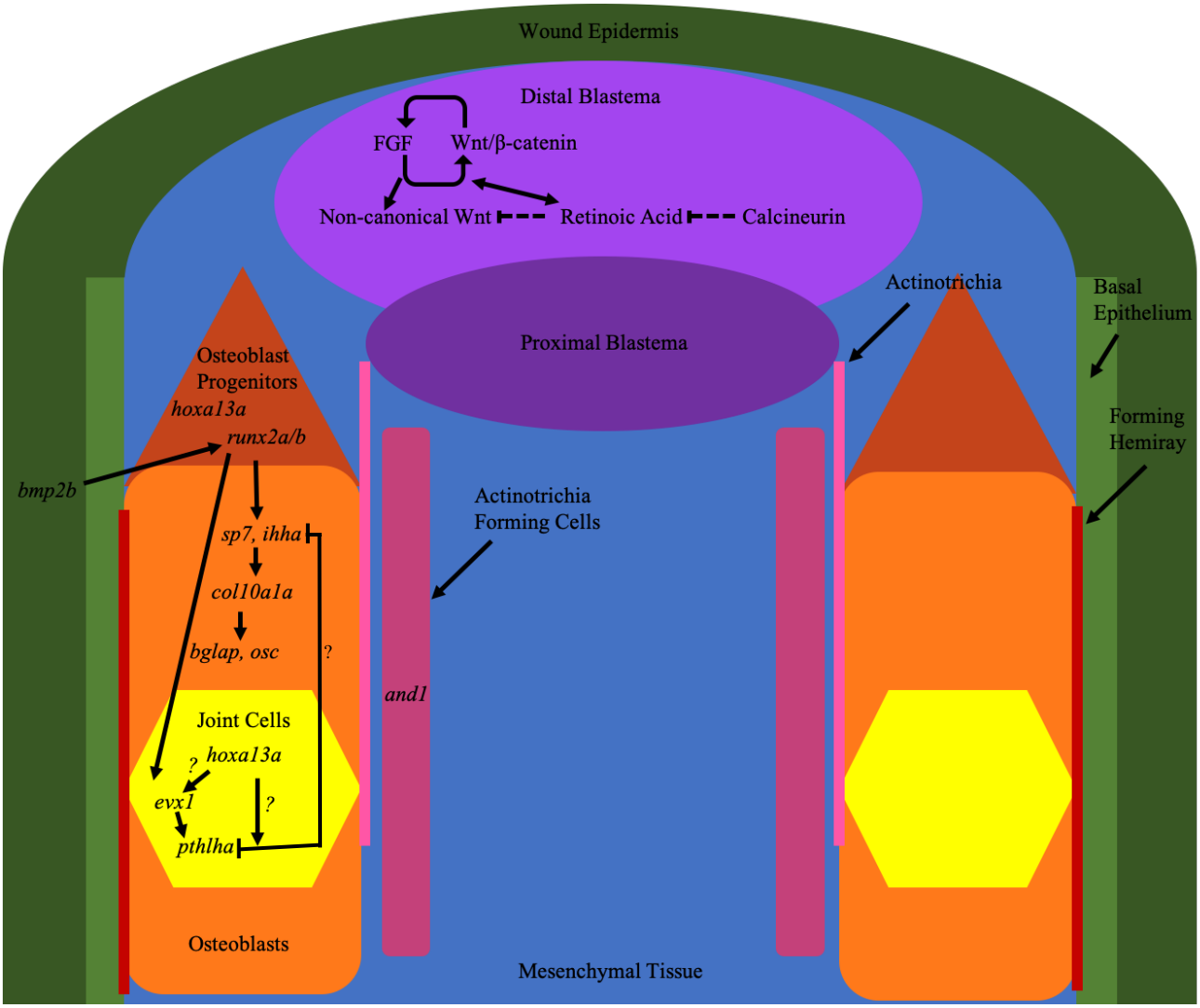

Figure 8. Schematic representation of the pathways discussed within this introduction. Joint genes: *hoxa13a, evx1, pthlha*; osteoblast genes: *sp7, ihha, col10a1a, bglap, osc*; osteoblast progenitor genes: *hoxa13a, runx2a/b*; actinotrichia-forming genes: *and1/2.*

1.6 Common Lineage of Bone and Joint Cells

In addition to the fate-restricted osteoblasts, Singh *et al.,* study suggested another unknown source of cells that can produce osteoblasts during fin regeneration (Singh et al., 2012). Singh *et al*., targeted osteoblasts for ablation using the zebrafish transgenic line (*sp7:NTR)* and treated with metronidazole to induce ablation (see section 1.11 for a description of the nitroreductase (NTR) mechanism). Although they ablated osteoblasts prior to fin amputation, bone

regeneration proceeded normally in the transgenic zebrafish suggesting the presence of another source of osteoblasts, potentially presumptive and joint-forming cells (Singh et al., 2012). The fin rays of the caudal fin are composed of bone segments separated by joints. The fin rays grow via the addition of bone to the distal part of the ray (Tu & Johnson, 2011). Joints form at regularly spaced intervals approximately 200μm apart, decreasing along the proximal distal axis of the ray. The joints form a gap in the bone segments which are then held together by ligaments forming the fibrous joint. Joints occur at the same position in the two hemirays and provide flexibility for the fin. In a previous study by Tu & Johnson, (2011) it was suggested that bone and joint cells of the caudal fin exoskeleton are derived from a common lineage. To investigate the lineage of bone and joint cells, a *ef1*α:GFP marker was used. The *Xenopus EF1*α promoter drives GFP (Johnson and Krieg, 1995) with ubiquitous expression, making it suitable to compare lineage relationship of different cell types in the fin. Over 1000 zebrafish embryos were injected with the *ef1*α:GFP transgene. Primary injected zebrafish are mosaic for the transgene. This approach allows for clonal analysis of cells expressing the transgene. Therefore, in this study embryos with GFP expression in the caudal fin were further investigated. Expression of GFP in joint cells was accompanied by positive expression in osteoblasts potentially indicating that they are derived from a common lineage (Tu & Johnson, 2011). Moreover, our lab has also recently discovered support for osteoblasts and joint cells sharing a common lineage. Expression of *runx2* was examined and recognized that it has an overlapping domain with *sp7* expression during regeneration. In addition, a small group of cells that created a protuberance in the pre-osteoblasts were $runx2^{+}$ but did not express *sp7* (figure 9). The position of the $runx2^{+}$ $sp7^{-}$ cells aligned with the positioning of where the next joint would be forming, suggesting that they are presumptive joint cells. Using immunohistochemistry (IHC) our lab noticed that these $runx2^{+}$ $sp7^{-}$ cells were also positive for

zns-5, a marker of zebrafish osteoblast at all differentiation stages, confirming that they were of osteoblast lineage (figure 10). Further examination of the expression of osteoblast commitment marker *sp7* and mature osteoblast marker *col10a1* show that, although there was expression of *runx2a/b* within the protuberance in the presumptive joint cells, *sp7* and *col10a1a* were not expressed (figure 9).

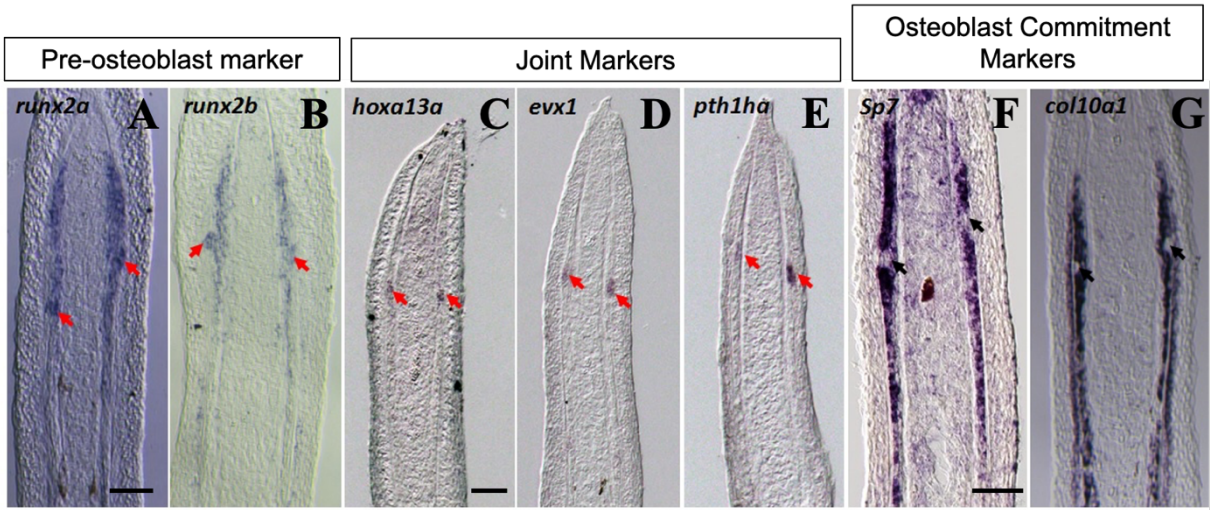

Figure 9. Expression of pre-osteoblast, joint, osteoblast commitment markers analyzed by *in situ* hybridisation on longitudinal cryosections of a 4DPA regenerate. Each panel is labelled with its respective marker Red arrows point to joint cells with positive expression, black arrows point to an absence of expression in joint cell clusters. Scale bar = 50 μm in (A) for (A&B), in (C) for (C, D&E), in F for (F&G). (McMillan et al., 2018). Reproduced/adapted with permission from Development, December 18, 2020.

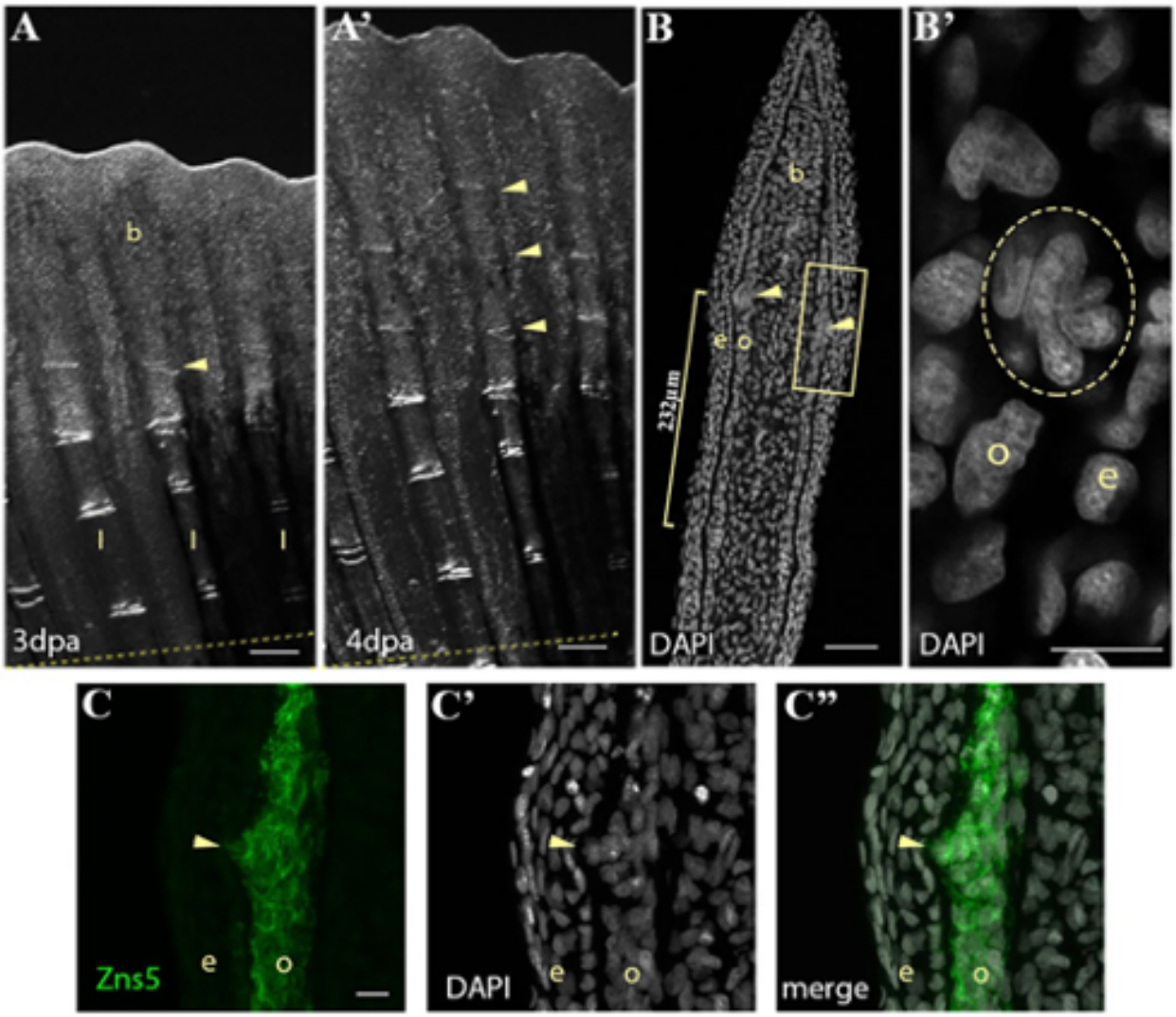

Figure 10. Formation of joint-forming cell clusters during fin regeneration and detection of Zns-5 protein using antibody staining. A-A′) Bright-field images of fin regenerate at 3 dpa A) and 4 dpa A′) illustration of the addition of joints shown by yellow arrowheads on the distal portion of rays. Dashed yellow line indicates amputation plane. B) DAPI staining on a longitudinal cryosection of a 4 dpa regenerate illustrates a cluster of nuclei (yellow arrowheads) 232 µm (yellow bracket) from the maturing joint. B′) Magnification of the boxed area in B showing a nuclei cluster inside yellow circle. C) Zns5 immunohistostaining labels pan-osteoblasts both joint cell cluster and osteoblasts are labeled. C′) DAPI staining of the same section showing the cell cluster nuclei. C′′) Merged image of C and C′. b, blastema; e, epidermis; l, lepidotrichia; o, osteoblast. Scale bars: 200 µm (A,A′); 50 µm (B); 10 µm (B′; in C for C-C′′) (McMillan et al., 2018). Reproduced/adapted with permission from Development, December 18, 2020.

1.7 Molecular Mechanisms of Joint Formation and Patterning After Amputation

Joint formation over the course of regeneration has not been extensively studied in zebrafish. As previously stated, the joint cells and osteoblasts share a common lineage however the derivation of joint fate is yet to be determined. Recent studies in our lab have shown that there are three stages of joint cell differentiation: presumptive joint cells, joint-forming cells, and mature joint cells (McMillan, Zhang et al., 2018). In a separate study it was shown that joint formation begins with the condensing of cells in the presumptive joint region at the distal end of the regenerate into a single row of cells, the presumptive joint cells. The row then divides into two rows of joint forming cells that encapsulate the forming joint (Pacifici et al., 2006; Sims et al., 2009). Following the separation of the two rows of joint forming cells a mature joint is formed and surrounded by mature joint cells (figure 11) (McMillan, Zhang et al., 2018).

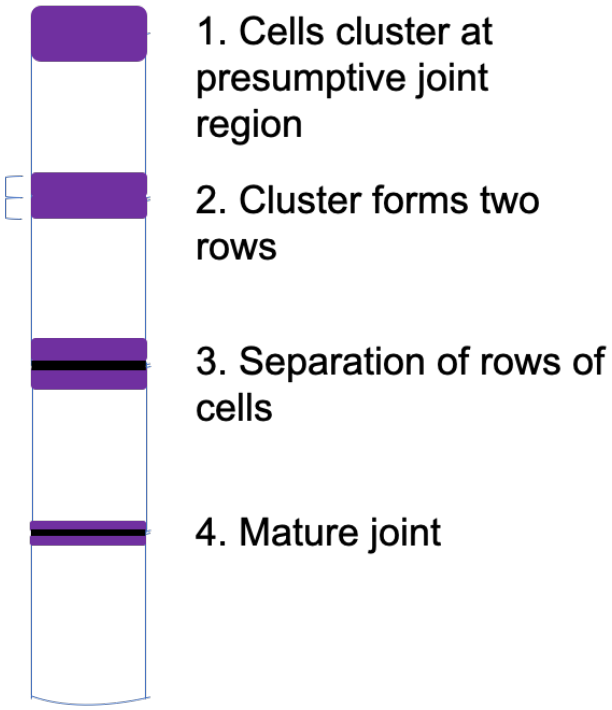

Figure 11. Maturation stages of joints along a fin ray. Mature joints toward the proximal portion of the fin ray immature joints (newly formed) toward the distal region of the fin ray.

1.7 .1 Molecular Mechanisms of *evx1* and *cx43* in Joint Formation

Despite the fact there is not a lot of studies on joint formation, most of them focused on the role of *evx1* and *cx43* regulation. The expression of a gene *even-skipped homeobox 1*, *evx1,* coding for a transcription factor was discovered to overlap where joints are present during fin development and regeneration (Borday et al., 2001). Mutants that are e*vx1*$^{-/-}$ null have fins that lack joints in the fin rays during development and regeneration, implicating that *evx1* is necessary for joint formation (Schulte et al., 2011). Further investigation has shown that zebrafish mutants of *connexin 43(cx43)* also show a disruption of joint patterning and *evx1* expression. The *cx43* gene codes for a component of connexons, necessary for the formation of gap junctions between cells (Ton & Iovine, 2013). Two mutant lines have been created that alter the length of the fin and bone segments. The *short fin, sof*^{b123} mutant, caused by mutations in *cx43,* has a shorter fin with decreased length in hemiray segments (Iovine et al., 2005). The second mutant *another long fin, alf*^{dty86} caused by mutations in *kcnk5b* has a longer fin length with increased and/or inconsistent length of hemiray segments (Ton & Iovine, 2013). The *cx43* gene is expressed in the joint cell clusters with *evx1* however *cx43* expression weakens as *evx1* becomes upregulated during joint formation (Ton & Iovine, 2013). Therefore, in mutant *cx43* null fish, *evx1* is expressed prematurely allowing for earlier joint formation and shorter hemiray segments (Ton & Iovine, 2013). Previous studies have also shown that an increase in *cx43* leads to a decrease in the expression of *evx1* as well as an increase in regenerate and hemiray segment length (Dardis et al., 2017; Ton & Iovine, 2013). In the second mutant, *alf* ^{dty86} *cx43* expression is increased creating decreased *evx1* expression (Ton & Iovine, 2013). These studies prompted further investigation into the expression patterns of bone markers in comparison to joint markers.

1.7 .2 Expression of Bone and Joint Markers in Presumptive and Joint-Forming Cells

To examine the molecular signature in the presumptive joint cells, expression of known and hypothesized fibrous joint markers were analyzed using *in situ* hybridization of antisense RNA probes (figure 9). *evx1* is expressed in the presumptive and joint-forming cells as well as a second known joint marker, *parathyroid hormone-related peptide I (pth1ha).* In *evx1* null mutants, expression of *pth1ha* is lost, suggesting *pthlha* is acting downstream of *evx1* (Figure 13). Research in mouse and chick embryos on the homologous protein of Pthlha show a negative-feedback loop between PTHrP (the homolog) and Ihh (homologous to Ihha) during endochondral ossification to allow control of chondrocyte proliferation and differentiation. (Lanske et al., 1996; St-Jacques et al., 1999; Vortkamp et al., 1998). In zebrafish, Pthlha inhibits intramembranous ossification and therefore may be involved in the inhibition of Ihha. Current hypotheses state that *pthlha* negatively regulates *ihha* inducing joint identity, osteoblast inhibition and subsequent joint formation (McMillan et al., 2018). *homeobox-A13a* (*hoxa13a*), coding for a transcription factor, is also expressed in the presumptive and joint-forming cells (Figure 9) as well as in all joint cells at all stages (figure 12). Moreover, *evx1* and *hoxa13a* are located in a close genomic proximity, and they often are expressed in similar domains (Ahn & Ho, 2008) suggesting that they may share some regulatory elements.

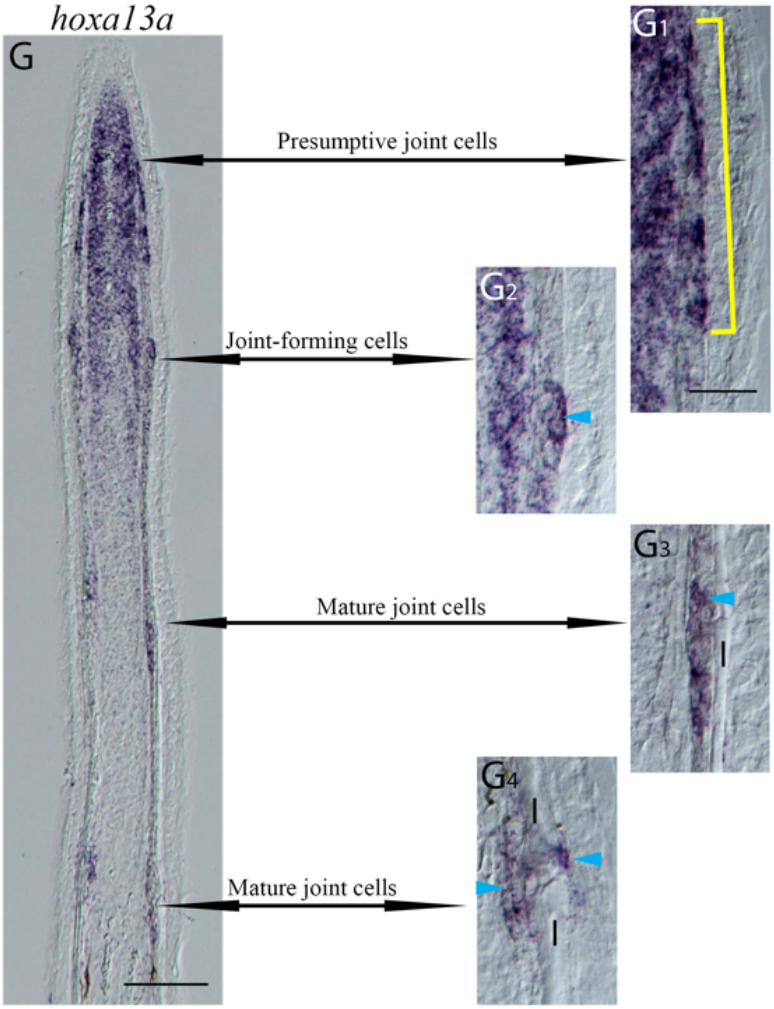

Figure 12. *in situ* hybridisation on a longitudinal cryosection of a 4DPA regenerate to show expression of *hoxa13a* in all joint stages as well as the blastema and actinotrichia forming cells. Scale bar = 30 µm. (McMillan et al., 2018). Reproduced/adapted with permission from Development, December 18, 2020.

Interestingly, *hoxa13a* is also expressed in joints of *evx1* null mutants suggesting that it is acting either upstream of *evx1* or in a parallel molecular mechanism (Figure 13). Double fluorescent *in situ* hybridization (FISH) confirmed that all three markers: *hoxa13a, evx1,* and *pthlha* are expressed in the presumptive, joint-forming, and mature joint cells. Additional work by McMilllan et al., (2018) also shows that *ihha* and *pthlha* possess complementary expression patterns in the regenerate indicating that they may interact during segment formation. While expression of *evx1* and *pthlha* is restricted to the joint cells, *hoxa13a* domain of expression extends in a few osteoblasts surrounding the joint cells at a lower level than in the joints (figure 12). In addition, *hoxa13a* is expressed in the presumptive / pre-osteoblasts characterised by the expression of *runx2a.* When a new joint is forming, *hoxa13a* expression is strongest and fades out in a gradient until no longer present (McMillan, Zhang et al., 2018). Refer to figure 8 for all aforementioned molecular pathways.

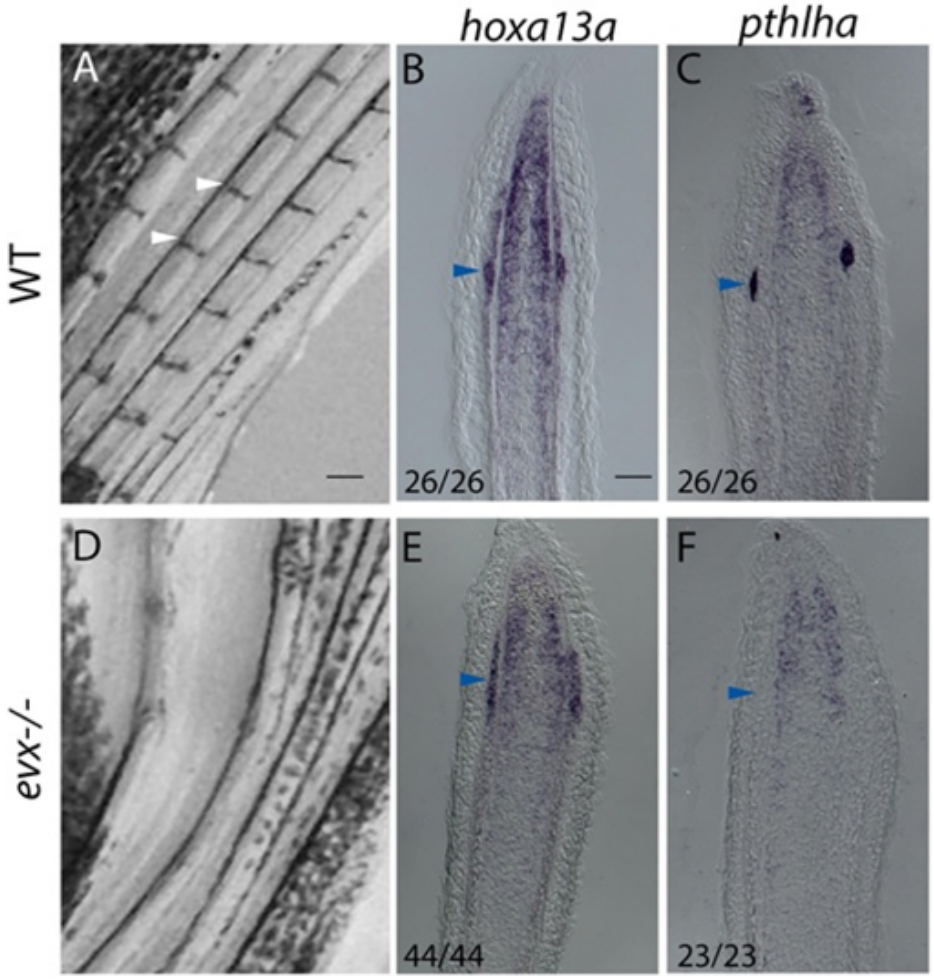

Figure 13. Expression of joint markers in WT and *evx1*$^{-/-}$ mutants. A) Wild-type fins, joints indicated by white arrowheads. B,C) ISH on longitudinal cryosections of 4 dpa wild-type regenerates *hoxa13a* B) and *pthlha* C) expression in joint cells (blue arrowheads). D) *evx1*$^{-/-}$ mutants fins joints are absent. E,F) ISH on longitudinal cryosections of 4 dpa *evx1*$^{-/-}$ mutant regenerates *hoxa13a* E) expression in presumptive joint cells but not *pthlha* F). Numbers in panels represent number of cryosections with similar expression pattern over the total number of sections analyzed. Scale bar = 200 μm (in A for A,D); 50 μm (in B for B, C, E, F) (McMillan et al., 2018). Reproduced/adapted with permission from Development, December 18, 2020.

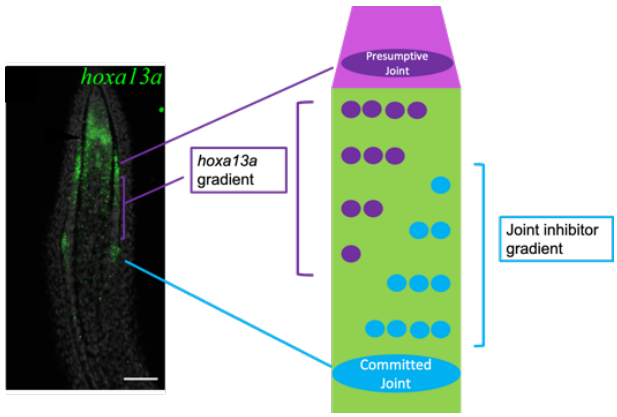

Figure 14. A proposed model of the *hoxa13a* gradient of expression. Scale bar = 100 µm. ISH image of *hoxa13a* taken from McMillan et al., 2018. Reproduced/adapted with permission from Development, December 18, 2020.

1.8 Proposed Model for the Role of *hoxa13a* in Joint Formation and Segment Length

Previously, a member in our lab was able to use laser photoablation, a technique used to ablate cells *in vivo,* to target *hoxa13a*-expressing joint cells responsible for the protuberance in the osteoblast layer during regeneration. The purpose of this ablation was to determine if the maturing joint cells can undergo regeneration if the *hoxa13a*-expressing cells were removed from the osteoblast layer. Following ablation, the joints cells failed to regenerate, an unusual result for zebrafish that have a high capacity for regeneration. The results suggested that joint cells can only regenerate if they follow the normal program of joint differentiation starting at the initial joint cell commitment stage. Coupling this result with a proposed joint cell commitment pathway, a joint formation model was created. The model is in part based on the discovered *hoxa13a* gradient of expression between the presumptive and maturing joint cells (figure 14). We propose that, when a new joint is forming, it leads to the synthesis of a joint inhibitor, and this inhibitor suppresses activation of *hoxa13a*. The expression of *hoxa13a* is greatest in the joint-forming cells and as the regenerate continues to form, *hoxa13a* expression progressively increases as it moves further from the source of the inhibitor until it meets a threshold and a subset of the most distal *runx2a/b*-expressing cells commit to joint lineage. After commitment of joint cells, the successive presumptive joint cells will undergo the same process. Based on the joint cell ablation described above, it is believed that joint cells can only form during the presumptive joint cell phase and if they are eliminated, the regenerate will form without joints.

Although the contributions of *hoxa13a* in joint cell differentiation have yet to be understood, the requirements of *evx1* in joint cell differentiation have been confirmed. Working to test this model, a past lab member, Derek Sheppard, used the metranidizole/nitroreductase system (discussed in section 1.11) to attempt ablation of the joint cells. Although full ablation of the cells was not obtained, the joint segments appeared irregularly spaced and shortened (figure 18). These results aligned with the proposed joint model; creating the hypothesis that the joint inhibitor is reduced allowing the next joint to form more proximal than in an untreated fish. However further research needed to be conducted to contribute to the elucidation of this model and molecular mechanisms of the *hox13* genes.

1.9 The Role of 5' *hox13* Genes in Ray/Joint Formation

The genes of the 5' *hox* gene clusters are highly involved in appendage patterning during development of all species including zebrafish (Amores, 1998). In mammals, there are four *Hox* clusters (*A-D)* and within each cluster paralogous genes are numbered from 1 to 13, *Hox1* paralogs are located at the 3' end of the cluster and the *Hox13* paralogs at the 5' end (Amores, 1998). The *Hox* genes encode transcription factors with a DNA binding domain called homeodomain. The Hox factors are responsible for the specificity of cell fate along the anterior-posterior axis of vertebrates (Amores, 1998). The order of *Hox* genes on the chromosome is reflective of the expression pattern observed on the anterior-posterior axis of the body (Amores, 1998). In addition to their role in the anterior-posterior axis, the 5' *Hox* genes of the A and D clusters play essential roles in limb patterning. In mouse models, *Hox* genes are specifying the fates along the three axes of the limb, *Hox13* genes are important for development of the autopod and distal parts of the appendages. More specifically, when the 5' *Hox* genes *Hoxa13* and *Hoxd13* are rendered inactive, phenotypic polydactyly and joint fusion are observed in the limb (Fromental-Ramain, *et al.,* 1996). Following the genome duplication event in teleost fish that occurred during evolution, zebrafish possess 7 *hox* gene clusters: *hoxaa, hoxab,*

hoxba, hoxbb, hoxca, hoxcb, and *hoxda*. The loss of the *hoxdb* cluster and a few *hox* genes within other clusters over the course of evolution now means that zebrafish have 49 *hox* genes.

In order to examine the role of the *hox13* genes in zebrafish compared to mouse, Nakamura et al., (2016) generated single and double frameshift mutants of *hoxa13a, hoxa13b, hoxd13a,* and mosaic triple *hox13* mutants. In zebrafish, the mosaic removal of the *Hoxa13* and *Hoxd13* orthologs: *hoxa13a, hoxa13b,* and *hoxd13a,* was shown to generate a lack of fin ray growth after the first bone segment in the pectoral fin, demonstrating the importance of the *hox13* genes in ray formation. This study also showed compensatory mechanisms between the paralogs, as variable length and number of segments in the pectoral fin were observed depending on allele dosage. While this study clearly shows the importance of the *hox13* genes for fin ray formation, it was solely focused on the pectoral fin. More specifically, emphasis was placed on the endoskeleton of the pectoral fin. Utilizing *in situ* hybridization it is shown that *hoxa13a, hoxa13b,* and *hoxd13a* are also expressed in the blastema of the regenerating caudal fin, as well *hoxa13a* also presents expression in all stages of the regenerating joint of the caudal fin. Therefore, additional studies need to be done to examine all the fins of the triple *hox13* mutants and to further explore different compensatory mechanisms that could occur between the different fins. Combining all the aforementioned knowledge, we decided to create our own mutants. These mutants were used for further examination of our proposed joint model during regeneration and to further determine the effects of the *hox13* gene removal on rays of all fins.

1.10 Generation of New *hox* Mutants

To study the role of *hoxa13a, hoxa13b,* and *hoxd13a* genes in relation to the molecular pathways involved in development and regeneration our lab created single knockout mutants encompassing the homeobox of each gene. Additionally, these single mutants were used to create

double and triple homozygous *hox13* deletion mutants. Generation of the *hox13* mutants in our lab was done by Dr. Qingming Qu using CRISPR/Cas9 genome editing technology. By injecting two guide RNAs (gRNA) designed for each gene and Cas-9 protein at the 1-cell stage in zebrafish embryos Dr. Qu was able to create the single *hox* mutants. The gRNAs used were created by Dr. Qu as well as some obtained from Nakamura et al., 2016, to create single deletion *hox13* mutants of *hoxa13a, hoxa13b,* and *hoxd13a*. The *hoxa13a* mutant was created with a 470 base pair (bp) deletion in the first exon. The *hoxa13b* mutant has a 790 bp deletion spanning part of the upstream intron and the majority of the second exon. The *hoxd13a* mutant has a 3154 bp deletion spanning half the first exon, the entirety of the intron, and the majority of the second exon. In each mutant the homeobox is removed or deleted rendering the transcription factor inactive (figure 15). In addition, Dr. Qu was compelled to create a single mutant with a deletion of the entire *hoxd* cluster (*hoxd13-hoxd3*). The *hoxd* cluster deletion was completed by injecting two gRNAs at once targeting each gene: *hoxd13,* and *hoxd3*. The F0 fish went from a cluster of 48 450 bp to 288 bp rendering the *hoxd* cluster inactive.

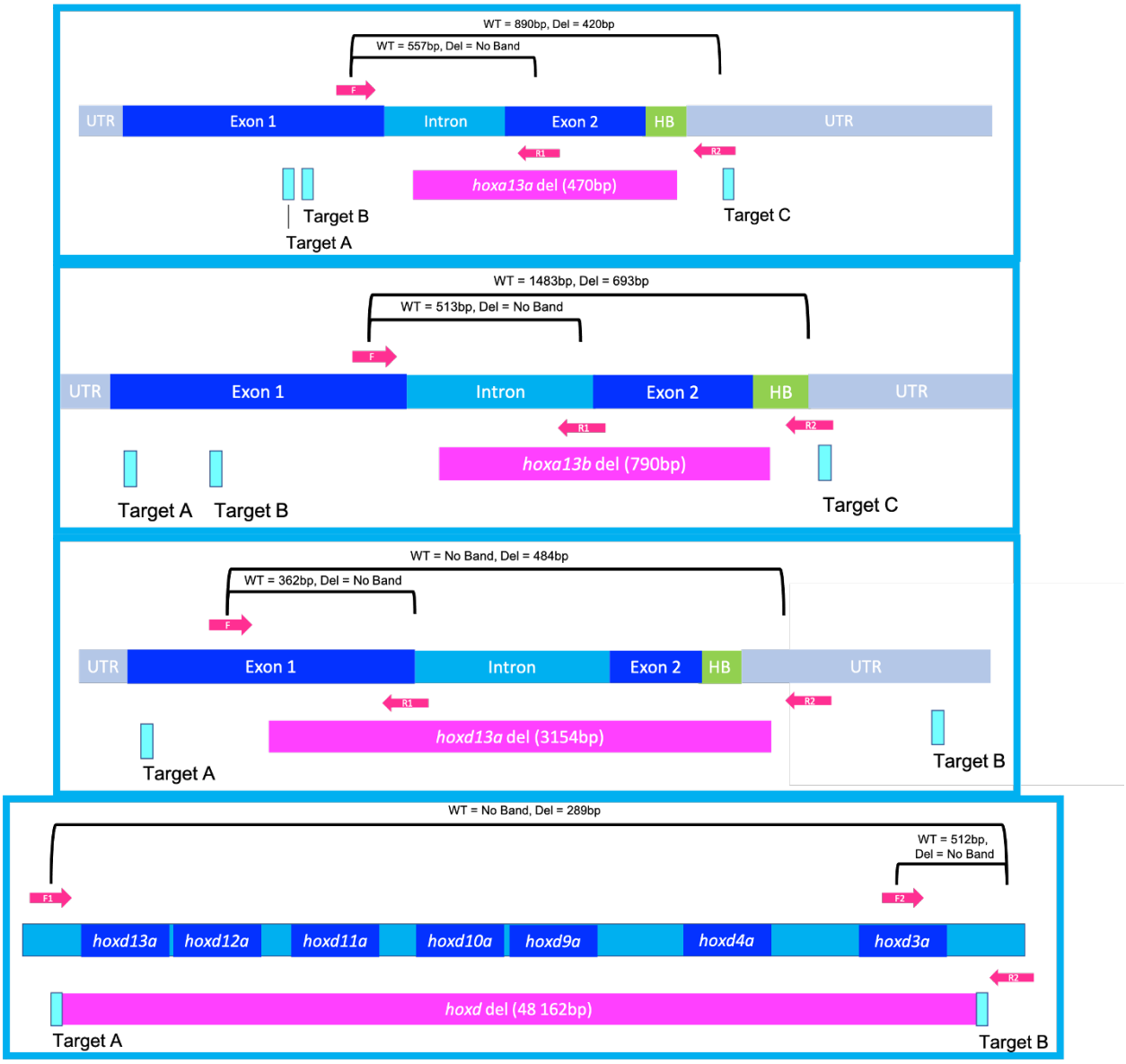

Figure 15. Schematic representation of the *hox* deletion mutations.
HB = homeobox.

1.11 Ablation of Joint Cells

Although the triple *hox13* mutants showed promising insight, the long rearing time allowed us to examine the ablation technique previously used by Derek Sheppard in our lab. The metronidazole/nitroreductase system (MTZ/NTR system) has been used as a technique for inducible targeted cell ablation *in vivo*. Nitroreductase (NTR) is a bacterial enzyme discovered in

E. coli, in the presence of certain prodrugs, including metronidazole (MTZ), metabolism will occur creating potent cytotoxins that kill the cells they are present in, specifically MTZ is converted into a DNA cross-linking agent leading to a caspase initiated apoptosis in the cell (Chen et al., 2011; Knox et al., 1988; Zenno et al., 1996). This method of inducible cell ablation has been studied heavily in zebrafish models targeting various cell types. Transgenic fish are created that express NTR controlled by tissue-specific regulatory elements. In theory, when placed in MTZ treated water, MTZ penetrates the tissue of the zebrafish inducing apoptosis in all cells expressing the NTR gene. Using concentrations of 10mM or lower will have minimal toxic effects however prolonged exposure can lead to toxicity and eventually death (Summersgill, Schupp, & Raff, 1982; White & Mumm, 2013; Chlebowski et al., 2017).

To target the joint cells, the NTR gene was expressed under the control of an enhancer named *m-Inta11,* that has been shown to be regulated by *Hoxa13* and *Hoxd13* in mice (Kherdjemil et al., 2016). In reporter transgenic zebrafish, this enhancer drives the expression of GFP in the joint cells at all differentiation stages and recapitulates *hoxa13a* gene expression (figure 16). The transgenic fish created in our lab to target and ablate joint cells uses this enhancer to drive expression of NTR as well as the yellow fluorescent protein (YFP) in joint cells. In this construct YFP and NTR proteins are linked via the 2A peptide. During translation, the 2A peptide is skipped by the ribosome, leading to the cleavage between the upstream (YFP) and downstream (NTR) (Ryan, King, & Thomas, 1991). In the absence of MTZ the joint cells express YFP, fluorescing yellow under UV light, and NTR which is neutral until exposed to a prodrug (Curado et al., 2007; Curado et al., 2008) (Figure 17). Past members of our lab have shown that treatment with MTZ during fin regeneration prior to the formation of the first joint (2.5 dpa) creates significantly shorter hemiray segments during the time of MTZ exposure compared to WT fish (figure 18). Although shorter segments were observed,

complete ablation of the joint cells was not observed as shown by the persistence of YFP expression. However, the impact of the cell loss in the *hoxa13a* domain still produced an abnormal joint pattern phenotype and warrants further research into the role of *hoxa13a* in the formation of joint cells. These results bring into question the efficiency of both the prodrug and our transgenic line.

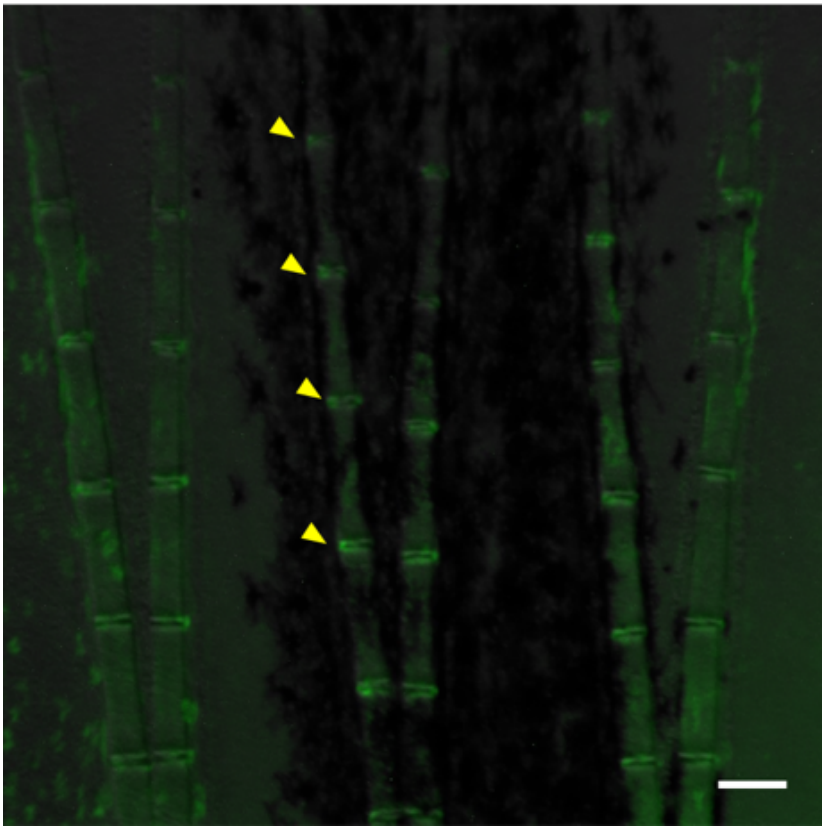

Figure 16. Fluorescence on intact caudal fin joints in a zebrafish with *tg(m-inta11-ß-globin:eGFP).* Scale bar = 100 μm (McMillan et al., 2018). Reproduced/adapted with permission from Development, December 18, 2020.

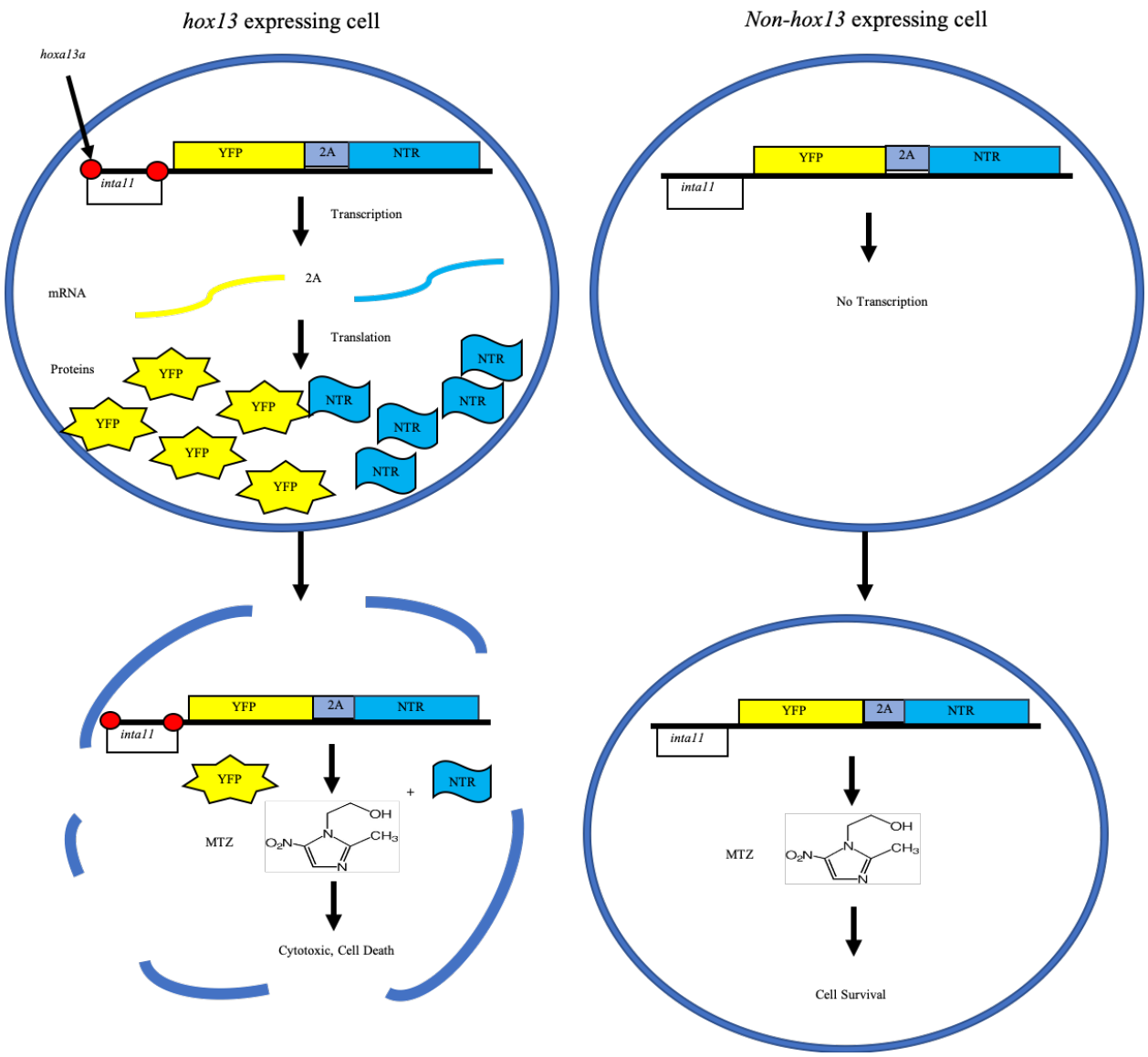

Figure 17. Schematic illustration of the MTZ/NTR mechanism under the m-*inta11* enhancer with a 2A self-cleaving peptide.

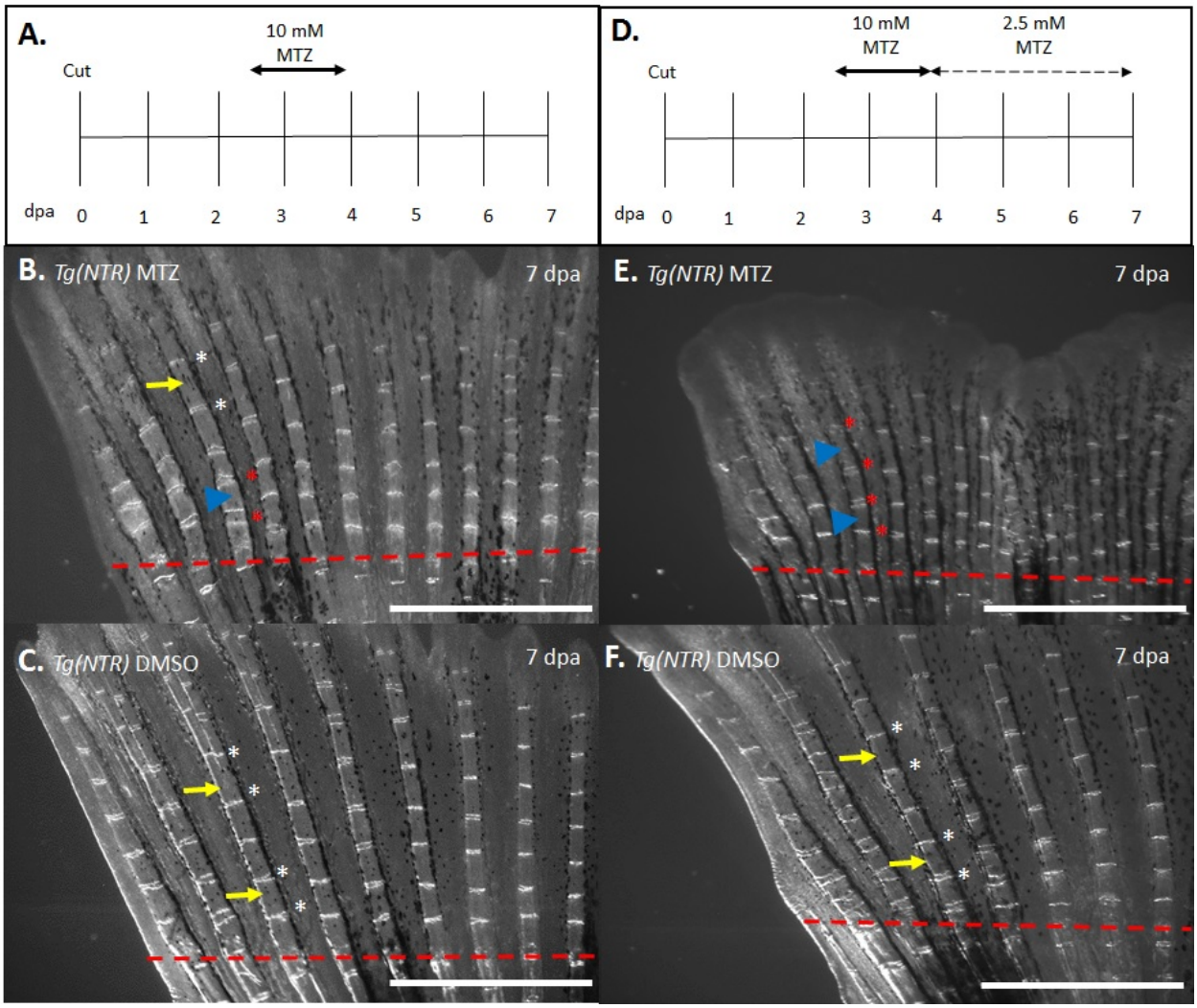

Figure 18. Metronidazole treatments results in joint development disruption. A) MTZ treatments at the 2.5dpa time point. B) A disruption of the joints that formed during 30 hours spent in MTZ (red asterisk) and shortened bone segments (blue arrow). After the MTZ treatment was over subsequent bone segments (yellow arrow) and joints (white asterisk) returned to normal. C) Compared to the DMSO controls bone segments (yellow arrow) and joints (white asterisk). D) Protocol was adjusted, after the initial 30 hours of 10 mM MTZ treatment fish were placed in 2.5mM MTZ for the remainder of the experiment. E) A continuation of the phenotype observed in the 30 hour 10mM MTZ with shortened bone segments (blue arrows) and disrupted joint formation (red asterisks) F) Compared to the bone segments (yellow arrow) and joints (white asterisks) of the controls. Scale bars are 1mm. Derek Sheppard, unpublished.

1.13 Hypotheses and Objectives

The *hoxa13a, hoxa13b,* and *hoxd13a* (*hox13)* genes have an incontrovertible role in the development and patterning of zebrafish fins. Previous studies in our lab showed that the partial ablation of *hox13*-expressing cells results in shorter hemiray segments. Furthermore, studies done by Nakamura et al., (2016) creating triple mosaic frameshift mutants of *hoxa13a, hoxa13b,* and *hoxd13a* show a phenotypic truncation of the pectoral fin after formation of the first joint. However, the extent to which *hox13* genes are involved in the growth and patterning of fin rays is unknown. This leads to my hypothesis: zebrafish *hox13* genes are involved in joint formation and patterning during development and regeneration. My two specific objectives within this thesis are listed below.

Objective 1: Test the efficiency of MTZ and our transgenic line for the ablation of *hox13* -expressing cells. The incomplete analysis using the transgenic line *Tg(m-inta11-ß-globin:yfp-2A-NTR)* in our lab has led to question the efficiency of both the MTZ prodrug as well as our transgenic line. To further explore this method, a cell death assay must be completed to determine if cell death is significant in the treated transgenic fish in comparison to WT. Moreover, additional prodrugs such as NFP should be tested to determine if a more significant phenotype can be observed in the transgenic treated fish. This objective will also explore the presence of molecular markers such as *hoxa13a,* and *sp7* in the treated transgenic fish.

Objective 2: Observe the effects of 5' *hox13* gene deletion mutations on zebrafish lepidotrichia growth and patterning. Characterisation of the phenotypes of our triple *hox13* knockout mutants in all fins are yet to be completed and is required. Furthermore, these mutants can be used to elucidate molecular mechanisms of joint formation during regeneration. This will be explored through the examination of bone and joint markers such as Zns5 and *evx1,*

respectively. Finally, these mutants will also be used to examine the function of *hox13* genes in the regulation of *and1/2* genes and subsequently the formation of actinotrichia.

Chapter 2: Material and Methods.

2.1 Zebrafish Husbandry

Zebrafish were raised and maintained in the University of Ottawa Aquatic Facilities. The zebrafish were housed in a constant temperature of 28.5˚C and following a 14 hours light / 10 hours dark cycle. The system water used in the tanks was UV sterilized and at a constant flow (Canadian Council on Animal Care, 2005). Fish were fed regularly according to Westerfield, (2007). The transgenic line *Tg(m-inta11:eGFP)* was previously described (Kherdjemil et al., 2016), and expresses eGFP under the control of *m-inta11*. The transgenic line *Tg(m-inta11-ß-globin:yfp-2A-NTR)* was previously described (Lalonde & Akimenko, 2018) (see introduction section 1.11 for a more detailed description). Zebrafish care and experiments were all certified by the Canadian Council on Animal Care and licensed under the Ontario Animals for Research Act. Tricaine was used for animal anesthesia and euthanasia. Wild type fish stock was originally obtained from a pet store and maintained through successive breeding for several years in our facilities to create a robust colony.

For breeding, false bottom traps were used (Westerfield, 2007). The male and female fish were fed more frequently the week prior to being placed in the breeding traps. The night before the fish were expected to breed, the male and female were separated by a plastic partition in the breeding trap. Immediately following the lights, the next morning, the water was replaced with clean water and the plastic partition was removed. A few hours later, embryos were collected and kept in embryo (E3) medium (5mM NaCl, 0.33mM $CaCl_2$, 0.33mM $MgSO_4$, 0.17mM KCl, 6-12 µM methylene blue). At 24 hpf, the embryos were sterilized using a low concentration of bleach (0.0003% NaOCL) for 10 minutes. Following exposure to bleach, embryos were placed in a neutralizing solution (0.05% $Na_2S_2O_3$) (Sigma-Aldrich) for one minute. Two subsequent washes

were done in E3 medium for five minutes to ensure neutralization. Embryos were then placed into clean petri dishes with fresh E3 medium and either used in the following days for experimentation or placed into the system at 5 dpf to be raised to adulthood.

2.2 Generation of Triple *hox13/hox* Homozygous Mutants

Zebrafish mutants for each gene (*hoxa13a, hoxa13b, hoxd13a,* and *hoxd* cluster) were identified. These primary fish were then crossed with WT fish to eliminate potential off-target effects. Three lines of each mutation were created and used to create triple homozygous mutants (see results section 3.2) The double *hoxa13a* and *hoxa13b* mutants were bred with the *hoxd* cluster deletion mutants to create an additional triple *hox* mutant (see section 3.5). Unfortunately, the triple *hox13/hox* mutants were unable to breed due to their truncated pectoral fin. Male zebrafish use their pectoral fin where breeding tubercles are located to coerce female fish to release their eggs. The pectoral truncation found in the triple homozygous *hox13/hox* mutants did not allow for proper stimulation of the female to release her eggs regardless of the fact they still possessed breeding tubercles. Therefore, to maintain a stable stock of triple homozygous mutants, double and single homozygous mutants were bred to maintain the population even though the triple homozygous fish were determined viable after examining the sperm of the males and eggs of the females.

2.3 DNA Extraction and Genotyping

DNA Extraction:

DNA was extracted from fin clip samples. Fish were anesthetized and a small piece of the caudal fin is clipped using a scalpel blade and placed in 50μL of 50mM NaOH. The samples were then placed at 95°C for five minutes, vortexed and then placed back at 95°C for an additional five

minutes. The samples were then cooled on ice for five minutes and then 5µL of 1M Tris HCl pH 8.0 is mixed into the sample.

Genotyping via Polymerase Chain Reaction (PCR):

The PCR reaction was made in a PCR tube: 0.2mM of sample DNA, 0.2µM of the forward primer, 0.2µM of the reverse primer, 2X GoTaq® Green Master Mix (Promega M7122), dd H_2O added to 25µL. The primers can be found in the table below. The samples were then run in a PCR program; initiation at 95°C for four minutes, denaturation at 95°C for one minute, annealing at 58°C for one minute, elongation 72°C for two minutes (denaturation, annealing, and elongation repeated 30 times) and a final extension period at 72°C for eight minutes.

Electrophoresis:

Following the PCR program, 10µL of PCR product was loaded on a 1.5% agarose gel and ran at 120 volts for approximately 20 minutes. For each gene, a forward (F) and reverse (R) primer outside the deletion were designed. If a small band was observed, the allele carries a deletion of the gene, the absence of a band indicates a wild type allele, since the WT allele is too large to be amplified under the PCR conditions. In addition, a third primer (F or R) was located inside the deletion and paired with one of the primers outside the deletion. If a band was present when these two primers were used the allele was wild type, absence of a band indicates a mutant allele.

Primer Name	Primer Sequence	Expected Band Size (when paired with F)
hoxa13a F	5'AGGCGAAGATTATACCAGCTCAC3'	
hoxa13a R2	5'CATCAAACAACTCATCCTTTGG3'	Paired with *hoxa13a* F: WT band = 890 bp, Deletion band = 420bp
hoxa13a R1 (inside)	5'CCTGTCGTTCAGATAGGTTGG3'	Paired with *hoxa13a* F: WT band = 557 bp, Deletion band = no band
hoxa13b F	5'CCACCACTTTGTTTCAGTTCAA3'	
hoxa13b R2	5'TGATGCCCTTGTACTTGTTGAC3'	Paired with *hoxa13b* F: WT band = 1483 bp, Deletion band = 693bp
hoxa13b R1 (inside)	5'ATATCCATAGGGCAAAGAAGCA3'	Paired with *hoxa13b* F: WT band = 513 bp, Deletion band = no band
hoxd13a F (F1)	5'TTTACCCATCTGCCTTCGGG3'	
hoxd13a R2	5'AGACCTCTTGCAGTCAAGGT3'	Paired with *hoxd13a* F: WT band = no band, Deletion band = 484bp
hoxd13a R1 (inside)	5'CTGCTGCAATTGTTTGACCAGT3'	Paired with *hoxd13a* F: WT band = 362 bp, Deletion band = no band
hoxd3a F2 (inside)	5'ATCCAGAGCCATTTTTGTAGCC3'	Paired with *hoxd3a* R: WT band = 512 bp, Deletion band = no band
hoxd3a R	5'CAAAAACTCGTCGCTTTCAGTC3'	Paired with *hoxd13a* F: WT band = no band, Deletion band = 289 bp

Table 1. Primer sequences used for genotyping *hox* mutants.

2.4 Fin Amputation

Prior to amputation fish were anesthetized using 0.17mg/mL tricaine diluted in clean system water (Westerfield, 2007). The fish was then placed on a petri dish with the desired fin fanned out. The caudal fin was amputated two segments proximal to the bifurcation plane (where the most proximal fin rays bifurcate into sister rays); known as the standard cut. Similarly, the ventral fin was amputated two segments proximal to the first bifurcation plane. Amputation was completed with a scalpel blade under a dissection microscope. The location where the fin is cut is

then named the amputation plane during regeneration. Following amputation, the fish were returned to their tanks and kept under the standard conditions mentioned above.

2.5 Cryosectioning

Following fin amputation, the regenerate was standardly grown for four days. After four days the fin regenerate was amputated once again, taking approximately one segment of the stump (area proximal to the amputation plane) with it. The fin regenerate was then laid flat in a 6-well plate containing 4% paraformaldehyde (PFA) and kept at 4°C overnight. The following day, the fin was washed in PBS (137 mM NaCl, 4.3 mM Na_2HPO_4, 2.7 mM KCl, 1.47 mM KH_2PO_4, adjusted to a final pH of 7.4) twice for five minutes. If fins were to be used immediately, they were placed in a solution of 30% sucrose in PBS and kept at 4°C overnight. If the fins were to be used for future experiments, dehydration was begun. The fins were taken from the PBS wash and placed in two washes of 100% methanol and then stored in -20°C. Once ready to be used, the fins were rehydrated in three, five-minute PBS washes and then soaked in a 30% sucrose solution as previously described. After retrieving the fins from the sucrose solution, they were placed in small square plastic molds aligning the fin ray to the edge of the mold. A solution containing 1:3 v/v 30% sucrose and Shandon™ Cryomatrix™ embedding resin (ThermoFisher Scientific) was then poured over top of the fin until the mold was full. Once in place, the mold containing the fin was submerged in isopentane that was stored at -80°C for 30 seconds or until completely frozen. The block was then either stored at -80°C or removed from the mold and placed on a chuck with additional Shandon™ Cryomatrix™ embedding resin and placed in the cryostat (Leica CM3050 S) at -20°C to be sectioned. The tissue was then sectioned at 16-18 μm and transferred to Fisherbrand™ Superfrost™ Plus microscope slides and left for 30 minutes at room temperature (RT) before being stored at -20°C for future use.

2.6 Metronidazole/Nifurpirinol Treatments

Metronidazole (MTZ)/Nifurpirinol (NFP) treatments were performed after amputation of the caudal fin of adult zebrafish approximately 8 months of age. The prodrug concentration for ablation was selected according to a survival curve. The MTZ concentrations of 10, 12, and 15 mM were tested as well as the durations of treatment 24, 30, and 36 hours. The treatment that was observed to be most effective with the lowest level of toxicity was a concentration of 10mM for a duration of 30 hours. Similarly, concentration trials of NFP were performed using different concentrations of 2.5, 5, and 7.5 µM. However, the time frame of 30 hours remained constant. It was determined that 5µm was the most effective concentration that also had the lowest toxicity. The fish were treated with a concentration of 10mM MTZ or 5µM NFP in clean system water with 1% dimethyl sulfoxide (DMSO) to aid in solubilization and increase penetrance of MTZ/NFP (Curado et al., 2008). The treatment began at 2.5 dpa and continued for 30 hours. The fish were kept in the dark during the treatment to avoid degradation of the MTZ/NFP, which will degrade in light, and the temperature remained constant at 28.5°C. After 30 hours, the MTZ-treated fish were placed in clean water and allowed to continue regeneration until 4dpa (additional 18 hours). After 30 hours, the NFP-treated fish were placed in clean water and allowed to continue regeneration until 4 dpa (additional 18 hours). At 4 dpa, the fin regenerate of treated fish was then collected and processed for further experimentation.

2.7 Probe Synthesis

Digoxigenin-labelled (DIG) antisense RNA and 2,4-dinitrophenyl (DNP) antisense RNA probes were made from cDNA plasmid templates listed in Table 2. The first step was linearization of 10µg of plasmid DNA with the corresponding enzyme at 37°C for two hours. The linearized plasmid was then purified using a GE Healthcare IllustraTM purification kit (VWR

CAT#CA95026-728L). A reaction mix was then created containing: 1µL linearized template DNA, 2µL DIG-labelling mix(10x concentrated dNTP labeling mixture: 1mM dATP, 1mM dCTP, 1mM dGTP, 0.65mM dTTP, 0.35mM DIG-dUTP, alkali-labile, pH 7.5) for DIG probes or 1µL nucleoside triphosphate (NTP) and 1µL dinitrophenol (DNP) labeled analog of uridine triphosphate (UTP) for DNP probes, 2µL 10x transcription buffer, 0.5µL RNAse inhibitor (40units/µL), 2µL RNA polymerase (T7, T3, or SP6), 12.5µL dd H_2O and incubated at 37°C for two hours. The reaction mix was then purified by precipitating with 2.5µL 4M LiCl and 75µL 100% cold ethanol at -80°C for 30 minutes. The solution was then spun at top speed (16000 rpm) in a 4°C centrifuge for 15-minutes. A second rinse was done with DEPC 70% ethanol before drying and resuspension in 25µL RNAse-free water. After resuspension, 1µL was loaded on a gel and the rest was mixed with 1µL EDTA (0.5M stock) and 9µL RNALater (Sigma R-0901) and stored at -80°C until use.

Probe Name	**Plasmid Vector**	**Restriction Enzyme**	**RNA Polymerase**
hoxa13a	pGEM-T	SmaI/XmaI	SP6
hoxa13b	pGEM-T	XhoI	SP6
hoxd13a	pDrive	HindIII	T7
evx1	pCS2+	BamHI	T3
pthlha	pDrive	XhoI	T7
sp7	pCRII-TOPO	HindIII	T7
runx2a	pDrive	XhoI	T7
and1	pBK-CMV	SalI	T7

Table 2. Antisense RNA probes used in double FISH experiments.

2.8 Double Fluorescence *in situ* hybridization (FISH) on Cryosections

Longitudinal cryosections of 4dpa regenerates were created using the aforementioned protocols and stored at -20°C until required. The protocol for double FISH on cryosections had been adapted from previous protocols described in Welten et al., 2006, Perkin-Elmer Manufacturers protocols of TSA Cyanine 3 and Fluorescein system (Perkin Elmer Cat# NEL753001KT), and TSA Cyanine 5 system (Perkin Elmer Cat# NEL745001KT).

Day 1: Hybridization. Slides containing the cryosections were defrosted at 60°C for one hour. All washes were performed in a coplin jar that holds approximately 40 mL of liquid. The tissue was then permeabilized beginning with a 15-minute rinse in 0.3% Triton-X 100 in DEPC-PBS (137 mM NaCl, 4.3 mM Na_2HPO_4, 2.7 mM KCl, 1.47 mM KH_2PO_4, adjusted to a final pH of 7.4) to remove lipids. Two five-minute washes in DEPC-PBS followed to remove Triton-X 100 residue. A proteinase K treatment was used to remove proteins blocking RNA hybridization as well as help digest the cell structure. Proteinase K solution was created making a final concentration of 5µg/mL (20µL stock Proteinase K [10mg/mL], 4mL 1MTris HCL pH 8.0, 4mL 0.5M EDTA, 32.80mL DEPC H_2O) and added to the coplin jar for an incubation of 15-minutes at room temperature; two five-minute rinses in DEPC-PBS followed. Next, a 20-minute fixation was done in 4% PFA and two five-minute rinses in DEPC-PBS followed. Acetylation was the final step before hybridization; the slides were incubated for five-minutes in acetylation mix (500µL triethanolamine, 108 µL acetic anhydride, 40mL DEPC H_2O) followed by two five-minute rinses in DEPC H_2O and finally laid out to dry. Once dry, slides were placed in a humidifying chamber with old solution A (1x SSC, 50% formamide, 0.1% tween 20, made up to 100mL with double distilled [dd] H_2O). The desired probes were diluted in hybridization buffer (1x salt [10x stock; 57g NaCl, 7.02g Tris HCl, 0.67g Tris base, 3.9g $NaH_2PO_4.H_2O$, 3.55g Na_2HPO_4, 50mL 0.5M

EDTA added dd H_2O to 500mL, adjust to pH 7.5 and autoclave], 50% deionized formamide, 10% dextran sulphate [50% stock], 1mg/mL yeast tRNA [stock 10mg/mL], 1x dd H_2O). The probe mix was then denatured at 70°C for 5-10 minutes before adding 300-500 µL to each slide. The slides were then covered with a cover slip, the humidifying chamber sealed and placed at 70°C overnight.

Day 2: DNP Antibody. The following day the coverslips were removed, and the slides placed back in coplin jars, the slides were rinsed twice for 30 minutes with solution A at 70°C. Two additional rinses were done for 30 minutes at RT in 1x TBST (made from 10x stock; 1.4 M NaCl, 27mM KCl, 0.25 M Tris HCl, 1% Tween 20, in dd H_2O made to a volume of 500mL and pH of 7.5, autoclaved). The next step was to inhibit endogenous Horseradish Peroxidase. The slides were incubated for 10-minutes in 2% H_2O_2 in TNT (0.1 M Tris-Hcl pH 7.5, 0.15 M NaCl, 0.5% Tween 20) followed by four five-minute rinses in TNT. The last step before the first antibody was applied was blocking; completed inside the humidifying chamber with H_2O instead of solution A. The tissue was blocked for 2-4 hours at RT with 300 µL of TBSTB (TNT with 0.5% Perkin-Elmer blocking powder) per slide and covered with coverslips. After incubation the coverslips were removed and 100µL anti-DNP-POD (1:500) in TBSTB was added onto each slide and incubated overnight at 4°C.

Day3: Tyr-Cy3 Stain and DIG Antibody. To remove antibody a sequence of TNT washes was performed, 2x5 minutes, 2x10 minutes, 20 minutes, and finally 30 minutes. The slides were then stained under coverslips for 10 minutes in 100µL Amplification diluent with 1:100 Tyr-Cy3 and rinsed with TNT three times for five-minutes. A second inhibition of Horseradish Peroxidase was done for 30 minutes in 2% H_2O_2 in TNT followed by four five-minute rinses in TNT. An additional blocking was done in the humidifying chamber with 300µL TBSTB per slide for 2-4

hours. Incubation with the second antibody was done in the same humidifying chamber. Each slide was incubated in 100µL of anti-DIG-POD diluted 1:500 in TBSTB overnight at 4°C.

Day 4: Tyr-fluorescein and DAPI Staining. To remove antibody a sequence of TNT washes was performed, 2x5 minutes, 2x10 minutes, 20 minutes, and finally 30 minutes. The slides were then stained under coverslips for 10 minutes in 100µL Amplification diluent with 1:100 Tyr-fluorescein and rinsed with TNT three times for five-minutes. A DAPI stain was then performed, to label cell nuclei, by diluting stock DAPI (5mg/mL) 1:10000 with TNT and incubated for five minutes followed by two five-minute rinses in TNT and finally left in fresh TNT overnight at 4°C.

Day 5: Mounting. Slides were rinsed twice in water to remove salt residue and allow to dry. Coverslips were then mounted using Aqua-Poly/Mount. Cryosections were imaged with Olympus FLUOVIEW FV1000 confocal laser scanning microscope with accompanying FV1000 Viewer software version 4.2b.

2.9 Fluorescent Immunohistochemistry on Cryosections

The immunohistochemistry protocol on longitudinal cryosections was adapted from protocols previously described in Smith et al., 2006. Longitudinal cryosections of 4DPA regenerates were thawed at RT for two hours and then rehydrated in 1x PBS for 30 minutes. The slides were then blocked in blocking solution (0.2% Triton X-100 and 2% Calf Serum in 1x PBS) for two hours at RT. After blocking slides were incubated in the primary antibody. The primary antibody anti-Collagen II protein (Developmental Studies Hybridoma Bank II-II6B3) was diluted to a suitable concentration (1:10) in blocking solution and 200µL was applied to each slide and incubated at RT for three hours or overnight 4°C in a humidifying chamber. The slides were rinsed four times with PBST (1x PBS with 0.1% Tween-20) at RT for 10 minutes. Fluorescently labelled

secondary antibody Alexa Fluor 488 goat and anti-rabbit IgG (Invitrogen, A11001) were used at a concentration of 1:500. Each slide had 200µL of secondary antibody applied and was incubated overnight at 4°C. The slides were then counterstained with DAPI by diluting stock DAPI (5mg/mL) 1:10000 with PBST and rinsed for five-minutes at RT. Three additional five-minute washes with PBST were required to remove excess stain. The slides were then rinsed twice in water to remove salt residue and allow to dry. Coverslips were mounted using Aqua-Poly/Mount. Cryosections were imaged with Olympus FLUOVIEW FV1000 confocal laser scanning microscope with accompanying FV1000 Viewer software version 4.2b.

2.10 TUNEL Assay on Cryosections

TUNEL assay protocol on longitudinal cryosections of 4dpa regenerates was adapted from Millipore Sigma; *In Situ* Cell Death Detection Kit, TMR red (Roche Cat#12156792910). The slides were defrosted at RT for a minimum of one hour before proceeding to permeabilization. To begin, a 15-minute rinse in 0.3% Triton-X 100 in 1xPBS was performed followed by two five-minute rinses in 1xPBS. Permeabilization was achieved with a 15-minute incubation in proteinase K (20µL stock Proteinase K [10mg/mL], 4mL 1MTris HCL pH 8.0, 4mL 0.5M EDTA, 32.80mL DEPC H_2O) followed by two five-minute washes in 1xPBS. Fixation with 4% PFA in 1xPBS for 20-minutes ensures tissue remains on the slide and was followed by two five-minute rinses in 1xPBS. A positive control was prepared by incubating one slide in; 1µL DNase I, 30µL 10x buffer, 269µL H_2O, for 10-minutes followed by two five-minute rinses in 1xPBS. Each slide was incubated in 50µL of TUNEL reaction mix (5µL enzyme solution, 45µL label solution) for 60-minutes at 37°C in the dark. A negative control was prepared by adding 50µL label solution to one slide only. The slides were then counterstained with DAPI by diluting stock DAPI (5mg/mL) 1:10000 with PBST and rinsed for five-minutes at RT. Three additional five-minute washes with

PBST were required to remove excess stain. The slides were then rinsed twice in water to remove salt residue and allow to dry. Coverslips were mounted using Aqua-Poly/Mount. Cryosections were imaged with Olympus FLUOVIEW FV1000 confocal laser scanning microscope with accompanying FV1000 Viewer software version 4.2b. Measurements were taken from the amputation plane to the distal tip for regenerate length. For segment length, measurements were taken from the center point of one joint cell cluster to the center point of the next.

2.11 Triton-X Treatment for Actinotrichia Visualization

When amputating the fin for regeneration studies the clipped portion was kept for better visualization of the actinotrichia. The goal was to clear the distal tissue of the fin. A previous student in our lab, Enzo Moretti, had tried different methods (Trypsin, Triton-X 100, and SDS) for clearing the tissue. Triton-X 100 was found to be the mildest keeping the actinotrichia intact while also digesting the tissue around them. The fin clipping was laid flat in a 6-well plate containing a concentration of 2x Triton-X 100 diluted with 1x PBS at RT overnight. Two additional rinses in 1xPBS were completed and the fin is stored in 100% glycerol until imaging. Images were taken using Lumenera Infinity 3-1UC camera mounted on a Leica MZ FLIII microscope, with Infinity Capture version 6.4.0 software.

2.12 Imaging

Fluorescent images were taken using Olympus FLUOVIEW FV1000 confocal laser scanning microscope with accompanying FV1000 Viewer software version 4.2b. Brightfield images were taken using Lumenera Infinity 3-1UC camera mounted on a Leica MZ FLIII microscope, with Infinity Capture version 6.4.0 software.

2.13 Generation of Statistics

GraphPad Prism 8.1.1 was used to conduct statistical tests and to generate graphs. Normality of all groups was tested using Shapiro-Wilks test for normality. In addition, the Q-Q plot was examined to visualize if the data followed a normal distribution. When comparing two groups, Unpaired two-tailed t-test (with Welch's correction) was performed. Mann Whitney was used when comparing two groups of a non-normal distribution (figure 25B, 35B). When comparing three groups (figure 19D, 20D) ANOVA was used with Dunnet's and Tukey's multiple comparison respectively. Mean ± SEM was presented. Adjusted p-values were reported, and significance was set at $p < 0.05$.

Chapter 3: Results

3.1 Partial ablation of *hox13* cell populations controlled by *m-inta11* cause a decrease in bone segment length during fin regeneration

Derek Sheppard, a former MSc student in the lab, used the nitroreductase (NTR) / metronidazole (MTZ) system to ablate the *hoxa13a*-expressing cells in the transgenic line *Tg(m-inta11-ß-globin:yfp-2A-NTR)*. As a reminder, this enhancer is regulated by *Hoxa13* and *Hoxd13*, and therefore, drives the transgene expression in *hoxa13*-expressing cells, including in the joint cells at all differentiation stages and blastema cells of the fin regenerate. Although a decrease in bone segment length was observed, this experiment did not lead to an absence of joint cells and YFP expression persisted suggesting partial cell ablation or a non –specific effect of the MTZ. To verify that the MTZ treatment induces apoptosis of *hoxa13a*-expressing cells, a similar experiment was repeated and a TUNEL assay was performed immediately after the end of the treatment at 4dpa. Three groups of two adult fish (8 months-1 year) were used: control transgenic fish that are not exposed to the drug but exposed to DMSO, the added solvent, control wild type fish that are exposed to the drug, and the experimental group of transgenic fish (called treatment-transgenic) that are exposed to the drug. The fish were exposed to 10mM of MTZ for 30 hours starting at 2.5 dpa, before the formation of the first presumptive joint cell cluster. Following 30 hours of treatment the fish were transferred to clean water until 4dpa. The TUNEL assay was performed on 4dpa regenerate longitudinal cryosections. This experiment was repeated three times to gain statistical significance.

The majority of cell death observed in the transgenic treatment group was found in the most proximal joint-forming cell clusters with little to no cell death in the more distal presumptive and joint-forming cell clusters (shown in enlargements of figure 19C). In addition, sporadic cell

death was observed in the blastema cell populations (outlined in a dashed yellow circle, figure 19C). Cell death in the superficial layers of the epidermis of the regenerate was also observed but may correspond to the natural shedding of epithelial cells as the fin grows. Although minimal cell death in *m-inta11* cell populations was observed, the regenerate length was significantly reduced in the transgenic fish treated with MTZ compared to controls as shown by a one -way ANOVA with Dunnett's multiple comparison (figure 19D). Additionally, an increased number of joints along the treated transgenic 4dpa regenerate was observed (figure 20C). A significant decrease in segment length was observed in the treated transgenic 4dpa regenerates determined by a one-way ANOVA with Tukey-Kramer multiple comparison (figure 20D). As expected from the morphological observations, double fluorescence *in situ* hybridisation (FISH) revealed that *hoxa13a* and *sp7* were still expressed in the joint cells and osteoblasts, respectively (figure 20). Additional *in situ* hybridization experiments performed to probe for joint marker expression of *evx1,* and *pthlha* revealed no absence in expression (data not shown).

In an attempt to increase cell death a different compound, Nifurpirinol (NFP), was used to treat the transgenic fish *Tg(m-inta11-ß-globin:yfp-2A-NTR).* Bergemann et al., (2018) showed that the prodrug Nifurpirinol (NFP) is a more potent and reliable substrate for cell ablation than MTZ. The experiment was repeated in the same fashion as for MTZ but using 5µMNFP which was determined to be the most effective concentration with the lowest toxicity (see section 2.6). For this experiment, two groups of two fish were used, treatment WT and treatment transgenic. To observe the effectiveness of this prodrug another TUNEL assay was performed on 4dpa longitudinal cryosections. This experiment was repeated three times, however one fish in the treatment WT group did succumb during treatment. Following the TUNEL assay cell death was similar to that of the MTZ treatments, producing a pattern of incomplete cell death in the joint cell

clusters. However, the more distal presumptive joint cell clusters do have cell death unlike the MTZ treated fish, eluding to a potentially more effective treatment (Figure 21). An unpaired t-test with Welch's correction confirmed that the transgenic regenerate was significantly shorter than the WT fish. However, the length of the transgenic regenerate had a comparable length to MTZ treated transgenic fish. Following low success ablating all the *m-inta11* cell populations it was still noticed that there were significant changes in fin and segment length.

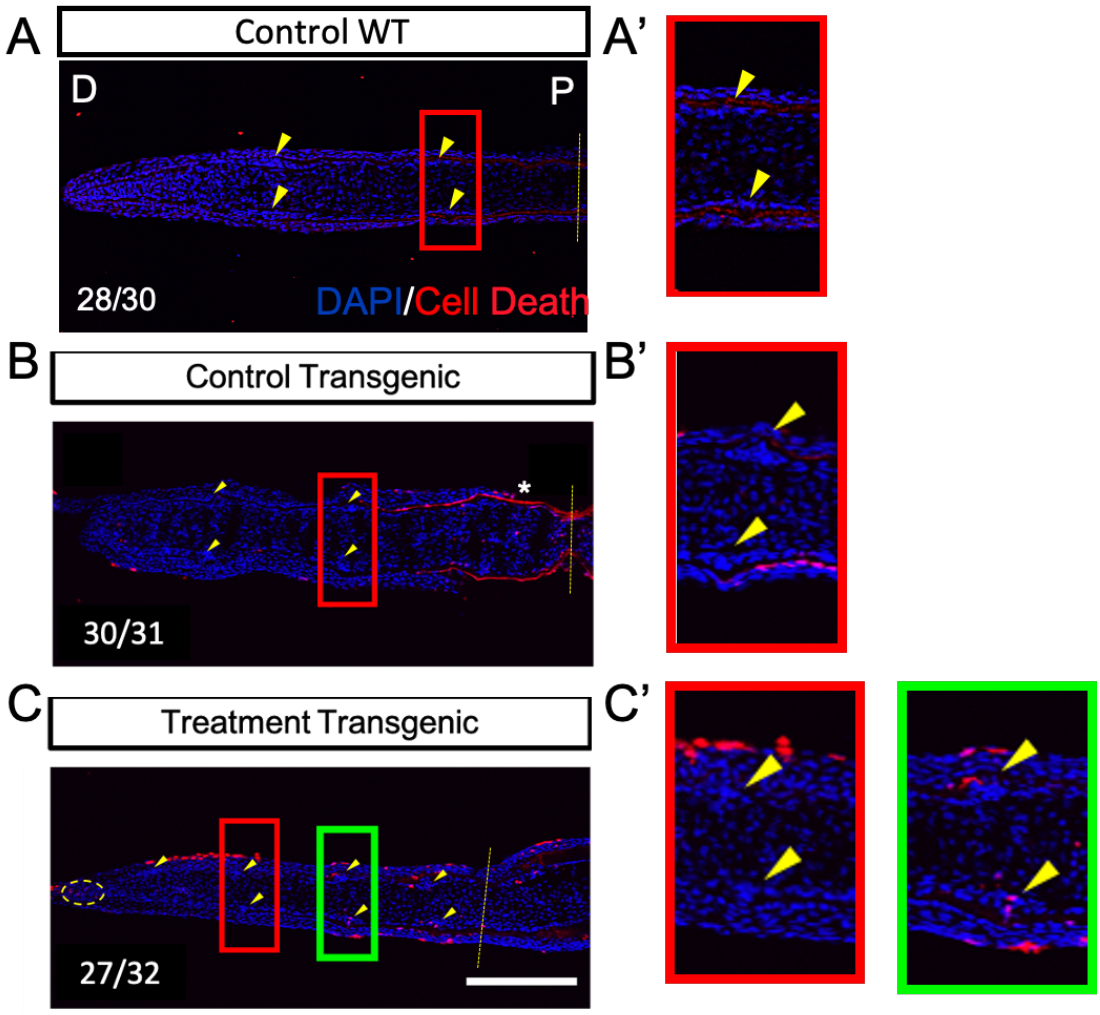
A
Control WT
D
P
28/30
DAPI/Cell Death
A'
B
Control Transgenic
30/31
B'
C
Treatment Transgenic
27/32
C'

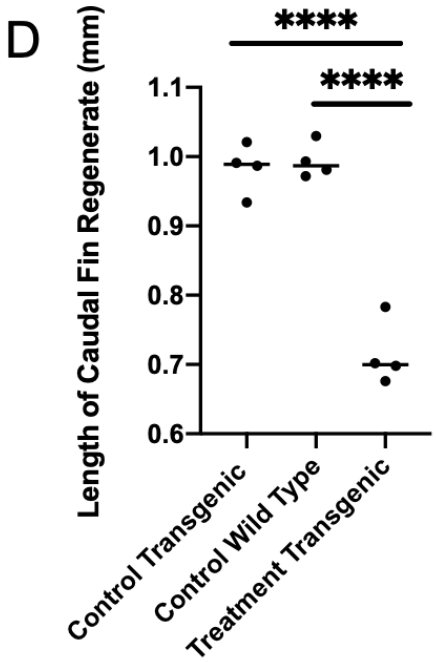
D
****
****
Length of Caudal Fin Regenerate (mm)
1.1
1.0
0.9
0.8
0.7
0.6
Control Transgenic
Control Wild Type
Treatment Transgenic

Figure 19. TUNEL assay shows increase in cell death (red) on 4dpa regenerate longitudinal cryosections of fish treated with MTZ; counterstained with DAPI. A) Control wild type samples, A') Enlargement of red box shown in A) shows no cell death (red) in the proximal joint-forming cell clusters B) Control (untreated) transgenic fish, B') enlargement of red box shown in B) shows no cell death in proximal joint-forming cell clusters (the asterisk indicates artefact red staining of bone matrix). C) MTZ treatment transgenic samples, C') Enlargement of red box in C) shows no cell death in distal presumptive joint cell clusters, enlargement of green box in C) shows sporadic cell death in proximal joint-forming cell clusters. Sporadic cell death is also observed in the blastema circled with yellow dashed line. White asterisk represents staining of epidermal tissue. D and P in panel (A) represent distal and proximal directions, respectively, of tissue sections in (A, B, C). Numbers in each panel represent the number of sections with similar phenotypes over total number of sections analyzed. Yellow arrows represent joint cell clusters. Yellow dotted line represents amputation plane. Scale bar in (C) for (A, B, C) = 200 μm. N = 6 fish per group. (D) Graph depicting the regenerate length of each group at 4dpa. One -way ANOVA with Dunnett's multiple comparison, significance (*) is set at $p<0.05$, (****) = p-value < 0.0001 adjusted p-values presented. N = 4 fish per group.

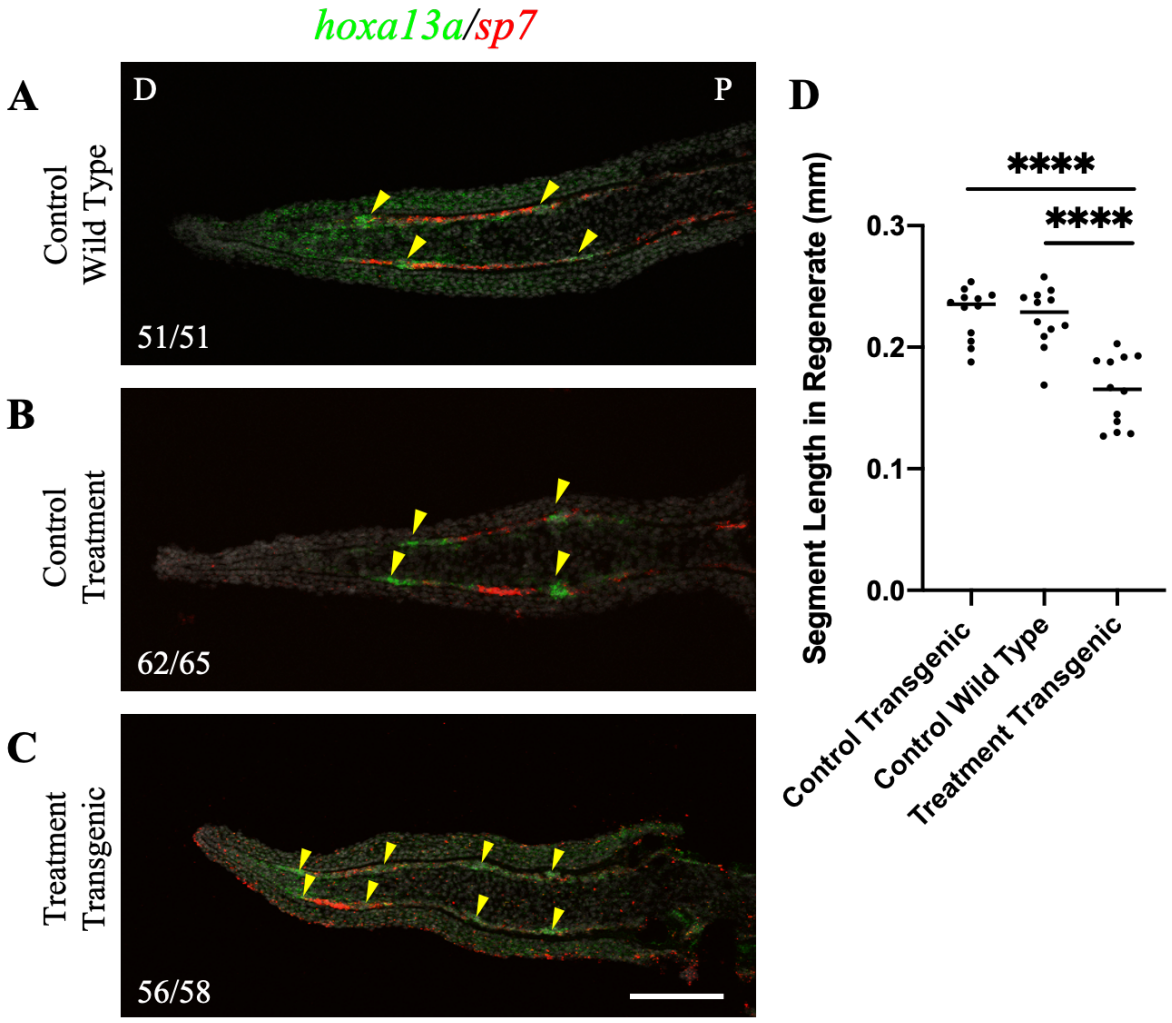

Figure 20. Expression of *hoxa13a* in 4dpa regenerate longitudinal cryosections of fish treated with MTZ via in situ hybridization. Green staining represents *hoxa13a* expression (joint) and red staining represents *sp7* expression (osteoblast) A) Transgenic fish without treatment; presumptive and joint-forming cell clusters are present. B) Wild type fish with treatment; two pairs of presumptive and joint-forming cell clusters are present. C) Transgenic fish with treatment; a set of presumptive joint cell clusters as well as three joint-forming clusters are present. White D and P in panel (A) represent distal (D) and proximal (P) directions of tissue sections in (A, B, C). White numbers in each panel represent the number of sections with similar phenotypes over total number of sections. Yellow arrows represent presumptive joint cell clusters. Scale bar in (C) for (A, B, C) = 100 µm. N = 6 fish per group. (D) Graph depicting reduction of segment length in the 4dpa regenerate of each group. One-way ANOVA with Tukey-Kramer multiple comparison, significance (*) is set at $p<0.05$, (****) = p-value < 0.0001 adjusted p-values presented. N = 4 fish per group.

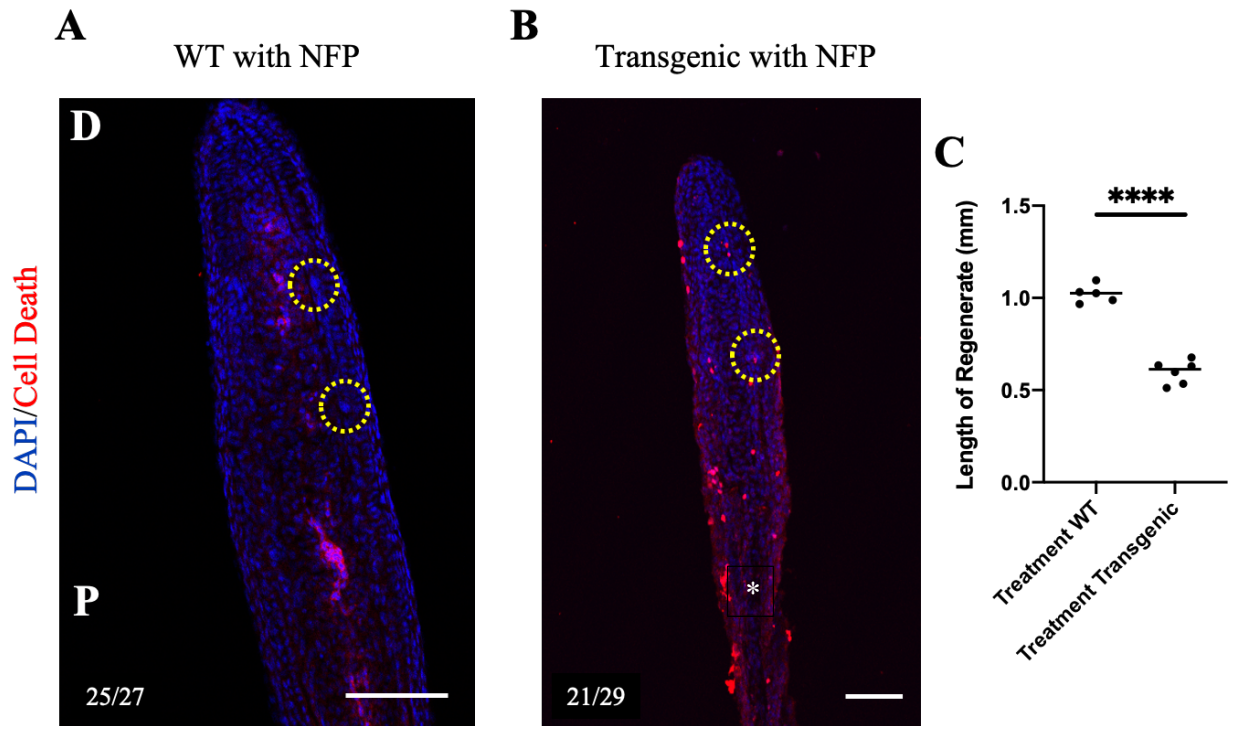

Figure 21. TUNEL assay showing cell death (red) on the 4dpa regenerate longitudinal cryosections of fish treated with NFP; counterstained with DAPI. A) Wild type fish treated with NFP no cell death is observed in presumptive and joint-forming cell clusters. B) Transgenic fish treated with NFP; cell death is observed in distal presumptive joint cell clusters as well as proximal joint-forming cell clusters. White asterisk represents staining of epidermal tissue. White D and P in panel (A) represent distal (D) and proximal (P) directions of tissue sections in (A, B, C). White numbers in each panel represent the number of sections with similar phenotypes over total number of sections. Yellow dashed circles represent presumptive joint cell clusters. Scale bar in (A) panel = 150 µm. Scale bar in (B) panel = 100 µm. WT fish N=5, Transgenic fish N=6. C) Graph depicting reduction of 4 dpa regenerate length of each group. Unpaired t-test with Welch's correction, significance (*) is set at $p<0.05$, (****) = p-value < 0.0001 adjusted p-values presented.

3.2 Triple *hoxa13a*$^{-/-}$, *hoxa13b*$^{-/-}$, *hoxd13a*$^{-/-}$ *(hox13)* mutants display defects in all fins and in regeneration of the fin

3.2.1 Analysis of the exoskeleton

The upregulation of *hox13* genes during joint formation and regeneration visualized with the *Tg(m-inta11:eGFP*) created an interest for further analyses of the role of the *hox13* genes in joint formation and regeneration. To examine the role of these *hox13* genes, single knockout mutants of *hoxa13a, hoxa13b,* and the *hoxd13a* were created via the CRISPR/Cas-9 technique.

The single homozygous *hox13* mutants were successively bred to create double and eventually triple *hoxa13a, hoxa13b,* and *hoxd13a* homozygous mutants. The adult fish were then genotyped to determine triple homozygosity and their phenotypes were examined. These triple *hox13*$^{-/-}$ mutants had a similar body size to their WT siblings. There were no noticeable defects in their morphology excluding the fins, however future studies should examine the structure and development of the vertebral column to ensure no skeletal defects. When first observing the pectoral fin, our phenotypic results were similar to those reported by Nakamura et al., (2016); the pectoral fin is severely truncated with no growth of the rays surpassing the first segment (Figure 22A). While Nakamura et al focused their analyses on the pectoral fins, we also catalogued all fins in the *hox13* triple knockout mutants, by taking brightfield images and measuring the length of the fins based on the length of the third fin ray from the most anterior ray. The second set of paired fins, the pelvic fins, were also severely truncated with no growth surpassing the first segment (Figure 22A). Both the pectoral and pelvic fins also had curling of the rays at the distal tips. The pectoral and pelvic fins were found to be significantly shorter in comparison to WT fish (figure 23A, B, respectively). When looking at the unpaired fins, the triple knockout mutants possessed significantly shorter dorsal and ventral fins compared to WT fish (figure 23C, D, respectively). In adult mutants, the dorsal and ventral fins also appeared to have a wavy phenotype in comparison to their normally straight trajectory (Figure 22B). Moreover, the rays of the dorsal and ventral fins both lacked joints as well as bifurcations. Significance in all fin comparisons was determined using an unpaired t-test with Welch's correction (Figure 23). The caudal fin was the least affected. Caudal fin measurements were taken on the third ray from each lateral edge and on the most central fin ray. The caudal fin of the triple *hox13* mutants was significantly shorter than the WT determined with an unpaired t-test with Welch's correction (Figure 25A). The fin of the triple

hox13 mutants was measured in three different locations (dorsal, medial, and ventral) to determine if the phenotype was consistent along the fin; significance values proved there was no significant difference in the proportions along the dorsal/ventral axis of the fin concluding that the fin maintained the same general shape as the WT caudal fin (figure 25A). In addition, the segment length was measured on each of the selected rays starting from the most proximal segment and extending to the tenth segment. The triple knockout mutants had irregular segment length shown by the spread of data in figure 26B in which the mean varied significantly in comparison to WT as well determined by a Mann-Whitney test (Figure 25B).

In order to determine the length of the regenerate, the fins were measured from the amputation plane to the distal edge in three locations along the dorsal-ventral axis and an average was subsequently taken. The number of joints each fin ray possessed was also counted and averaged between all rays present in the regenerate. The triple *hox13* knockout mutants were significantly delayed in regeneration at both four and seven dpa tested using an unpaired t-test with Welch's correction (Figure 25C). Moreover, significantly fewer joints were found in the regenerate of triple *hox13* mutants at four and seven dpa determined using an unpaired t-test with Welch's correction (Figure 25D).

After reviewing all the morphological analyses, the lack of joints in all the fins except for the caudal lead us to the conclusion that *hox13* genes are necessary for joint formation within the two paired and dorsal and ventral fins. Even though the caudal fin still possessed joints the segment length varied greatly, and regeneration was delayed drawing us to the conclusion; the *hox13* genes are involved in regulating segment length and consequently joint patterning.

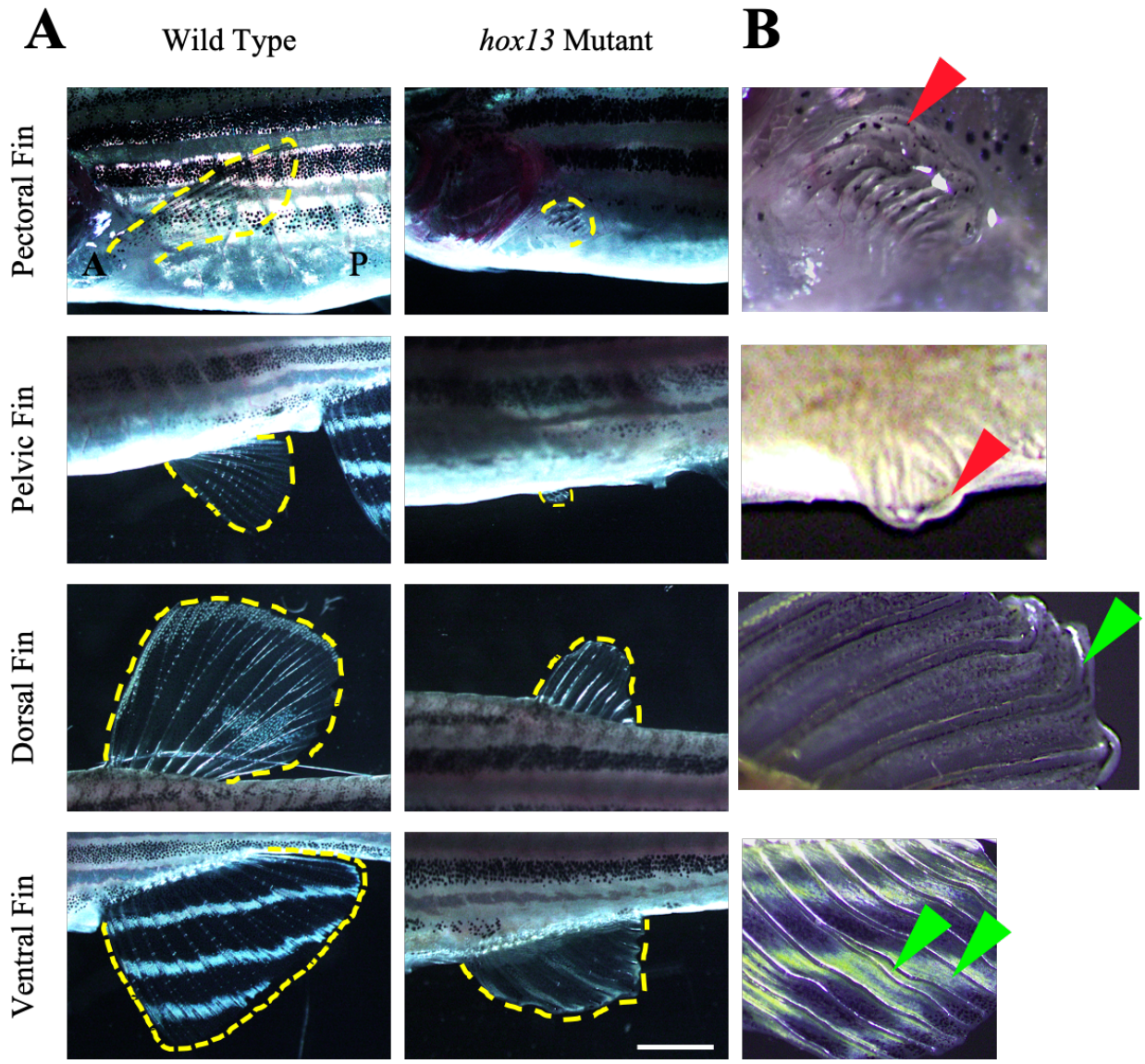

Figure 22. Triple *hox13* mutants have a pectoral, pelvic, ventral, and dorsal fin phenotype of reduced fin length and absence of joints. A) Visual comparison of WT versus *hox13* mutant pectoral, pelvic, dorsal, and ventral fins. A (anterior) and P (posterior) in first panel represent orientation of fish in all panels. Scale bar = 2mm in last panel for all images in A). B) Enlarged images of the triple *hox13* mutant fin phenotypes: curled (indicated with red arrows) and wavy (indicated with green arrows). N=8 fish per group.

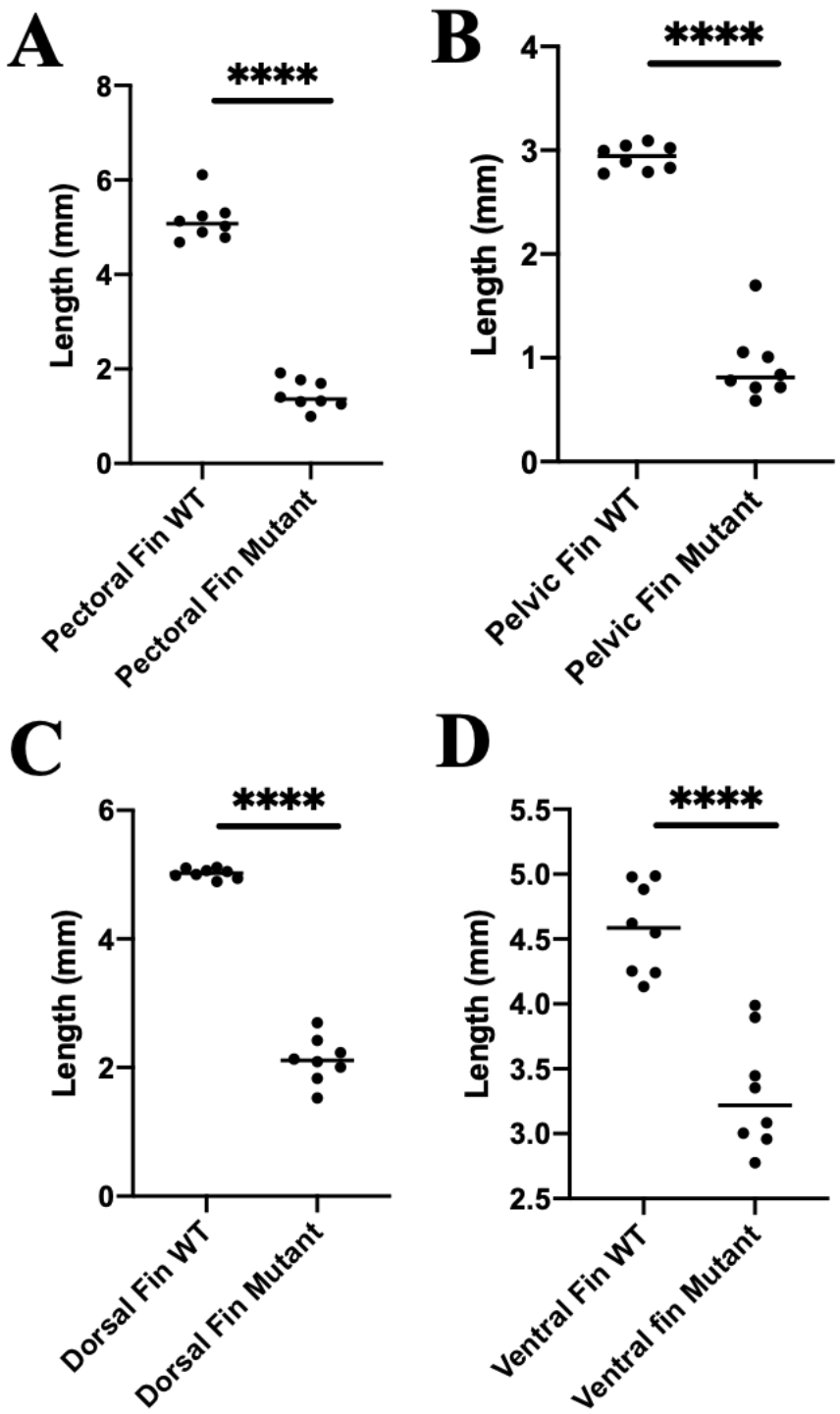

Figure 23. Measurements of the pectoral, pelvic, ventral, and dorsal fin of triple *hox13* knockout mutants show they are reduced in length. A) Length of pectoral fin in WT versus triple *hox13* mutant fish. B) Length of pelvic fin in WT versus triple *hox13* mutant fish. C) Length of dorsal fin in WT versus triple *hox13* mutant fish. D) Length of ventral fin in WT versus triple *hox13* mutant fish. For all graphs: unpaired t-test with Welch's correction, significance (*) set at $p<0.05$, (****) = p-value < 0.0001. N=8 fish per group.

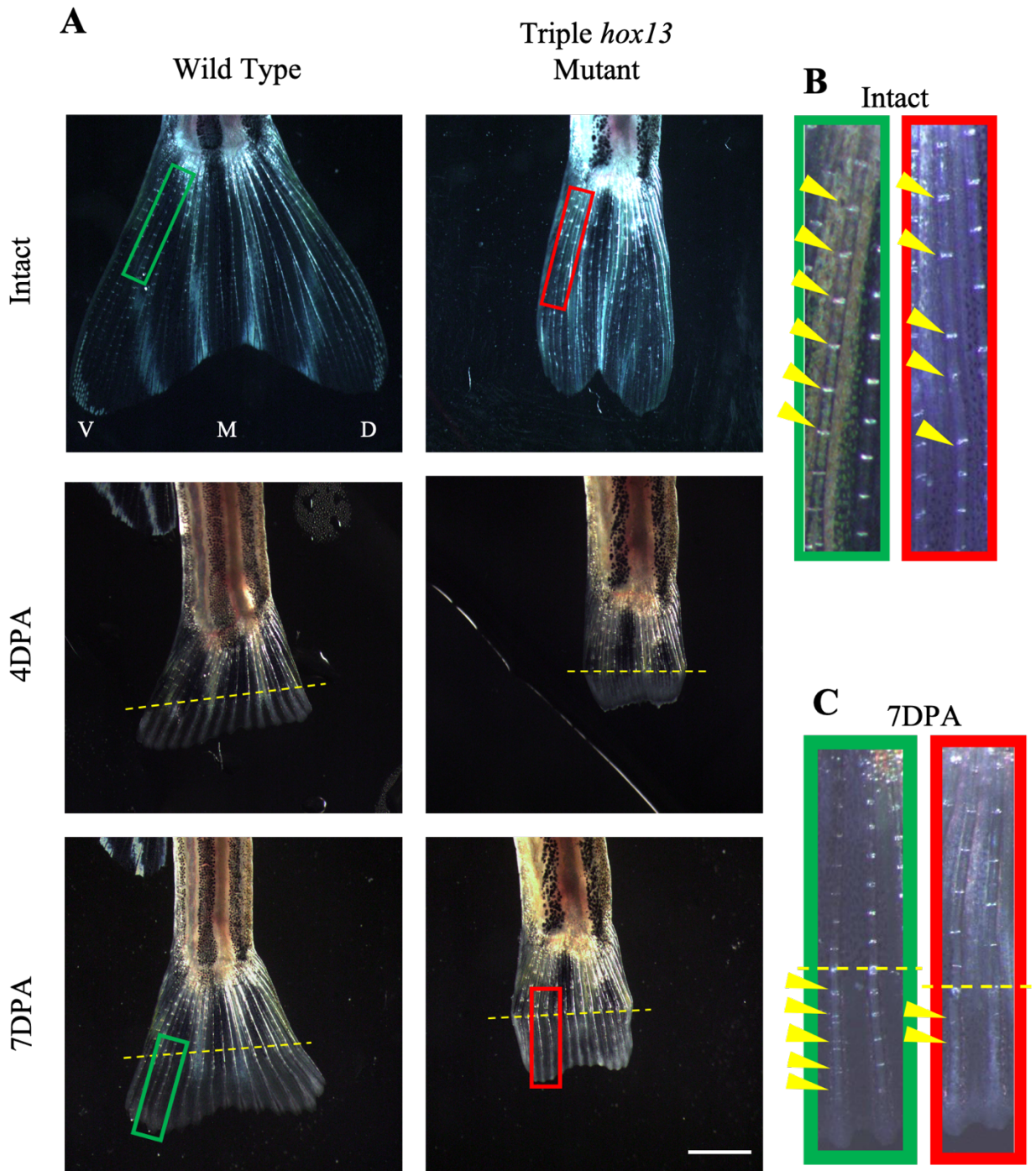

Figure 24. The caudal fin of triple *hox13* possesses defects in segment length and regeneration. A) Intact, 4dpa, and 7dpa comparison of WT versus triple *hox13* mutant caudal fins. B) and C) Enlarged green and red boxes correspond to green and red boxes in A). B) Enlarged green box corresponds to the green box on the intact WT fin and the enlarged red box corresponds to the red box on the triple *hox13* knockout caudal fin. Boxes show the irregularity in joint positioning in the triple *hox13* mutant. C) Enlarged green box corresponds to the green box on the

7dpa WT fin and the enlarged red box corresponds to the red box on the 7dpa triple *hox13* knockout caudal fin. Boxes show lack of joints formed in the 7dpa regenerate of the triple *hox13* mutant. Yellow arrows in B and C indicate joints after the amputation plane. Yellow dotted line represents the amputation plane. V (ventral), M (medial), and D (dorsal) in first panel represent orientation of all panels. N=8 fish per group. Scale bar = 1mm in bottom panel for all panels in A.

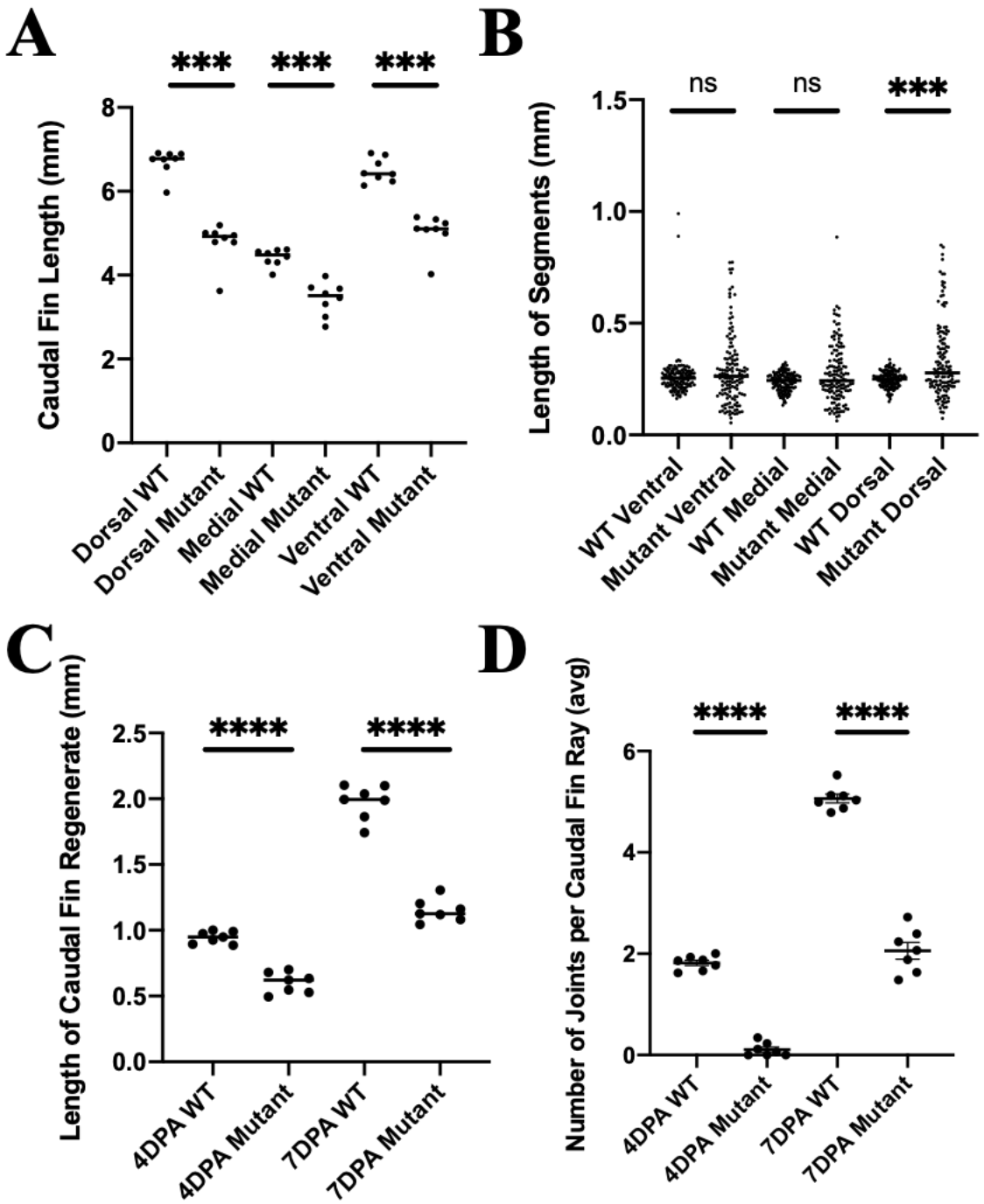

Figure 25. Measurements of the caudal fin of triple *hox13* knockout mutants show they are reduced in size and regeneration is delayed. A) Length of the intact caudal fin compared by unpaired t-test with Welch's correction. B) Length of the caudal fin ray segments in intact fins

compared by Mann Whitney test. N=8 fish per group (in A/B). C) Length of the caudal fin regenerate at 4 and 7dpa compared using an unpaired t-test with Welch's correction. D) Average number of joints per fin ray found at 4 and 7dpa compared with an unpaired t-test with Welch's correction. Significance (*) set at $p<0.05$, (***) = p-value <0.001, (****) = p-value < 0.0001. N=7 fish per group (in C/D).

3.2.2 *hox13* may regulate downstream joint marker expression *pthlha*

As previously mentioned, *evx1* is necessary for joint formation during development and regeneration. Prior studies done in our lab have shown that *hox13* genes are working in a downstream or parallel pathway to *evx1* during joint formation. Complete absence of joints was found in the pectoral, pelvic, ventral, and dorsal fins Although joints were still present in the caudal fin, patterning defects, such as irregular spacing, were observed both during fin development and fin regeneration. We examined the effects of the loss of *hox13* genes on other joint markers. To begin, fluorescence i*n situ* hybridization (FISH) was performed on fin regenerate 4dpa longitudinal cryosections of six triple *hox13* mutants and six WT fish and analyzed by confocal microscopy. *evx1* expression was observed in the regenerate of the triple *hox13* mutants however not at regularly spaced intervals. Expression of *evx1* in the triple *hox13* mutants was both misaligned between the two parallel hemirays and at shorter intervals than observed in WT (Figure 26A). *pthlha* was expressed in the joint cell clusters of the regenerate in 78% of the sections analyzed, however expression was weaker in the triple *hox13* mutants compared to WT (Figure 26B). Interestingly, *pthlha* expression was not detected in 22% of the sections analyzed. The expression of *evx1* suggests that the *hox13* genes are likely acting in a parallel pathway to the *evx1* gene in the joint forming cells. The reduction in expression of *pthlha* shows that the *hox13* genes may regulate *pthlha*. To ensure morphology of osteoblast cells was not affected immunohistochemistry (IHC) was performed on cryosections using Zns5, a pan osteoblast marker which stains all stages

of differentiation. Zns5 staining in triple *hox13* knockout mutants was comparable to the wildtype (Figure 27).

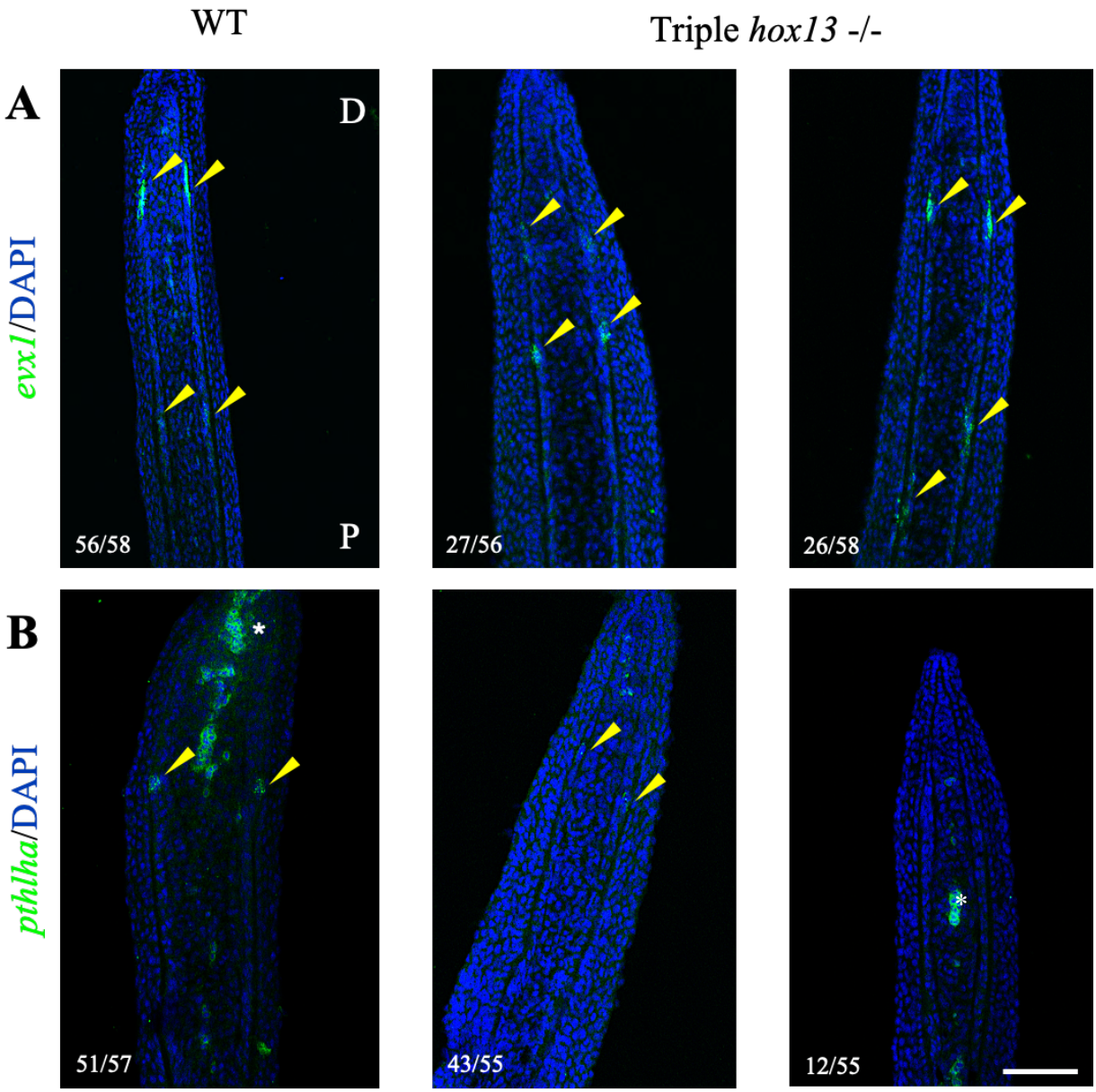

Figure 26. Expression of joint markers *evx1* and *pthlha* persists in triple *hox13* knockout mutants. A) Expression of the joint commitment marker *evx1* represented with green in 4 dpa caudal fin longitudinal cryosections WT and triple *hox13* knockout mutants; counterstained with DAPI. B) Expression of the joint commitment marker *pthlha* represented with green in 4 dpa caudal fin longitudinal cryosections WT and triple *hox13* knockout mutants; counterstained with DAPI. White D and P in panel A) represent distal (D) and proximal (P) directions of tissue sections in (A, B, all panels). White numbers in each panel represent the number of sections with similar phenotypes over total number of sections. Yellow arrows represent presumptive joint cell clusters

with expression. White asterisks indicate artifact staining of blastemal tissue. Scale bar in B) final. panel = 100 μm for all images. N= 6 fish per group.

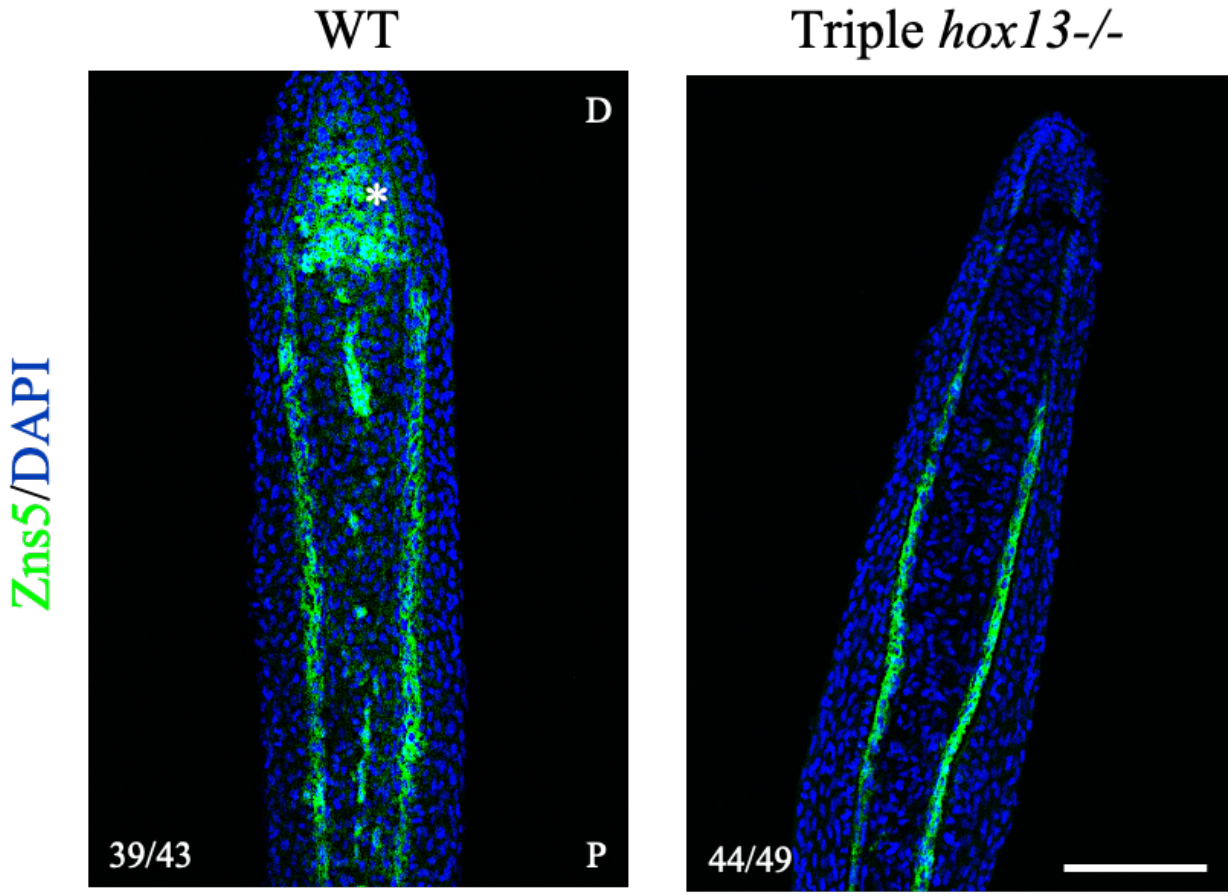

Figure 27. Early osteoblast blast commitment marker, Zns5, shows no significant difference in expression in triple *hox13* mutants and WT fish. The 4dpa caudal fin longitudinal cryosections of the triple *hox13* knockout mutants' domain of Zns5 expression (green) and cell morphology is comparable to wild type longitudinal cryosections; counterstained with DAPI. White D and P in first panel represent distal (D) and proximal (P) directions of tissue sections in both panels. White numbers in each panel represent the number of sections with similar phenotypes over total number of sections. White asterisk represents artifact staining of blastemal tissue in first panel. Scale bar in final panel = 100 μm for both images. N= 6 fish per group.

3.2.3 Triple *hox13* knockout mutants show actinotrichia defects

Actinotrichia are the first exoskeletal elements formed during fin development and fin regeneration and they provide support for cell migration. Actinotrichia fibres are comprised of two components collagen and actinodin. To examine for the presence of actinotrichia in the triple

hox13 mutants, brightfield images were taken following a Triton-X 100 treatment on the larger intact fins (ventral and caudal fins). The Triton-X 100 treatment was used to digest tissue bulk around the actinotrichia fibres for improved imaging on six triple *hox13* mutants and six WT fish. Triton-X 100 treatment revealed a lack of actinotrichia at the distal tip of the ventral fin in triple *hox13* mutants (Figure 28B). Moreover, it revealed that the lateral rays of the caudal fin in triple *hox13* mutants also lacked actinotrichia, medial rays appeared to have fewer actinotrichia fibres (Figure 29A). To further examine for the presence of actinotrichia, IHC using antibodies against the two main structural components of actinotrichia, collagen and actinodin, were performed on longitudinal cryosections of fin regenerates at 4 dpa of eight triple *hox13* mutants and eight WT fish. IHC using Col2 and And1 (actinodin 1) antibodies revealed a decreased amount of fluorescence and therefore of actinotrichia fibers in the triple *hox13* knockout mutants compared to WT (figure 29). Furthermore, Col2 immunostaining revealed a disorganization of actinotrichia fibres throughout the regenerate. The Col2 antibody was also used to analyse longitudinal 4dpa cryosections of the ventral fin, which lacks actinotrichia, in six triple *hox13* mutants and six WT fish. The triple *hox13* knockout mutants failed to fully form bundles of actinotrichia fibres at the distal tip of the fin ray (Figure 30). This is potentially caused by defects in the extracellular matrix disrupting the ability of Col2 and And1 fibres to bundle correctly. It should be noted that proper regeneration of the triple *hox13* knockout mutant ventral fins was also affected and regenerates were smaller at 4dpa than in WT (Figure 30). Lastly, an ISH was performed to examine *and1* mRNA expression in the caudal fin regenerate at 4dpa. There was no difference in the expression patterns of *and1* between the triple *hox13* mutants and the WT fish (Figure 31). This result is surprising since IHC with Col2 and Triton-X 100 show defective actinotrichia. However, it is important to note that *and1* is expressed at a very high level in the normal fin regenerate; it is

therefore possible that a lower expression level in the fins of the triple mutants may not be detectable using ISH. A quantitative method, such as qRT-PCR should be used to determine if *and1* transcript levels are reduced. Col2, IHC, and Triton-X100 analysis indicate that an absence of *hox13* does disrupt the orthodox formation of actinotrichia, which influences the outgrowth of the fin rays. Howbeit, the compensation mechanism which is responsible for the presence of joints (although mis-patterned) and of some actinotrichia within the caudal fin in comparison to the ventral, dorsal, and paired fins is still unknown. In an attempt to examine whether compensation by other *hoxd* genes may explain this differential phenotype found in the caudal fin, a second triple *hox* mutant was created that lacked *hoxa13a, hoxa13b,* as well as the entire *hoxd* cluster.

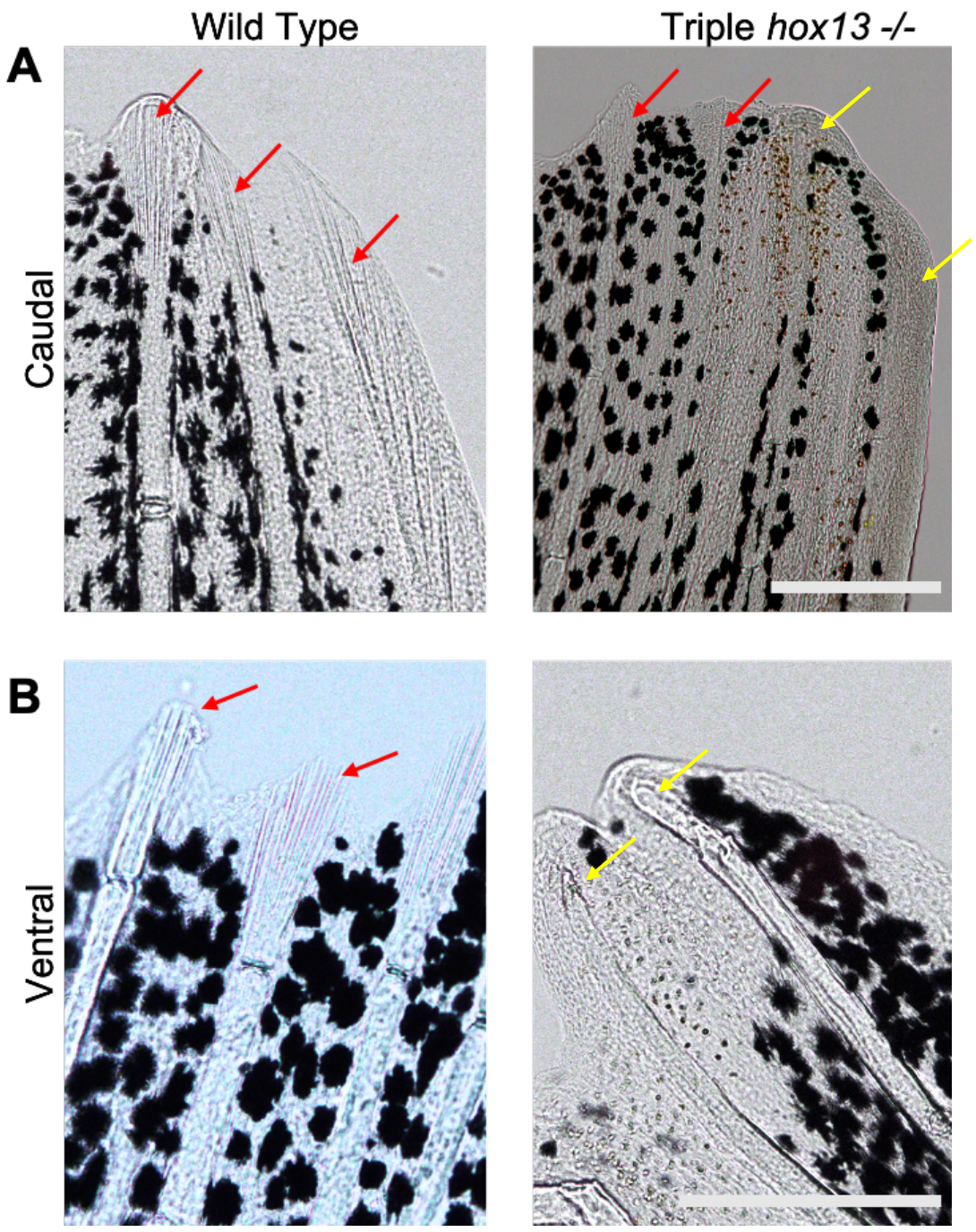

Figure 28. Lateral rays of the caudal fin and all rays of the ventral fin lack actinotrichia at the distal tips of triple *hox13* knockout mutants. Fins were treated with Triton-X 100 to improve visibility of the actinotrichia. (A) All caudal fin rays of the triple *hox13* knockout mutant possess actinotrichia at the distal tip with the exception of the lateral rays. (B) All fin rays of the ventral fin lack actinotrichia at the distal tips in triple *hox13* knockout mutants. Red arrows denote presence of actinotrichia, yellow arrows denote a lack of actinotrichia at distal tips of fin rays. Scale bar in second panel of (A) = 200 µm. Scale bar in final panel of (B) = 200 µm for other three images. WT N=6, triple *hox13*-/- N=6.

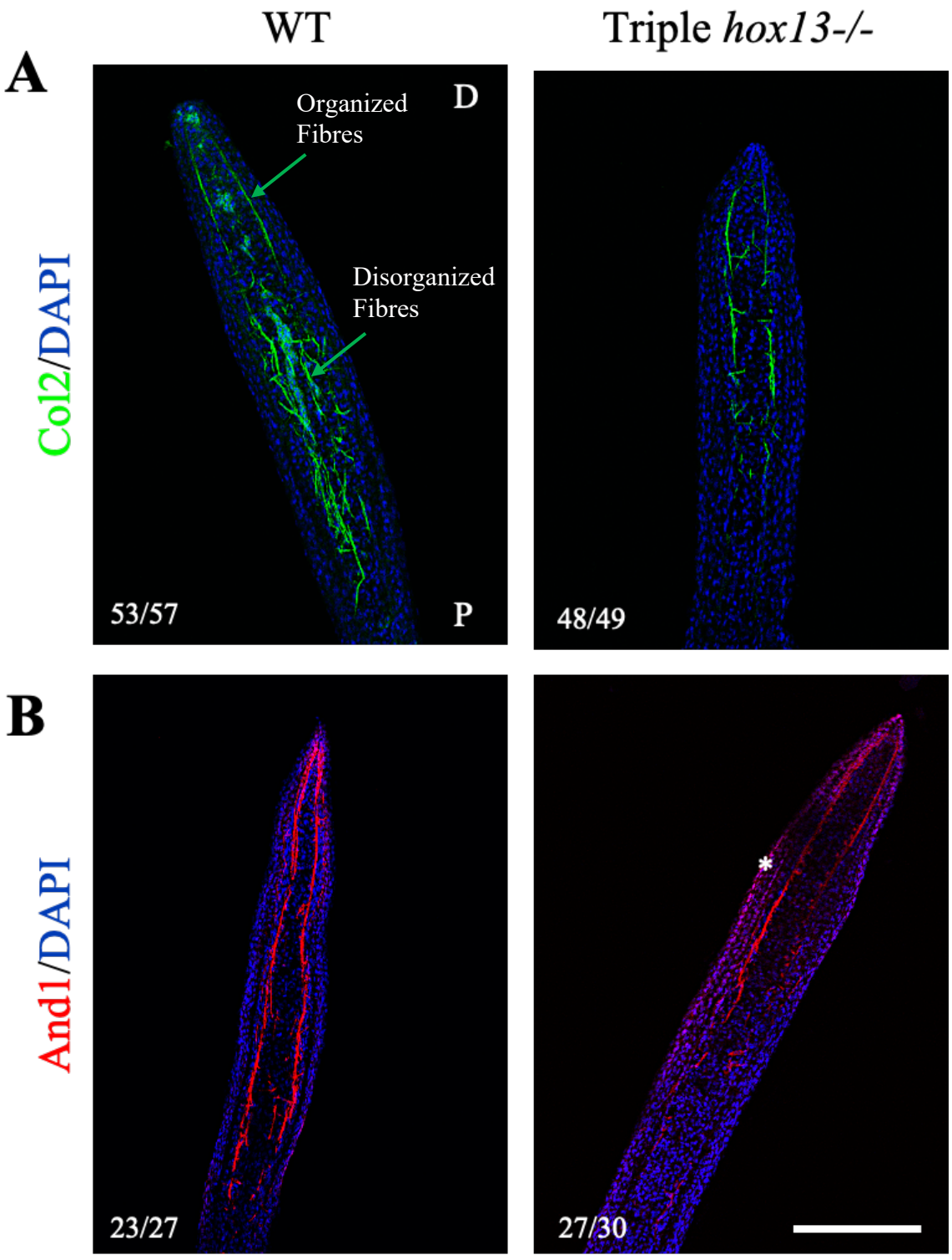

Figure 29. Triple *hox13* knockout mutants display a reduction in expression of actinotrichia components; Col2 (green) and And1 (red), in the caudal fin regenerate. (A) 4dpa caudal fin longitudinal cryosections of the triple *hox13* knockout mutants display a decrease in Col2 expression in the distal portion as well as a decrease in Col2 fibre disorganization in the proximal

portion of the regenerate, counterstained with DAPI. (B) 4dpa caudal fin longitudinal cryosections of the triple *hox13* knockout mutants display a decrease in And1 expression, counterstained with DAPI. White D and P in first panel represent distal (D) and proximal (P) directions of tissue sections in both panels. White numbers in each panel represent the number of sections with similar phenotypes over total number of sections. White asterisk represents artifact staining of epidermal tissue in final panel. Scale bar in final panel = 100 μm for all images. WT N=8, triple *hox13-/-* N=8.

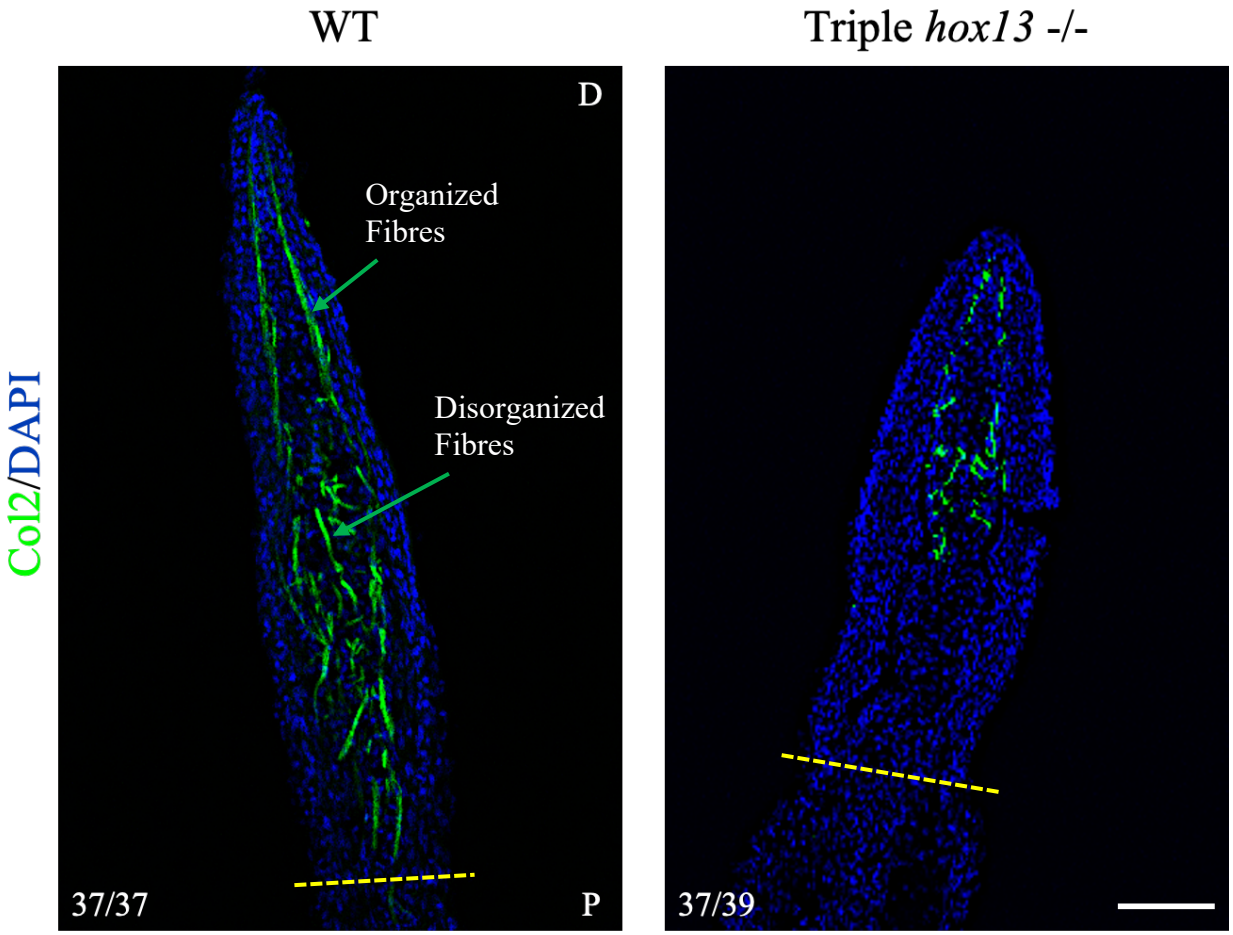

Figure 30. Expression of Col2 (green) is greatly reduced in the ventral fin of the triple *hox13* knockout mutants. The 4dpa ventral fin longitudinal cryosections of the triple *hox13* knockout mutants lack fully formed actinotrichia fibers highlighted by Col2 antibody staining at the distal tip of the fin ray and express and overall reduction in Col2 expression; counterstained with DAPI. White D and P in first panel represent distal (D) and proximal (P) directions of tissue sections in both panels. White numbers in each panel represent the number of sections with similar phenotypes over total number of sections. Yellow dashed lines represent the amputation plane. Scale bar in final panel = 50 μm for both images. WT N=6, triple *hox13-/-* N=6.

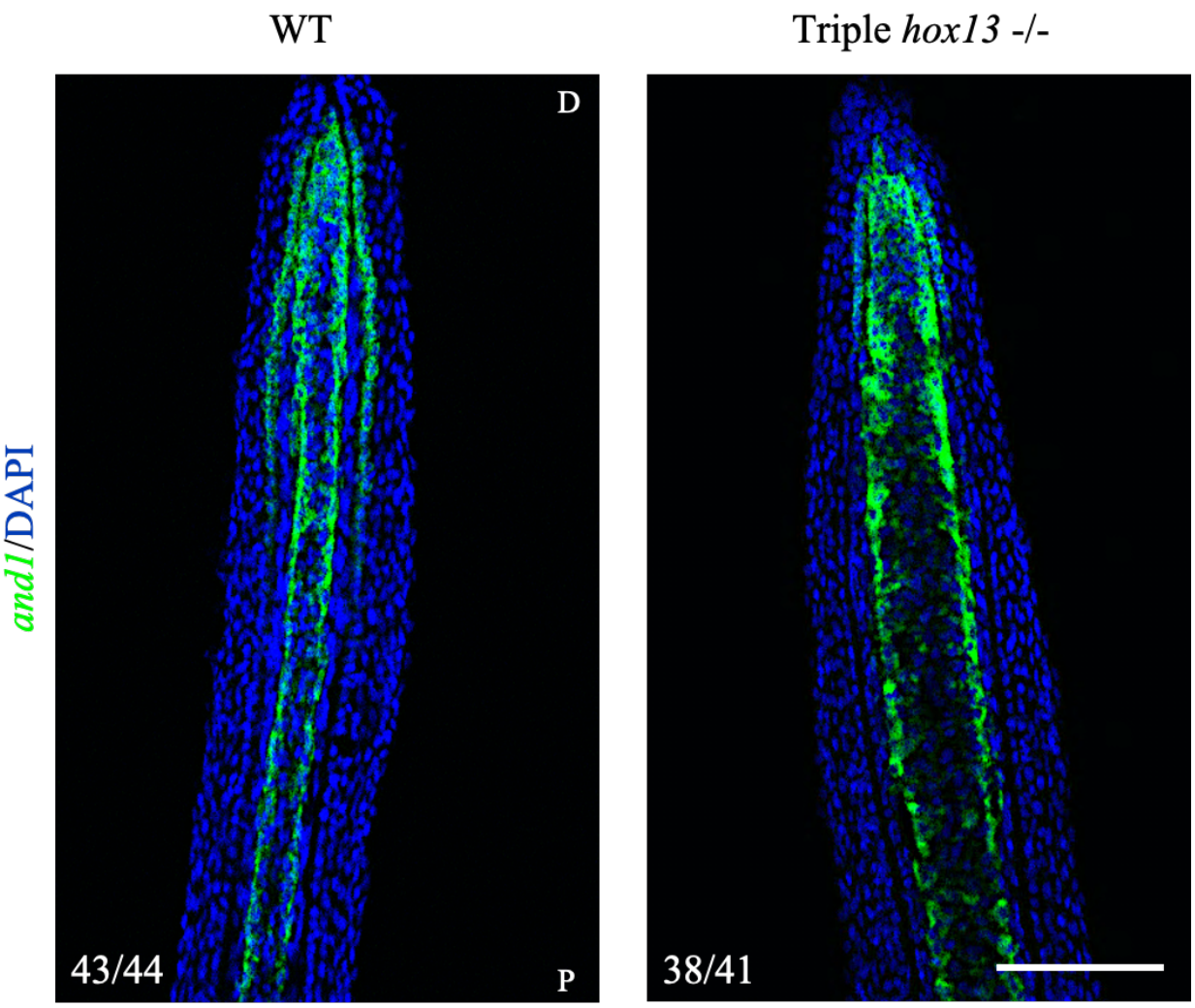

Figure 31. Expression pattern of *and1* (green) remains the same in triple *hox13* knockout mutants. The *and1* expression domain remains in the same in 4dpa caudal fin longitudinal cryosections of the triple *hox13* knockout mutants as the wild type; counterstained with DAPI. White D and P in first panel represent distal (D) and proximal (P) directions of tissue sections in both panels. White numbers in each panel represent the number of sections with similar phenotypes over total number of sections. Scale bar in final panel = 100 μm for both images. WT N=5, triple *hox13-/-* N=5.

3.3 Triple *hoxa13a*$^{-/-}$, *hoxa13b*$^{-/-}$, and *hoxd*$^{-/-}$ *(hox)* mutants display defects in all intact fins and in regenerating fins

3.3.1 Analysis of the exoskeleton

Over the course of analyses in our triple *hox13* knockout mutants, a second *hox* mutant was created with the hopes to elicit a more severe phenotype. The second mutant was created using a

double homozygous *hoxa13a* and *hoxa13b* mutant and a homozygous *hoxd* cluster deletion mutant. Through serial breeding, the two mutants were combined to create a triple mutant: *hoxa13a*$^{-/-}$, *hoxa13b*$^{-/-}$, and *hoxd*$^{-/-}$. Qingming Qu, postdoctoral fellow in our lab, who made the *hoxd* cluster deletion, showed that the *hoxd* cluster deletion alone had no effect on either paired fins as well as on the dorsal or ventral fins, the only phenotype was a size asymmetry of caudal fin lobes. Brightfield images were taken of all the fins in five triple *hox* knockout mutants as well as five WT fish. When first observing the pectoral fin, phenotypic results were similar to those found in the triple *hox13* mutants; the pectoral fin is severely truncated with no growth surpassing the first segment (Figure 32A). Furthermore, the fin rays curl toward the distal ends of the ray. Interestingly, the second set of paired fins, the pelvic, were no longer present on the triple *hox* mutant fish (Figure 32A). When looking at the unpaired fins, the triple *hox* knockout mutants possessed significantly shorter dorsal and ventral fins than WT (Figure 32D, E). Length measurements were taken from the third fin ray from the most anterior ray for all fins except for the caudal. Significance in all fin comparisons was determined using an unpaired t-test with Welch's correction, significance was set at $p<0.05$ (Figure 33). In adult mutants, the dorsal and ventral fin rays also appear to have a wavy phenotype in comparison to their normally straight trajectory (Figure 32A). Moreover, rays of the dorsal and ventral fins lacked bifurcation as well as joints (Figure 32A).

The caudal fin of the triple *hox* knockout mutants did not produce a stronger phenotype than in the triple *hox13* mutants (figure 34). Length measurements were taken from the third fin ray from the lateral edge as well as the most central ray. Additionally, segment lengths were taken from the same fin rays beginning at the most proximal segment and extending 10 segments distally. The caudal fin of the triple *hox* mutants was significantly shorter than the WT also determined

with an unpaired t-test with Welch's correction (Figure 35). In addition, the triple *hox* knockout mutants had irregular joint spacing shown by the spread of data in figure 35B; these segments also varied in the mean length significantly when compared to WT determined by a Mann-Whitney test (Figure 35B). To examine regeneration, the fins were amputated and examined at four and seven dpa. Following amputation, the fins were measured from the amputation plane to the distal edge in three locations along the dorsal ventral axis and an average was subsequently taken. Regeneration was significantly delayed in the triple *hox* knockout mutants at both four and seven dpa tested using an unpaired t-test with Welch's correction (Figure 35C). The number of joints in each fin ray was also counted and averaged between all rays present in the regenerate. Results show a significantly fewer number of joints at four and seven dpa determined using an unpaired t-test with Welch's correction (Figure 35D).

Overall, the removal of the *hoxd* cluster did not have any additional effect on the phenotype on the pectoral, dorsal, ventral and caudal fins when compared to the triple *hox13* knockout mutants. Intriguingly, the pelvic exoskeleton was significantly impaired by the removal of the *hoxd* cluster. Further analyses were needed to determine if this is caused by a lack of endosketetal elements or loss of only the exoskeleton.

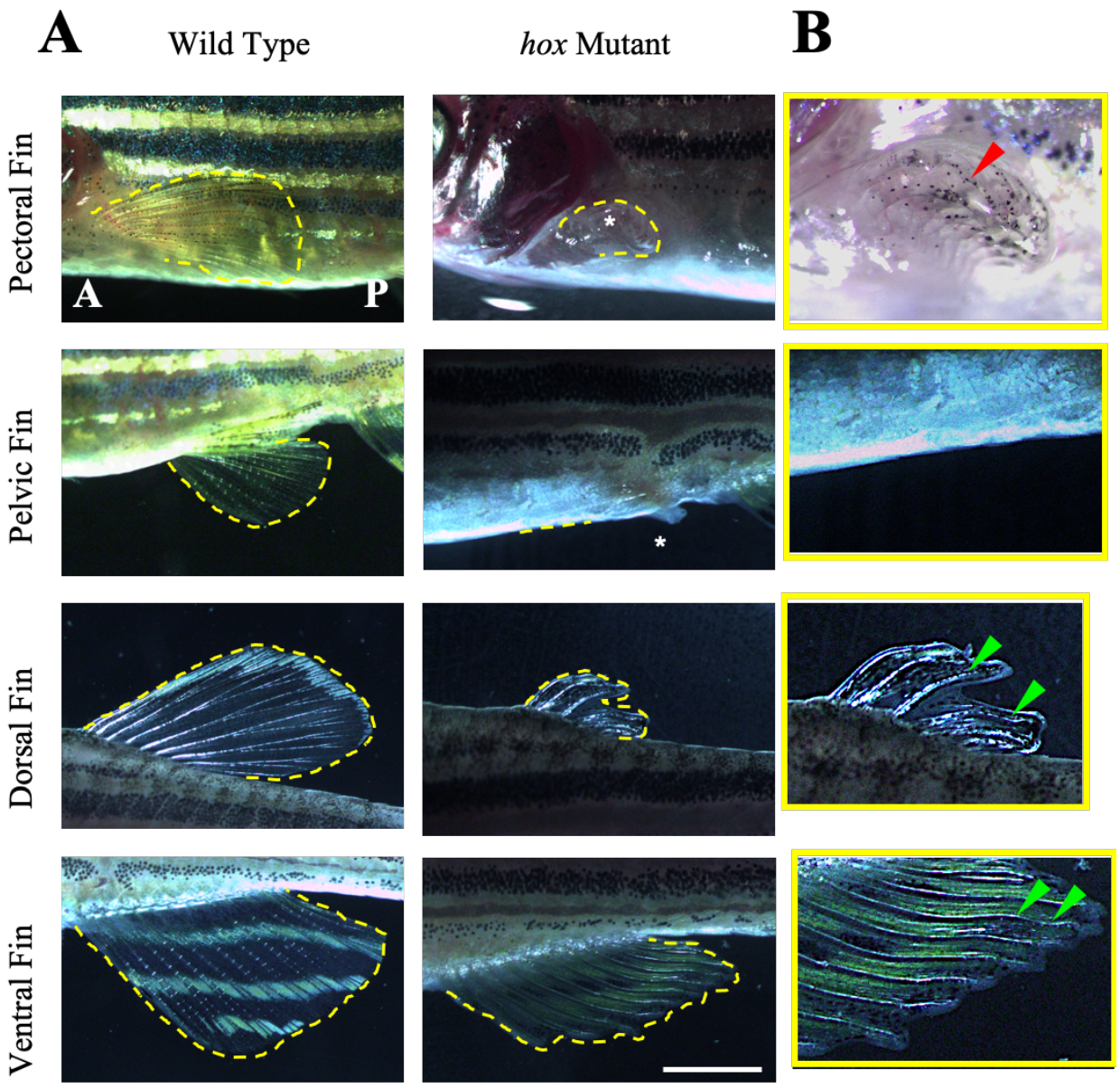

Figure 32. Triple *hox* mutant pectoral, pelvic, ventral, and dorsal fins have a phenotype of reduced fin length and absence of joints in comparison to WT. A) Comparison of WT versus *hox* mutant pectoral, pelvic, dorsal, and ventral fins. A (anterior) and P (posterior) in first panel represent orientation of fish in all panels. Scale bar = 3mm in last panel for all images in A). B) Enlarged images of triple *hox* mutant fin phenotypes: curled (indicated with red arrows) and wavy (indicated with green arrows). N= 5 fish per group.

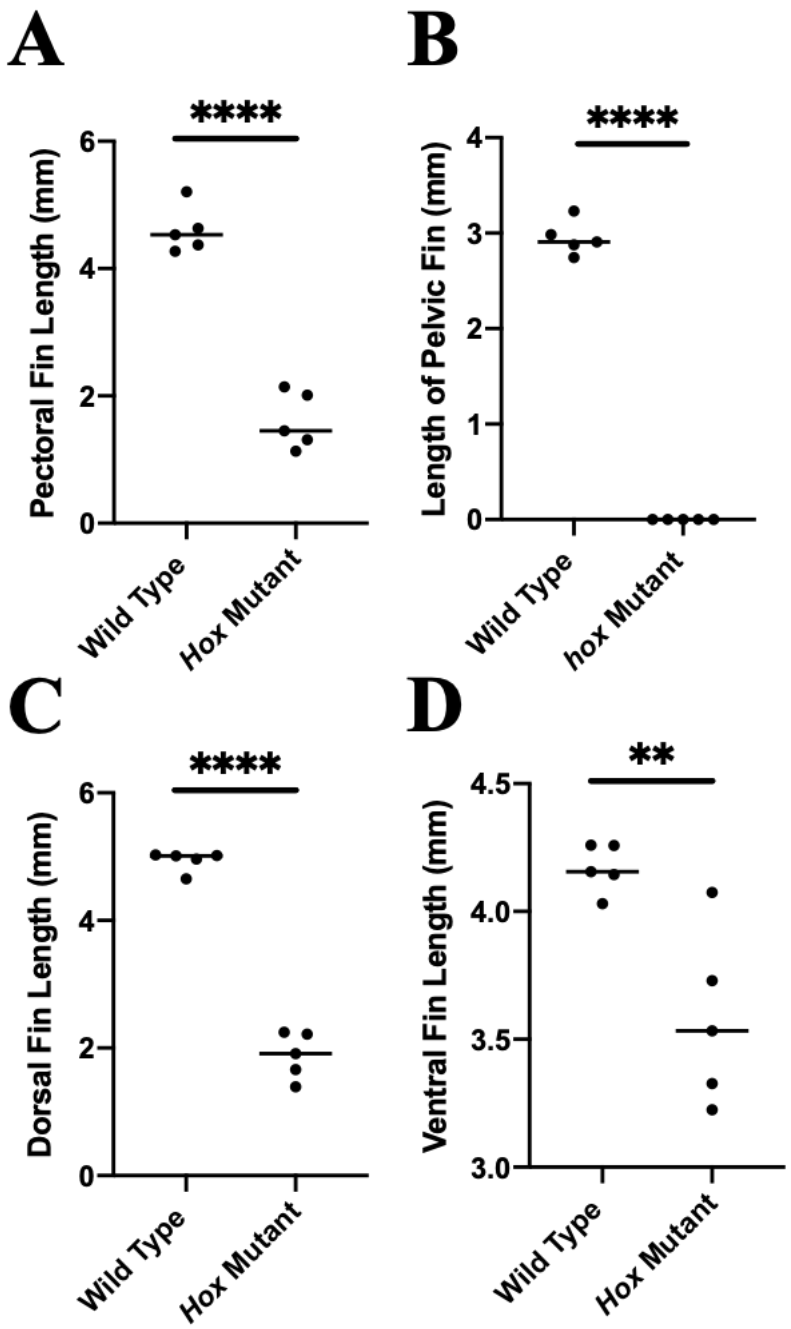

Figure 33. Measurements of the pectoral, pelvic, ventral, and dorsal fin of triple *hox* knockout mutants show they are reduced in length. A) Length of pectoral fin in WT versus triple *hox* mutant fish. B) Length of pelvic fin in WT versus triple *hox* mutant fish. C) Length of dorsal fin in WT versus triple *hox* mutant fish. D) Length of ventral fin in WT versus triple *hox13* mutant fish. For all graphs: unpaired t-test with Welch's correction, significance (*) set at $p<0.05$, (**) = p-value <0.01, (****) = p-value < 0.0001. N=5 fish per group.

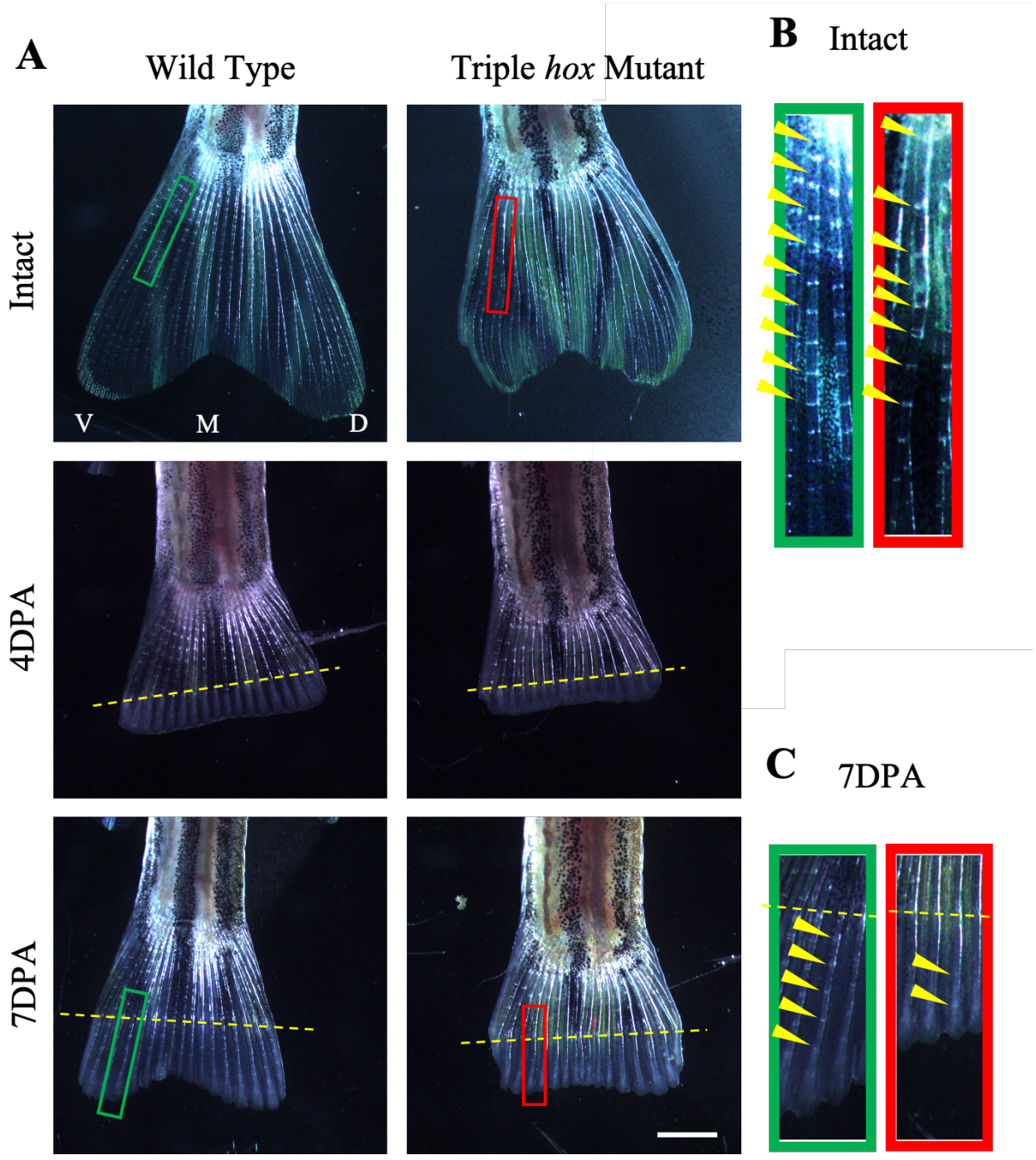

Figure 34. The caudal fin of triple hox knockout possesses defects in segment length and regeneration. A) Intact, 4dpa, and 7dpa comparison of WT versus triple *hox* mutant caudal fins. White V (ventral), M (medial), and D (dorsal) in first panel represent orientation of all panels. B) and C) Enlarged green and red boxes correspond to green and red boxes in A). Yellow dashed line represents amputation plane. Scale bar = 1mm in final panel for all panels. B) Enlarged green box corresponds to the green box on the intact WT fin and the enlarged red box corresponds to the red box on the intact triple *hox13* knockout caudal fin. Yellow arrows represent joints along the fin

ray. C) Enlarged green box corresponds to the green box on the 7dpa WT fin and the enlarged red box corresponds to the red box on the 7dpa triple *hox13* knockout caudal fin. Yellow arrows represent joints after the amputation plane. Yellow dotted line represents the amputation plane. N=5 fish per group.

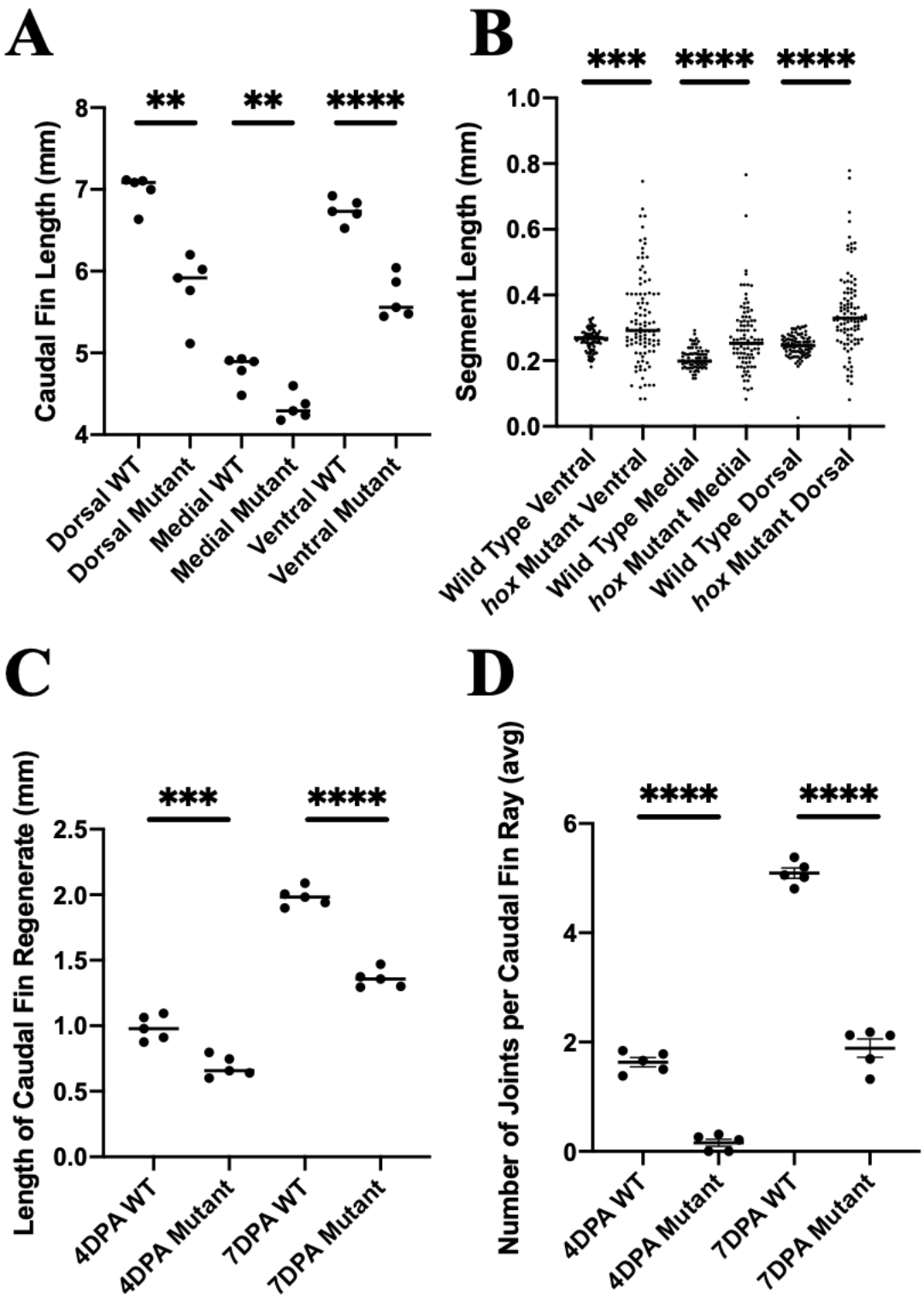

Figure 35. Measurements of the caudal fin of triple *hox* knockout mutants show they are reduced in size and regeneration is delayed. A) Length of the intact caudal fin compared by unpaired t-test with Welch's correction. B) Length of the caudal fin ray segments in intact fins compared by Mann Whitney test. C) Length of the caudal fin regenerate at 4 and 7 dpa compared using an unpaired t-test with Welch's correction. D) Average number of joints per fin ray found at 4 and 7 dpa compared with an unpaired t-test with Welch's correction. Significance (*) set at $p<0.05$, (**) = p-value <0.01, (***) = p-value <0.001, (****) = p-value < 0.0001. N=5 fish per group.

3.3.2 The endoskeleton of the paired fins triple *hox* knockout mutants displays defects

The triple *hox* knockout mutants lacked external tissue of the pelvic fins (Figure 32A). To further examine this phenotype and determine if the entire fin structure (exoskeleton and endoskeleton) was absent a few fish were sent for a computerized tomography (CT) scan completed by Dr. Qingming Qu (School of Life Sciences, Xiamen University, China). Two fish with a WT genotype, two fish with the genotype: *hoxa13a*$^{-/-}$ *hoxa13b*$^{-/-}$ *hoxd*$^{+/-}$ (double homozygous *hoxa13*; *hoxd* heterozygous), and two fish with the genotype: *hoxa13a*$^{-/-}$ *hoxa13b*$^{-/-}$ *hoxd*$^{-/-}$, were fixed in PFA and sent for analysis. The CT scan was taken to closely examine the pectoral and pelvic endoskeleton and orientation. Although, not enough fish were sent to perform a statistical analysis, the observations were still carried out to determine if more scans should be completed in the future. Surprisingly, the triple homozygous *hox* knockout mutants and the double homozygous *hoxa13*; *hoxd* heterozygous fish displayed many of the same phenotypes. However, symmetry between the left and right endoskeletons was rarely observed and variation in phenotypes did occur between fish. The pectoral endoskeleton of the triple *hox* knockout mutants possessed a greater number of distal radials (~9) in comparison to wildtype (~5) (figure 36A, outlined in yellow). The proximal radials of the pectoral fin normally consist of four long bones that articulate together. The *hox* mutants of both genotypes possessed two different phenotypes, additional proximal radials in some locations as well as a lack of proximal radials in others,

suggesting that some of the elements separated and fused as a result of the mutation (figure 36A, outlined in red). Analysis of the endoskeleton of the triple *hox* mutants' pelvic fin showed an absence of the endoskeleton on one side of one of the double homozygous *hoxd* heterozygous fish (figure 36B) and a reduction in size and a change in orientation of the seven other pelvic fins (figure 36B, red arrows). The posterior process appeared to be enlarged in the triple *hox* mutant fish (figure 36B, yellow arrows). Moreover, adult WT fish regularly possess ~3 radials, many of the *hox* mutants lacked the proper number of radials (figure 36B, blue arrows); however, it should be noted that the change in orientation could have made them harder to visualize. Further tests using bone staining should be done to confirm the presence or absence of the radials. Withal the pelvic fin endoskeleton of the triple *hox* knockout mutants was in a different orientation on the anterior posterior axis in comparison to the WT pelvic fin endoskeleton (Figure 36B, red arrows).

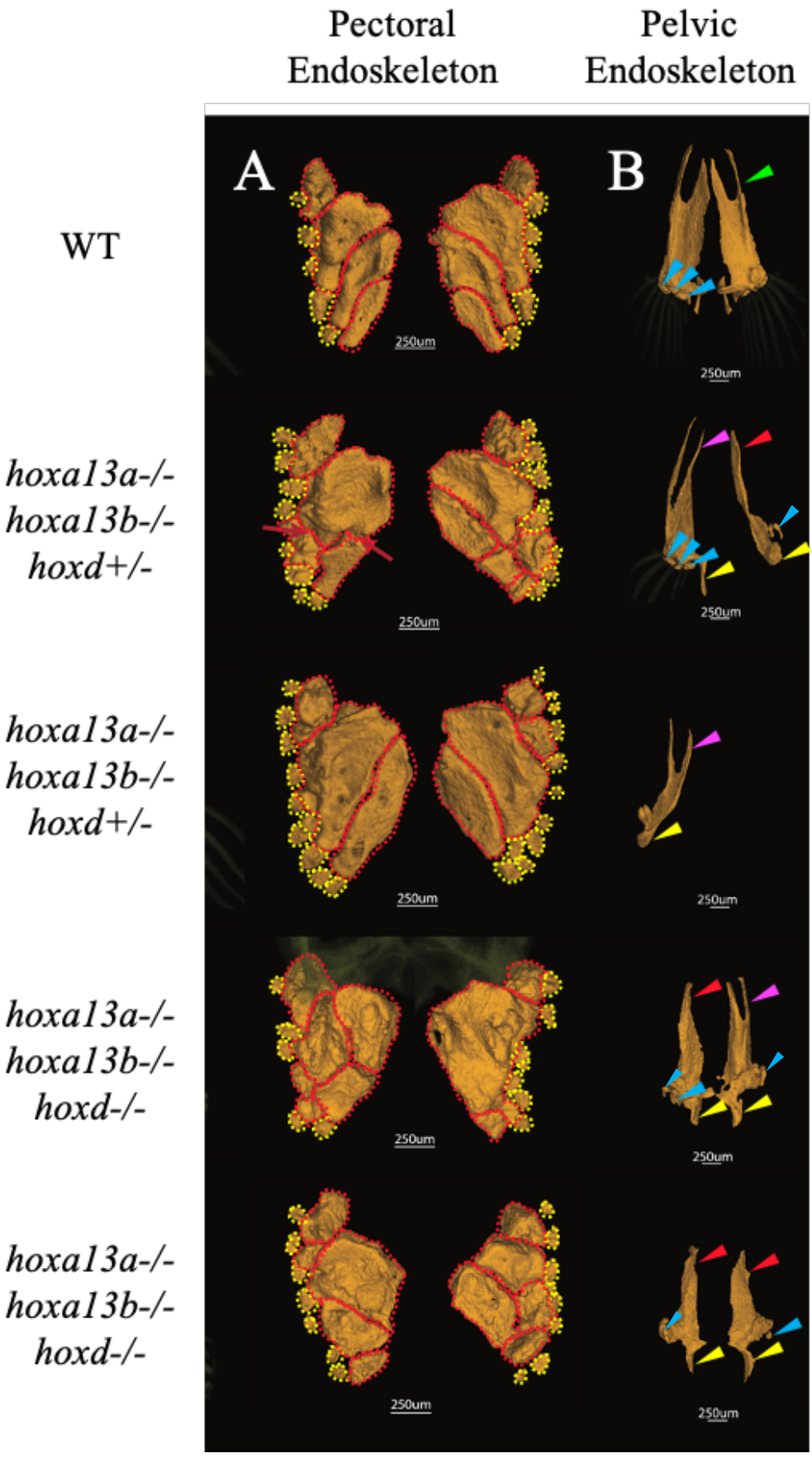
Pectoral Endoskeleton
Pelvic Endoskeleton
A
B
WT
hoxa13a-/-
hoxa13b-/-
hoxd+/-
hoxa13a-/-
hoxa13b-/-
hoxd+/-
hoxa13a-/-
hoxa13b-/-
hoxd-/-
hoxa13a-/-
hoxa13b-/-
hoxd-/-
250um

Figure 36. Triple *hox* knockout mutants display varying morphology in pectoral and pelvic endoskeleton. A) The pectoral endoskeleton of the triple *hox* mutants possess a greater number of distal radials in comparison to WT fish. Red dashed lines outline proximal radials, yellow dashed lines outline distal radials. B) The pelvic endoskeleton has an altered orientation of the pelvic girdle (red arrows) and variation in sizing of the posterior process (yellow arrows). Moreover, most endoskeleton elements lack radials (blue arrows) Magenta arrows indicate a pelvic girdle with correct orientation but altered sizing, green arrow points at a WT pelvic girdle with a correct orientation, size and posterior process. WT N= 2 fish. *hoxa13a-/- hoxa13b-/- hoxd-/-* N=2 fish. *hoxa13a-/- hoxa13b-/- hoxd+/-* N=2 fish. Scale bars in each image = 250 μm.

Chapter 4: Discussion

The goal of this thesis was to determine the role of *hox13* expressing cells/genes in joint/fin ray formation and patterning during development and regeneration. Our first objective was to extend the previous analysis by Derek Sheppard, by exploring new treatment options as well as examining the amount of cell death following cell ablation of *hox13* positive cells. After showing that the reduction of *hox13* positive cells using the MTZ/NTR mechanism had a profound effect on segment length and therefore joint displacement we decided to look more closely into the role of *hox13/hox* genes within the scope of development and regeneration of the fins. Our second objective was to create triple *hox13* deletion mutants in an effort to produce a severe phenotype we can use to analyze the role of these genes in joint formation and regeneration.

4.1 Minimal reduction of *m-inta11* cell populations cause a decrease in segment length

A previous student within the lab, Derek Sheppard used the MTZ/NTR system to explore a concentration gradient most effective at treating adult transgenic zebrafish fins. While doing this he noticed that the fin ray segments had a decreased length during the time of treatment. To confirm the results obtained by Derek Sheppard, the ablation of *m-inta11* cell populations was repeated with modification to allow for the observation of cell death. Although cell death was relatively limited in the joint cells, it was restricted to the *m-inta11* cell populations, regulated by *hox13,* eliminating the possibility of a non-specific effect. In comparison to control fish, cell death was observed at the level of the more proximal joint-forming cells. Cell death was not observed in the most distal presumptive joint cells. The reason why there was no cell death in the distal presumptive joint cells is still unclear, however, it is possible that there is a decrease in the effectivity of the MTZ drug over time. Over time, small amounts of MTZ are degraded/metabolised creating a lower concentration of MTZ in the water while the newest (the

most distal) joint is forming. Despite a modest effect on cell death based on the results of the TUNEL assays, a significant decrease in segment length was observed. Control WT fish that were treated with MTZ confirm that the decrease in segment length was not due to a non-specific effect of the drug as no difference in segment length was observed in these fish. Since the *m-Inta11* is active in presumptive, joint-forming, and mature joint cells, actinotrichia forming cells, and the blastema, the observed phenotypes could be attributed to a specific effect on these cell populations (McMillan et al., 2018). However, results from FISH did not show obvious changes in *hoxa13a* expression in the treated *Tg(NTR)* fish most likely caused by the inability of MTZ to eliminate the entire m-*inta11* cell populations. In order to attempt complete ablation of *hox13*-expressing cells, a second pro-drug was tested. Nifurpirinol (NFP) was found to be a more reliable substrate than MTZ for cell ablation in a recent study by Bergemann et al., (2018). This pro-drug can be used at a significantly lower concentration (5µM) with a significant reduction in overall toxicity seen in the fish (Bergemann et al., 2018). In addition, this pro-drug produced greater amounts of cell death with increased specificity and penetrance (Bergemann et al., 2018). After attempting this treatment on adult transgenic zebrafish, DAPI staining showed the morphology of the regenerating fin had been affected; the regenerated fin was significantly smaller and seemingly more immature than controls. However, after completing the TUNEL assay, there was not an obvious increase in the cell death signal in the regenerate tissue. The reason cell death was not observed while using MTZ or this new pro-drug could be due to three factors. First, the TUNEL assay may have been ineffective at recognizing cell death. To test this possibility a second cell death assay based on Annexin V detection with IHC, should be completed in the future. Secondly, the *Tg(NTR)* fish used had YFP fused upstream of NTR; this could have led to issues with translation of the NTR and also made it difficult to determine how much NTR was being translated. To determine if NTR

is being translated a western blot analysis could be done to determine if NTR is present in the sample. However, future transgenic lines of fish could be made with the 2A and YFP downstream of NTR to ensure the proper translation of NTR independently of YFP. The third reason limited cell death was observed, could be that the NTR/ MTZ or NFP approach is not very efficient for ablating regenerative tissue as is shown in many studies. The regenerative capabilities of the zebrafish supersede the ability of the NTR/MTZ mechanism to completely ablate a cell population (Curado et al., 2008; Lalonde & Akimenko, 2018). The only plausible way to target this inefficiency is to maintain prolonged exposure which can induce non-specific effects and toxicity to the fish (Curado et al., 2008; Lalonde & Akimenko, 2018). The results suggest an inefficient ablation of the targeted cells, it is interesting to see that the partial loss of the joint cells and of blastema cells has an effect on patterning of the bone segments / joints and on the length of the regenerate. The increased number of joints and the shortening of segments in the treated *Tg(NTR)* fish suggests a disruption of the regulation of joint positioning.

4.2 Results of MTZ treatment on *Tg(NTR)* fish support proposed joint forming model

In the mechanism proposed by Rolland-Lagan et al., (2012) a joint inhibiting molecule, currently unknown, is responsible for inhibiting the formation of a joint in the immediate area surrounding the joint. Within this model, the unknown compound decays quickly as outgrowth proceeds distally away from the more proximal joint. Therefore, the concentration begins to reduce toward the distal end of the segment. Once the concentration is low enough a threshold is met, and the new joint begins to form. Our research has expanded upon this knowledge introducing *hoxa13a* as a regulatory factor responsible for the patterning and induction of the newly forming joint. As the concentration of the inhibitor decreases the concentration of *hoxa13a* increases until a threshold is met, and a new joint can begin to form, ensuring even spacing between joints and

regulated segment length (figure 14). Treatment results of the *Tg(NTR)* fish bring further evidence to our proposed joint model. Within our proposed model, the subset of *runx2a*-expressing cells that are to become a presumptive joint cell cluster begin to produce a joint inhibitor. The joint inhibitor is effective until the concentration threshold is met and increasing amounts of *hoxa13a* are present (McMillan et al., 2018). The most distal joint cell cluster has the highest concentration of *hoxa13a* with limited expression directly following (McMillan et al., 2018). In addition, this threshold is thought to be the reason for the initial introduction of a presumptive joint cell cluster with upregulated expression of *hoxa13a* (McMillan et al., 2018).

Following treatment with MTZ on the *Tg(NTR)* fish, the observed cell death in the joint-forming cells led us to hypothesize that the concentration of the joint inhibitor is reduced allowing the threshold for *hox13* expression to be met sooner reducing the segment length and consequently distance between joints (figure 37). Moreover, since in the *Tg(NTR)* fish, NTR expression is driven by the *m-inta11* enhancer which, in addition to the joint cells, is also active in the blastema, it is expected that, MTZ treatment beginning at 2.5 dpa, is affecting blastema cells. Such effect may have an impact on the outgrowth of the fin while regeneration is proceeding. Therefore, it is likely that MTZ treatment may have a combined effect where both: outgrowth was impaired, and the distance to the *hox13* threshold required to form a joint was reduced, resulting in the shortened segment length and additional joint formation as well as the overall reduction in size of the regenerate.

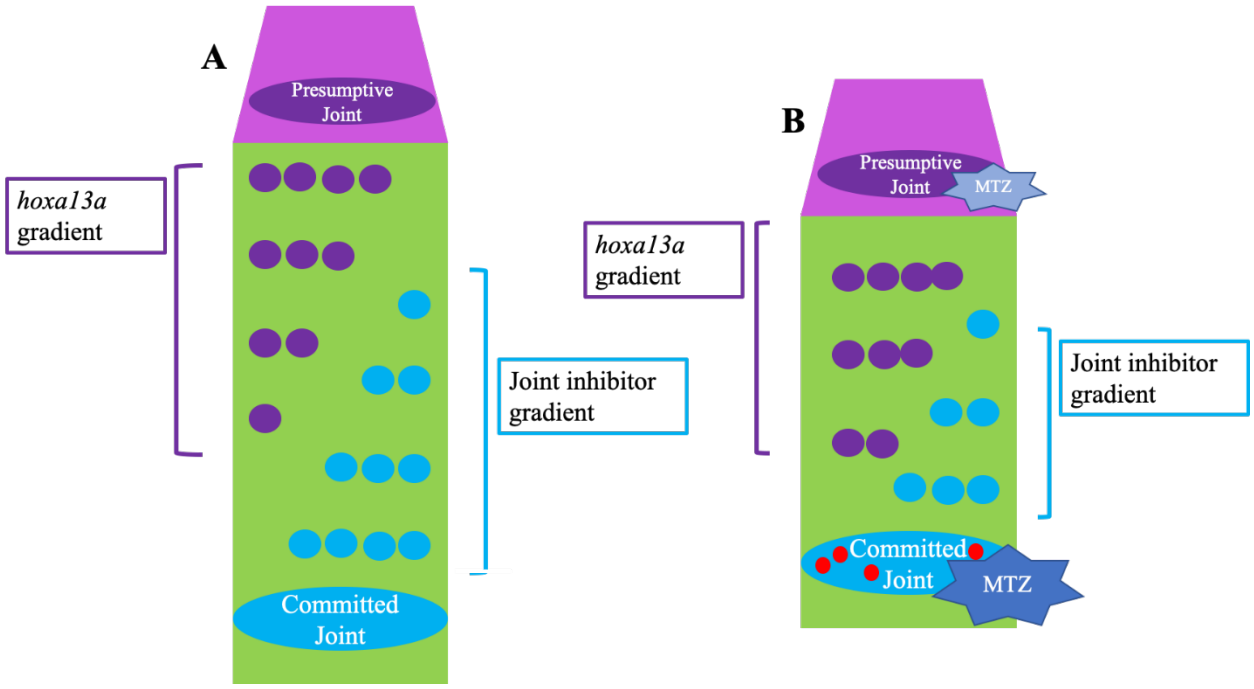

Figure 37. Schematic representation of proposed joint inhibitor model with the effects of MTZ. (A) Normal regeneration of a fin ray. Committed joint produces an inhibitor gradient (blue dots) that acts on *hoxa13a*. The threshold of *hoxa13a* is met and the presumptive joint begins to form. (B) Impaired regeneration of an NTR transgenic fin ray with MTZ. The committed joint produces an inhibitor gradient (blue dots) that acts on *hoxa13a*. MTZ induces apoptosis on some NTR positive cells (red dots) in the committed joint reducing the amount of joint inhibitor produces. The threshold of *hoxa13a* gradient is met sooner due to a lack of inhibitor, the presumptive joint begins to form reducing the size of the segment. MTZ is present at the presumptive joint but in a lower concentration.

Studies have also shown inhibition of members in the joint formation pathway can perturb and eliminate joints. The expression of *connexin43* (*cx43*) negatively regulates *evx1* expression (Bhattacharya et al., 2020). Dardis et al., (2017) showed via ISH a decrease in *evx1* expression after altering *cx43* expression. Our lab showed that *hoxa13a* is expressed in presumptive joint cells earlier than *evx1* and that *hoxa13a* expression persists in *evx1*$^{-/-}$ mutants. One hypothesis is that *cx43* expression is reducing *hoxa13a* expression in a similar way to how it reduces expression of *evx1*. Furthermore, the zebrafish short fin mutant (*sof* ^{b123}) is characterized by reduced fin length, bone segment length, and cell proliferation resulting from reduced levels of *cx43* mRNA and

protein (Iovine et al., 2005). This phenotype was also shown in caudal fins of WT fish that underwent morpholino-mediated knockdown of *cx43* (Hoptak-Solga et al., 2008). Based on these studies, it is possible that a reduction of *cx43* expression causes an increase in *hoxa13a* expression. According to our model an increase in *hoxa13a* expression would lead to the premature formation of a new joint, the effect that is also seen with a decrease in *cx43* expression. Reduction of *cx43* as well as the partial ablation of the joint-forming cells both resulted in a reduction of bone segment length in the fin regenerate. To determine if *cx43* and *hoxa13a* do in fact have an inverse relationship, qRT-PCR for *cx43* should be done in the triple *hox13* knockout mutants, to determine if an increase in the *cx43* transcript is present. In conclusion, it is interesting to note that, although the technique of ablation is only moderately efficient, there is an effect of joint patterning and fin length. Therefore, it shows that a small change has a strong effect suggesting a tight control, possibly through the expression of regulators such as the Hox13 transcription factors. These experiments lead to our hypothesis that the complete inhibition of *hox13* genes during regeneration, through successful ablation or CRISPR/Cas-9 knockout, would produce a fin that does not possess joints.

4.3 Triple *hox13* mutants display defects in all fins and in regeneration of the caudal fin

To begin examining the role of *hox13* genes Dr. Qu, a post-doctoral fellow in our laboratory, originally generated single *hoxa13a, hoxa13b,* and *hoxd13a* knockout mutants. Single mutants did not show any phenotype as expected from the study by Nakamura et al., 2016. Therefore, we created triple mutants through serial breeding of the single mutants. Fins of adult fish were greatly affected by the triple *hox13* deletion mutations. Rays of the paired fins and of the dorsal and ventral fins had similar patterning phenotypes: truncations (more severe in the paired fins), absence of joints and of ray bifurcations, and a wavy ray pattern when compared to WT.

This supports our hypothesis that *hox13* genes are necessary for joint formation as well as proper ray formation in these fins. The caudal fin of the triple *hox13* mutant had a very different phenotype from the rest of the fins; overall the fin was also found to be significantly shorter but still possessed joints however, segment length varied greatly along the fin (due to abnormal joint patterning). The removal of the *hox13* genes also impaired the caudal fins ability to regenerate properly, leaving the mutant regenerate shorter and with fewer joints in the rays. The caudal fin phenotype still shows that *hox13* genes are required for proper ray patterning and segment length. However, it is also suggesting a compensatory mechanism by other factor(s) acting to rescue or to moderate the phenotype. The caudal fin is one of the most conserved fins among fish used in propelling and guiding fish during swimming. The caudal fin also has the greatest importance for survival to maintain proper swimming for escape of predators as well as catching prey (reviewed in: Fu et al., 2013; Iovine, 2007). The caudal fin's importance for survival in many fish species suggests that the caudal fin would be the most resistant to genetic change with many compensatory mechanisms in place. However, future studies using RNA-seq (discussed in 4.8.3) will need to be completed to examine this hypothesis.

4.4 Triple *hox13* mutants display defects joint marker expression

To explore the molecular profile of the presumptive joint cells in the triple *hox13* mutants, two genes, *evx1,* and *pthlha,* were used. The genes *evx1*, and *pthlha* are known joint cell markers that are important for the proper formation of joints. Previous experiments have shown that *pthlha* is acting downstream of *evx1,* and as previously discussed, the position of *hoxa13a* in this molecular pathway is relatively unknown. The expression of *hoxa13a* persists in *evx1* null mutants elucidating that it is either upstream or in a parallel pathway with *evx1* (figure 38A). In the triple *hox13* knockout mutants' expression of *evx1* still persists, supporting the hypothesis that the

hoxa13a gene is working in a parallel pathway. Although there is expression in the *evx1*, defects in the expression patterns can be observed. Interestingly, *pthlha* expression is weaker or absent in the triple *hox13* knockout mutants. The weakened expression or absence of *pthlha* suggest that *hoxa13a* may be regulating *pthlha* expression (figure 38B). Therefore, the elimination of *hox13* genes reduces expression of *pthlha.* Furthermore, the interaction of *hoxa13* and *pthlha* supports the hypothesis proposed by McMillan et al., (2018) that regulation of segment length occurs via the interaction of *pthlha* with *ihha*. Interestingly, *hoxa13a* and *evx1* are close to each other in the genome (~8kb). It is therefore possible that they may share some regulatory elements. However, reduction in expression found by ISH can be misleading without quantitative data. To determine if this hypothesis is correct qRT-PCR for *evx1* and *pthlha* should be done on triple *hox13* knockout mutants as a quantitative measure. This would determine if transcript levels of *evx1* are affected by the removal of the *hox13* genes even if not visible by ISH and would also aid in determining if our hypothesis involving *pthlha* is correct.

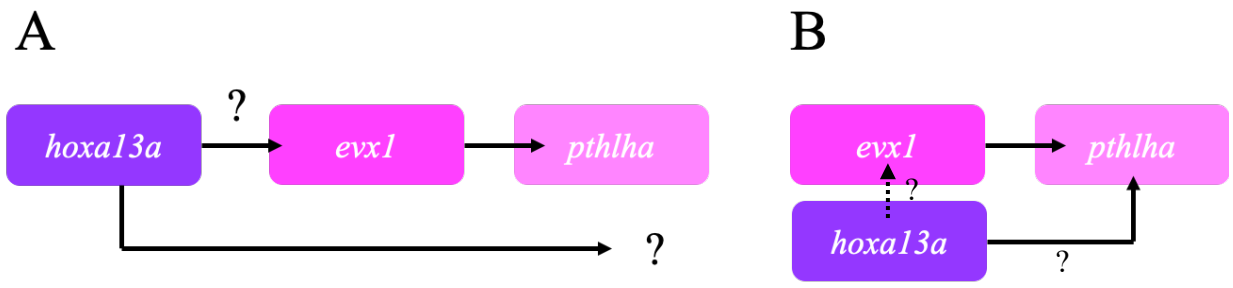

Figure 38. Schematic of the novel regulatory pathway between *hoxa13a* and *pthlha*. A) Previous model created by members in our lab based on data from *evx1* null mutants. B) Updated model based on our observations in the triple *hox13* knockout mutants.

4.5 Actinotrichia defects found in triple *hox13* knockout mutants

Actinotrichia are important for support and cell migration in the fin regenerate (Figure 3). Actinotrichia are collagenous fibres that provide a scaffold for cells to migrate along in the

forming regenerate (Akimenko et al., 2003; Duran et al., 2011; Pfefferli and Jazwinska, 2015). Actinotrichia are organized in longitudinal bundles at the distal end of the rays. The distal end of the actinotrichia is located in the subepithelial space of the regenerate. However, as osteoblasts migrate, they intercalate between the actinotrichia and the epithelial layers. Therefore, the proximal end of the actinotrichia is no longer close to the epithelial tissue but located between the osteoblasts and the internal connective tissue of the regenerate. In more proximal part of the regenerate, the actinotrichia fibres will break apart into fibre debris that localizes within the connective tissue. (Akimenko et al., 2003; Duran et al., 2011; Pfefferli and Jazwinska, 2015). It has previously been shown that *hoxa13* and *hoxd13* binding sites in the regulatory region of *actinodin 1 (and1)* are essential for this gene expression in the developing fins. This may suggest the importance of the Hox13 factors for the synthesis of this important structural component of the actinotrichia (Lalonde & Akimenko, 2018; Phan, et al., 2019).

The caudal fin of the triple *hox13* mutant presented a unique phenotype, lacking actinotrichia only on the lateral edges. However, the ventral fin of the triple *hox13* mutant lacked actinotrichia over the entirety of the fin. We hypothesized the presence of a few fibers in some rays of the caudal fin, may be due to other genes (*hox* perhaps) in addition to the *hox13* that are necessary (and partially compensating) for actinotrichia formation.

Immunostaining of the triple *hox13* mutant showed lower and abnormal patterns of Col2 and And1 proteins, the two major components comprising actinotrichia, in the caudal fin regenerate. However, ISH analysis did not reveal obvious defects in levels of *and1* expression. It is important to note that *and1* is strongly transcribed in WT fins. Therefore, although the mRNA levels did not seem affected in triple *hox13* mutants the strong expression of *and1* may supersede the ability of the ISH to detect change, as suggested by the immunostaining analyses for the

actinotrichia proteins, And1. Interestingly, CRISPR/Cas-9 double *and1* and *and2* knockout mutants created in our lab, which produce no actinotrichia, also present defects of ray patterning similar to those observed in the triple *hox13* mutants: a reduction in overall fin length, reduction in segment length, sporadic bifurcation, and a "wavy" fin ray (figure 39). The similarities in phenotype of the *and1/2* and *hox13* mutants supports our hypothesis that; *hox13* genes are playing a regulatory role in *and1/2* during development and regeneration. However, in order to determine if *and1* transcripts are reduced a qRT-PCR would be necessary. Although there are phenotypic similarities between the *and1/2* knockout mutants and the triple *hox13* knockout mutants, the reasoning as to why each fin of the *hox13* triple mutants possess slightly different phenotypes is still unknown. To determine if the *hoxd* cluster genes were compensating for the removal of *hoxa13a, hoxa13b,* and *hoxd13a* in the caudal fin the triple *hoxa13a, hoxa13b* and *hoxd* cluster mutant was created.

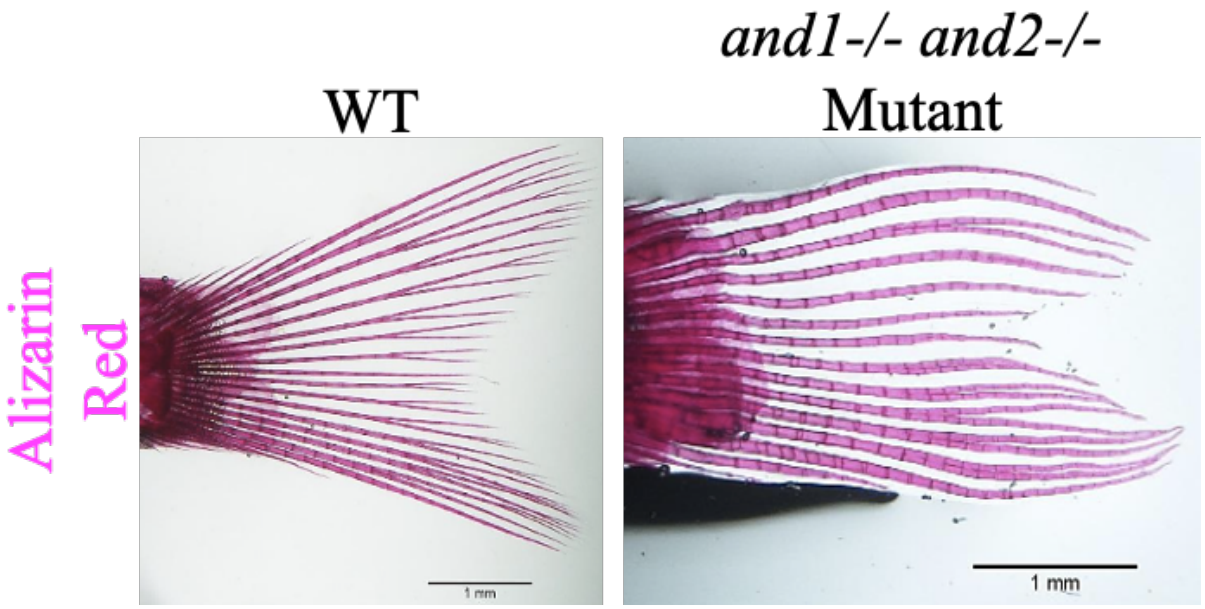

Figure 39. Alizarin red staining of the caudal fin, fin rays of a WT and double and1/2 knockout mutant. The *and1/2* -/- mutants show sporadic bifurcation, and "wavy" fin rays in comparison to WT fish. Images taken by Reeham Kadhom, unpublished.

4.6 Triple *hox* mutants display defects in rays of all fins

In an attempt to create a more severe phenotype in the caudal fin we chose to alter the triple *hox13* mutant and create a triple *hox* mutant, a combinatorial deletion mutant of *hoxa13a, hoxa13b,* and the *hoxd* cluster deletion. At first observation of the triple *hox* mutants, the phenotypes of the fins did not vary greatly from the triple *hox13* mutants. The most significant difference was the absence of the pelvic fin in the triple *hox* mutant. The other paired fin, the pectoral fin of the triple *hox* mutant had no growth surpassing the first joint and was significantly shorter than the WT control. In the unpaired fins, the dorsal and ventral fins had similar phenotypes however the caudal fin once again produced a third and less severe phenotype in the overall fin phenotypes. The caudal fin of the triple *hox* mutants still possessed joints and the segment length varied greatly along the fin. Overall, the fin was also found to be significantly shorter and the regeneration of the caudal fin was impaired resulting in a significantly shorter length of regenerate as well as fewer joints. The similarities between the two types of triple mutants (*hox13* and *hox*) suggest that the genes of the *hoxd* cluster, other than *hoxd13* do not play major regulatory role in the development of the pectoral, dorsal, ventral, and caudal fins. These results further demonstrate the importance of the *hoxd13a* gene in the phenotype of the zebrafish fins.

4.7 The endoskeleton of the triple *hox* knockout mutants displays defects after development

Despite the many similarities of the phenotype observed between the triple *hox13* mutants and the triple *hox* mutants, the main difference was the absence of the pelvic fin. This suggests that the *hoxd* cluster genes play a role in the development of the posterior paired fin substantially affecting the exoskeleton and the endoskeleton. The lack of external pelvic fin on the triple *hox* mutants prompted us to examine the internal portion of the pelvic fin, the pelvic girdle. The

genotypes we chose to examine were: two fish with a WT genotype, two fish with the genotype: *hoxa13a*$^{-/-}$ *hoxa13b*$^{-/-}$ *hoxd*$^{+/-}$, and two fish with the genotype: *hoxa13a*$^{-/-}$ *hoxa13b*$^{-/-}$ *hoxd*$^{-/-}$. The number of fish and corresponding genotypes were chosen due to the availability at the time of the experiment. Surprisingly, the triple homozygous *hox* knockout mutants and the double homozygous *hoxa13*, *hoxd* heterozygous fish displayed many of the same phenotypes. However, symmetry between the left and right endoskeletons was rarely observed and in addition, variation in phenotypes such as, number of proximal radials or distal radials, did occur between fish. The observed variation could be created from varying expressivity of the *hox* genes causing variation between fish. In addition, this could also be explained by developmental instability which can cause fluctuating asymmetry, a concept largely still unexplored in developmental and evolutionary biology. Although fluctuating asymmetry and developmental instability are often observed phenotypically in a population, the underlying genetic modalities in which they occur are still unknown. These concepts are explored by Dongen (2006), in their review paper where they also mention competing theories.

A consistent phenotype recognised in the triple *hox* knockout mutants was a different orientation of the pelvic fin endoskeleton in comparison to the WT pelvic fin endoskeleton. The pelvic endoskeleton of the triple *hox* mutants was rotated on its anterior-posterior axis on three of the four fish. Previous literature illustrates that the pelvic girdle/fin rays have led to the evolution of the hind limbs (Don et al., 2012). The pelvic fins of fish express key limb positioning and outgrowth genes in a similar manner to what is seen in hindlimb development of tetrapods. This change in orientation has direct implications in the fin to limb transition, where the pelvic fin is adjusted beneath the centre of mass allowing it to become weight-bearing (Don et al., 2012; Coates,

1995). However, more replicates of the study will have to be performed to provide conclusive evidence.

Overall, it seems that the *hox13* genes are involved in the regulation of distal radial formation of the pectoral fin, a phenotype also observed by Nakamura et al., (2016). In addition to extra distal radials in the pectoral fin of our triple *hox13* mutants, the positioning of the proximal radials to one and other was affected. More work should be completed to determine if these proximal radials are potentially articulated together with additional joints caused by the removal of the *hox* genes. Moreover, the endoskeleton of the unpaired fins should be examined to determine if similar phenotypes such as extra distal radials or the segregation or fusing of radials is observed. Nakamura et al., (2016) claim that the addition of endochondral bone along with the reduction of exoskeletal bone found in their triple *hox13* frameshift mutants, supports the theory of the fin to limb transition, characterized by the transformation of to elaborate endochondral skeleton and the loss of the exoskeleton during evolution the fin skeleton of an ancestral fish. However, further studies need to be completed to determine the evolutionary relationship between the distal radials and the autopod to determine if this hypothesis could be implicated in our work.

The severity of the impact of the *hox* deletions on the endoskeleton of the unpaired fins could be a result of the impaired development of the endoskeletal disc. The endoskeletal disc also gives rise to the exoskeleton which may in turn cause a disruption in outgrowth of the exoskeleton. However, additional studies based on the development of the endoskeletal disc will be necessary to discern if the observed phenotypes in the exoskeleton are a result of mis-patterning in the endoskeletal disc.

4.8 Future Directions

4.8.1 Analysis of all fins

Within this study, the fins were analysed using longitudinal cryosections of 4dpa fin regenerates. Furthermore, comparisons were only made with the caudal and ventral fin, due to their easily accessible nature. Future work on this project should incorporate all fins as well as whole fin analysis of each fin. Specifically, IHC with antibodies for And1 and Col2 should be performed on each fin type to determine if there is still expression at the distal tips following development, including the paired fin where the curling of the distal tips makes visualizing the phenotypes more difficult. All fins should be examined to help elaborate on why the majority of the fins present with different phenotypes.

4.8.2 Cell type-specific fluorescent reporter transgenic lines in the *hox13* mutants genetic background

Generating lines of fish expressing a fluorescent reporter transgene for specific cell types in the triple *hox13* mutant background would allow us to visualize specific cell types *in vivo* while the fish are developing and during fin regeneration. Such lines can be done through a serial breeding of transgenic reporter lines of fish (already available) with homozygous *hox13* deletion fish. Two of the transgenic lines that would be feasible and practical to create a transgenic mutant are *Tg(sp7),* and *Tg(runx2a:ßg:kaede)*. Each of these lines would provide expansive knowledge on a specific cell type during development and regeneration. The first line *Tg(sp7),* expresses EGFP in the committed osteoblasts. This line could help identify any changes in the fin exoskeleton over the course of development and regeneration. In addition, this *Tg* would aid in visualization of any changes in the migration or size of the osteoblast layers. The second line *Tg(runx2a:ßg:kaede),* uses *runx2a* to drive expression of the photoconvertible *kaede* which switches from green fluorescence to red, after exposure to specific violet UV wavelengths

(Schuster & Ghysen, 2013). The gene *runx2a* is a pre-osteoblast marker but is also present in dedifferentiated osteoblasts as well as presumptive joint cells (Knopf et al., 2011). The r*unx2*$^{+}$ cells are restricted to the lateral sides of the blastema under the epidermis (Knopf et al., 2011). Moreover, *runx2*$^{+}$ cells have an overlapping domain with *hoxa13a* expression (McMillan et al., 2018). By using *kaede* driven by the enhancer elements of *runx2a,* we would be able to follow the fate of a single cell in a regenerating fin. Using a confocal microscope set to the violet UV wavelength, a group of presumptive joint cell cluster could be photoconverted from green to red fluorescence and followed throughout regeneration to determine their migratory path and life span. In addition, early osteoblasts could be photoconverted to determine their migration and life span as outgrowth proceeds. This would provide insight to the migratory paths of osteoblast cells following the deletion of *hox13* genes potentially shedding light on the "wavy" bone phenotype observed in the triple *hox13* mutants. This line could also provide insight to the differentiation of bone and joint cells during regeneration or development in the triple *hox13* mutants. These transgenic mutant lines help us to better track specific cell types and morphologies that could be contributing to the phenotypes that are observed following development and in regeneration in the triple *hox13* mutants. However, the underlying molecular mechanisms that control cell differentiation and movement require additional experiments.

4.8.3 RNA-Seq on triple *hox13* mutant fins

To understand why each fin is affected differently by the triple *hox* deletion mutations a more in-depth and quantifiable transcriptomic read is necessary. To obtain this transcriptomic read every fin type (pectoral, pelvic, dorsal, ventral, and caudal) would have to be amputated and kept separately to facilitate comparison of each of the fins with each other and moreover with wild type. RNA-Seq allows for full sequencing of the entire transcriptome (Qian et al., 2014; Metzker, 2009).

RNA-Seq uses next generation sequencing to reveal both presence and quantity of total RNA in the sample (Qian et al., 2014; Metzker, 2009). Within this process, mRNA is converted into a cDNA library and mapped against our WT reference transcriptome (Qian et al., 2014; Metzker, 2009). RNA-Seq will provide a wide scope of information to compare the differences in gene expression between the triple *hox13* knockout mutants and wildtype fish as well as the differences in gene expression between each fin type. Moreover, fluorescent cell sorting could be completed using some of the aforementioned fluorescent reporter transgenic mutant lines that will be created. Cell sorting would allow us to look at specific cell subtypes within each fin. By using the transgenic *sp7:EGFP* mutant lines, we would be able to examine transcript expression specific to the committed osteoblast cells. This could provide insight into genes that are affected by the triple *hox13* mutation and potentially upregulating bone matrix secretion in the fins that lack joints (paired, dorsal, and ventral). In a similar manner the *Tg(runx2a:ßg:kaede*) mutants could be used to determine transcript expression in: pre-osteoblasts, isolated presumptive joint cells, and joint-forming cells. These cell subsets would provide insight for the transcriptomic reasoning behind the lack of joint formation in the paired or dorsal and ventral fins in comparison to the caudal, which still possess joints after the deletion mutations. The results of this analysis could provide reasoning for why we observed different phenotypes in each of the fins of the triple *hox13* mutants.

Conclusion

In this thesis we examine the hypothesis: zebrafish *hox13* genes are responsible for joint formation and patterning during development and regeneration. This hypothesis is based on previous studies performed in our laboratory examining the role of *hoxa13a* in joint formation and regeneration. In this thesis, a conditional cell ablation approach was used to target *m-inta11* cell populations (*hoxa13a*-expressing cells) in the regenerating caudal fin. We show that partial ablation of the cells leads to important patterning defects of the joints and growth of the ray. This indicates that proper patterning and growth depends on a tight control of factors produced by *m-inta11* cell populations. Among the factors that may be critical in this control is the Hoxa13a transcription factor that was also previously shown to be a factor involved in joint formation. To explore the function of this factor and of other Hox13 paralogs, we examined the fins of a triple knockout mutant for *hoxa13a, hoxa13b,* and *hoxd13a* and found that each fin presents with defects in patterning or loss of joints in the rays as well as shorter fin length. These defects confirm the role of the *hox13* genes in the development and patterning of joints. Further examination of the fins of the triple *hox13* mutant showed that actinotrichia are not structurally intact, a potential reason for a disruption in the migration of the osteoblast cells. Although, the phenotypes of the fins possess commonalities, the paired, dorsal/ventral, and caudal fins do present differences; however, the reason for these differences is still unknown. Additional studies involving transcriptome analysis will have to be completed to determine the underlying molecular mechanisms that are acting in response to the deletion of the *hox13* genes. Furthermore, gene expression analyses done on the triple *hox13* knockout mutants support the hypothesis that Hoxa13 is acting in parallel to Evx1 and may directly regulate *pthlha* expression (as does Evx1), which may in turn be involved in segment length regulation through its interaction with Ihha. Finally, since deletion of the entire *hoxd* cluster in the

triple *hox13* mutants had no major additional effects on the rays other than those observed with the triple *hox13* knockout mutants, we can conclude of the importance of the hoxd13 gene for the structure of the rays. Overall, this thesis demonstrates the necessity of the *hox13* genes for joint and actinotrichia formation in the paired, dorsal, and ventral fins and, for the regulation of bone segment length in the caudal fin.

References

Abzhanov, A., Rodda, S. J., McMahon, A. P., & Tabin, C. J. (2007). Regulation of skeletogenic differentiation in cranial dermal bone. *Development (Cambridge, England)*, *134*(17), 3133–3144. doi:10.1242/dev.002709

Ahn, D., & Ho, R. (2008). Tri-phasic expression of posterior Hox genes during development of pectoral fins in zebrafish: Implications for the evolution of vertebrate paired appendages. *Developmental Biology*, *322*(1), 220-233. doi: 10.1016/j.ydbio.2008.06.032

Akimenko, M. A., Mari-Beffa, M., Becerra, J., & Geraudie, J. (2003). Old questions, new tools, and some answers to the mystery of fin regeneration. *Developmental, 226*(2), 190-201.

Amores, A. (1998). Zebrafish hox Clusters and Vertebrate Genome Evolution. *Science*, *282*(5394), 1711-1714. doi: 10.1126/science.282.5394.1711

Avaron, F., Hoffman, L., Guay, D., & Akimenko, M. A. (2006). Characterization of two new zebrafish members of the hedgehog family: Atypical expression of a zebrafish *indian hedgehog* gene in skeletal elements of both endochondral and dermal origins. *Developmental Dynamics, 235*(2), 478-489.

Bensimon-Brito, A., Cancela, M., Huysseune, A., & Witten, P. (2012). Vestiges, rudiments and fusion events: the zebrafish caudal fin endoskeleton in an evo-devo perspective. *Evolution & Development*, *14*(1), 116-127. doi: 10.1111/j.1525-142x.2011.00526.x

Bergemann, D., Massoz, L., Bourdouxhe, J., Carril Pardo, C., Voz, M., Peers, B., & Manfroid, I. (2018). Nifurpirinol: A more potent and reliable substrate compared to metronidazole

for nitroreductase-mediated cell ablations. *Wound Repair And Regeneration*, *26*(2), 238-244. doi: 10.1111/wrr.12633

Bhattacharya, S., Hyland, C., Falk, M., & Iovine, M. (2020). *Connexin 43* gap junctional intercellular communication inhibits *evx1* expression and joint formation in regenerating fins. *Development*, *147*(13), dev190512. doi: 10.1242/dev.190512

Bird, N., & Mabee, P. (2003). Developmental morphology of the axial skeleton of the zebrafish, Danio rerio (Ostariophysi: Cyprinidae). *Developmental Dynamics*, *228*(3), 337-357. doi: 10.1002/dvdy.10387

Borday, V., Tharon, C., Avaron, F., Brulfert, A., Casane, D., Laurenti, P., & Graudie, J. (2001). evx1 Transcription in bony fin rays segment boundaries leads to a reiterated pattern during zebrafish fin development and regeneration. *Developmental Dynamics*, *220*(2), 91–98. doi:10.1002/1097-0177(2000)9999:9999

Carleton, K. L. (2011). Quantification of Transcript Levels with Quantitative RT-PCR. *Methods in Molecular Biology Molecular Methods for Evolutionary Genetics,*279-295. doi:10.1007/978-1-61779-228-1_17

Chen, C. F., Chu, C. Y., Chen, T. H., Lee, S. J., Shen, C. N., & Hsiao, C. Der. (2011). Establishment of a transgenic zebrafish line for superficial skin ablation and functional validation of apoptosis modulators in vivo. *PLoS ONE*, *6*(5). doi:10.1371/journal.pone.0020654

Chlebowski, A., La Du, J., Truong, L., Massey Simonich, S., & Tanguay, R. (2017). Investigating the application of a nitroreductase-expressing transgenic zebrafish line for high-throughput toxicity testing. *Toxicology Reports*, *4*, 202-210. doi: 10.1016/j.toxrep.2017.04.005

Coates, M. (1995). Limb Evolution: Fish fins or tetrapod limbs — a simple twist of fate?. *Current Biology*, *5*(8), 844-848. doi: 10.1016/s0960-9822(95)00169-2

Curado, S., Anderson, R. M., Jungblut, B., Mumm, J., Schroeter, E., & Stainier, D. Y. R. (2007). Conditional targeted cell ablation in zebrafish: A new tool for regeneration studies. *Developmental Dynamics*, *236*(4), 1025–1035. doi:10.1002/dvdy.21100

Curado, S., Stainier, D. Y. R., & Anderson, R. M. (2008). Nitroreductase-mediated cell/tissue ablation in zebrafish: a spatially and temporally controlled ablation method with applications in developmental and regeneration studies. *Nature Protocols*, *3*(6), 948–954. Doi:10.1038/nprot.2008.58

Dardis, G., Tryon, R., Ton, Q., Johnson, S. L., & Iovine, M. K. (2017). *Cx43* suppresses *evx1* expression to regulate joint initiation in the regenerating fin. *Developmental Dynamics,246*(9), 691-699. doi:10.1002/dvdy.24531

Don, E., Currie, P., & Cole, N. (2012). The evolutionary history of the development of the pelvic fin/hindlimb. *Journal of Anatomy*, *222*(1), 114-133. doi: 10.1111/j.1469-7580.2012.01557.x

Dongen, S., (2006). Fluctuating asymmetry and developmental instability in evolutionary biology: past, present and future. *Journal of Evolutionary Biology*, *19*(6), 1727-1743. doi: 10.1111/j.1420-9101.2006.01175.x

Duran, I., Mari-Beffa, M., Santamaria, J. A., Becerra, J., & Santos-Ruiz, L. (2011). Actinotrichia collagens and their role in fin formation. *Developmental Biology, 354*(1), 160-172.

Fromental-Ramain, C., Warot, X., Messadecq, N., LeMeur, M., Dolle, P., & Chambon, P. (1996). *Hoxa-13* and *Hoxd-13* play a crucial role in the patterning of the limb autopod. *Development, 122*(10), 2997-3011.

Fu, C., Cao, Z., & Fu, S. (2013). The effects of caudal fin loss and regeneration on the swimming performance of three cyprinid fish species with different swimming capacities. *Journal of Experimental Biology,216*(16), 3164-3174. doi:10.1242/jeb.084244

Gavaia, P. J., Simes, D. C., Ortiz-Delgado, J. B., Viegas, C. S. B., Pinto, J. P., Kelsh, R. N., Cancela, M. L. (2006). Osteocalcin and matrix Gla protein in zebrafish (Danio rerio) and Senegal sole (Solea senegalensis): Comparative gene and protein expression during larval development through adulthood. *Gene Expression Patterns*, *6*(6), 637–652. doi:10.1016/j.modgep.2005.11.010

Geraci, F., Saha, I., & Bianchini, M. (2020). Editorial: RNA-Seq Analysis: Methods, Applications and Challenges. *Frontiers in Genetics*, *11*. doi: 10.3389/fgene.2020.00220

Geraudie, J., & Borday Birraux, V. (2003). Posterior *hoxa* genes expression during zebrafish bony fin ray development and regeneration suggests their involvement in scleroblast differentiation. *Development Genes and Evolution, 213*(4), 182-186.

Geraudie, J., & Meunier, F. J. (1980). Elastoidin actinotrichia in coelacanth fins: A comparison with teleosts. *Tissue & Cell, 12*(4), 637-645

Grandel, H., & Schulte-Merker, S. (1998). The development of the paired fins in the zebrafish (*danio rerio*). *Mechanisms of Development, 79*(1-2), 99-120.

Grotek, B., Wehner, D., & Weidinger, G. (2013). Notch signaling coordinates cellular proliferation with differentiation during zebrafish fin regeneration. *Development (Cambridge, England)*, *140*(7), 1412–23. Doi: 10.1242/dev.087452

Hamada, H., Uemoto, T., Tanaka, Y., Honda, Y., Kitajima, K., Umeda, T., Kawakami, A., Shinya, M., Kawakami, K., Tamura, K., Abe, G. (2019). Pattern of fin rays along the antero-posterior axis based on their connection to distal radials. *Zoological Letters,5*(1). doi:10.1186/s40851-019-0145-z

Iovine, M. (2007). Conserved mechanisms regulate outgrowth in zebrafish fins. *Nature Chemical Biology*, *3*(10), 613-618. doi: 10.1038/nchembio.2007.36

Johnson A. D., Krieg P. A. (1995). A *Xenopus laevis* gene encoding EF-1 alpha S, the somatic form of elongation factor 1 alpha: sequence, structure, and identification of regulatory elements required for embryonic transcription. *Dev. Genet*. 17, 280-290.

Johnson, S. L., & Weston, J. A. (1995). Temperature-sensitive mutations that cause stage-specific defects in Zebrafish fin regeneration. *Genetics,141*(4), 1583-1595. doi:10.1093/genetics/141.4.1583

Kawakami, A. (2010). Stem cell system in tissue regeneration in fish. *Development, Growth & Differentiation*, *52*, 77–87. doi:10.1111/j.1440-169X.2009.01138.x

Kawakami, Y., Rodriguez Esteban, C., Raya, M., Kawakami, H., Marti, M., Dubova, I., et al. (2006). Wnt/beta-catenin signaling regulates vertebrate limb regeneration. *Genes & Development, 20*(23), 3232-3237.

Kherdjemil, Y., Lalonde, R. L., Sheth, R., Dumouchel, A., de Martino, G., Pineault, K. M., Kmita, M. (2016). Evolution of *Hoxa11* regulation in vertebrates is linked to the pentadactyl state. *Nature*, *539*(7627), 89–92. Doi:10.1038/nature19813

Kimmel, C., Ballard, W., Kimmel, S., Ullmann, B., & Schilling, T. (1995). Stages of embryonic development of the zebrafish. *Developmental Dynamics*, *203*(3), 253-310. doi: 10.1002/aja.1002030302

Knopf, F., Hammond, C., Chekuru, A., Kurth, T., Hans, S., Weber, C. W., Weidinger, G. (2011). Bone regenerates via dedifferentiation of osteoblasts in the zebrafish fin. *Developmental Cell*, *20*(5), 713–724. doi:10.1016/j.devcel.2011.04.014

Knox, R. J., Friedlos, F., Jarman, M., & Roberts, J. J. (1988). A new cytotoxic, DNA interstrand crosslinking agent, 5-(aziridin-1-yl)-4-hydroxylamino-2-nitrobenzamide, is formed from 5-(aziridin-1-yl)-2,4-dinitrobenzamide (CB 1954) by a nitroreductase enzyme in walker carcinoma cells. *Biochemical Pharmacology*, *37*(24), 4661–4669. Doi:10.1016/0006-2952(88)90335-8

Konig, D., Page, L., Chassot, B., & Jaźwińska, A. (2017). Dynamics of actinotrichia regeneration in the adult zebrafish fin. *Developmental Biology*, 433(2), 416-432.

Laforest, L., Brown, C. W., Poleo, G., Géraudie, J., Tada, M., Ekker, M., & Akimenko, M. A. (1998). Involvement of the *sonic hedgehog, patched 1* and *bmp2* genes in patterning of the zebrafish dermal fin rays. *Development (Cambridge, England)*, *125*(21), 4175–4184.

Lalonde, R., & Akimenko, M.A. (2018). Contributions of 5'*HoxA/D* regulation to actinodin evolution and the fin-to-limb transition. *The International Journal Of Developmental Biology*, *62*(11-12), 705-716. doi: 10.1387/ijdb.180248rl

Lalonde, R., & Akimenko, M.A. (2018). Effects of fin fold mesenchyme ablation on fin development in zebrafish. *PLOS ONE*, *13*(2), e0192500. doi: 10.1371/journal.pone.0192500

Lanske B, Karaplis AC, Lee K, Luz A, Vortkamp A, Pirro A, Karperien M, Defize LH, Ho C, Mulligan RC, Abou-Samra AB, Jüppner H, Segre GV, Kronenberg HM. PTH/PTHrP

receptor in early development and Indian Hedgehog-regulated bone growth. Science. 1996 Aug 2;273(5275):663-6. doi: 10.1126/science.273.5275.663. PMID: 8662561.

Li, J., Meng, X., Zong, Y., Chen, K., Zhang, H., Liu, J., Li, J., and Gao, C. Gene replacements and insertions in rice by intron targeting using CRISPR-Cas9. *Nat. Plants*. 2016; 2:16139.

Mackie, E. J., Tatarczuch, L., & Mirams, M. (2011). The skeleton: A multi-functional complex organ. The growth plate chondrocyte and endochondral ossification. *Journal of Endocrinology,211*(2), 109-121. doi:10.1530/joe-11-0048

Mari-Beffa, M., Carmona, M. C., & Becerra, J. (1989). Elastoidin turn-over during tail fin regeneration in teleosts. *Anatomy and Embryology,180*(5), 465-470. doi:10.1007/bf00305121

Mathavan, S., Lee, S., Mak, A., Miller, L., Murthy, K., & Govindarajan, K. et al. (2005). Transcriptome Analysis of Zebrafish Embryogenesis Using Microarrays. *Plos Genetics*, *1*(2), e29. doi: 10.1371/journal.pgen.0010029

McMillan, S., Géraudie, J., & Akimenko, M. (2015). Pectoral Fin Breeding Tubercle Clusters: A Method to Determine Zebrafish Sex. *Zebrafish*, *12*(1), 121-123. doi: 10.1089/zeb.2014.1060

McMillan, S., Zhang, J., Phan, H., Jeradi, S., Probst, L., Hammerschmidt, M., & Akimenko, M.A. (2018). A regulatory pathway involving retinoic acid and calcineurin demarcates and maintains joint cells and osteoblasts in regenerating fin. *Development*, *145*(11), dev161158. doi: 10.1242/dev.161158

Metzker, M. (2009). Sequencing technologies — the next generation. *Nature Reviews Genetics*, *11*(1), 31-46. doi: 10.1038/nrg2626

Münch, J., Gonzalez-Rajal, A., & Pompa, J. L. (2013). Notch regulates blastema proliferation and prevents differentiation during adult zebrafish fin regeneration. *Development,140*(7), 1402-1411. doi:10.1242/dev.087346

Nakamura, T., Gehrke, A., Lemberg, J., Szymaszek, J., & Shubin, N. (2016). Digits and fin rays share common developmental histories. *Nature*, *537*(7619), 225-228. doi: 10.1038/nature19322

Pacifici, M., Koyama, E., Shibukawa, Y., Wu, C., Tamamura, Y., Enomoto-Iwamoto, M., & Iwamoto, M. (2006). Cellular and molecular mechanisms of synovial joint and articular cartilage formation. In *Annals of the New York Academy of Sciences* (Vol. 1068, pp. 74–86). Doi:10.1196/annals.1346.010

Parinov, S., Kondrichin, I., Korzh, V., & Emelyanov, A. (2004). Tol2 transposon-mediated enhancer trap to identify developmentally regulated zebrafish genes in vivo. *Developmental Dynamics*, *231*(2), 449-459. doi: 10.1002/dvdy.20157

Pfefferli, C., & Jaźwińska, A. (2015). The art of fin regeneration in zebrafish. *Regeneration,2*(2), 72-83. doi:10.1002/reg2.33

Phan, H., Northorp, M., Lalonde, R., Ngo, D., & Akimenko, M.A. (2019). Differential *actinodin1* regulation in embryonic development and adult fin regeneration in *Danio rerio*. *PLOS ONE*, *14*(5), e0216370. doi: 10.1371/journal.pone.0216370

Poss, K. D., Keating, M. T., & Nechiporuk, A. (2003). Tales of regeneration in zebrafish. *Developmental Dynamics, 226*(2), 202-210.

Qian, X., Ba, Y., Zhuang, Q., & Zhong, G. (2014). RNA-Seq Technology and Its Application in Fish Transcriptomics. *OMICS: A Journal Of Integrative Biology*, *18*(2), 98-110. doi: 10.1089/omi.2013.0110

Rath, D., Amlinger, L., Rath, A., & Lundgren, M. (2015). The CRISPR-Cas immune system: Biology, mechanisms and applications. *Biochimie,117*, 119-128. doi:10.1016/j.biochi.2015.03.025

Ryan, M. D., King, A. M. Q., & Thomas, G. P. (1991). Cleavage of foot-and-mouth disease virus polyprotein is mediated by residues located within a 19 amino acid sequence. *Journal of General Virology*, *72*(11), 2727–2732. Doi:10.1099/0022-1317-72-11-2727

Sander, J. D., & Joung, J. K. (2014). CRISPR-Cas systems for editing, regulating and targeting genomes. *Nature Biotechnology,32*(4), 347-355. doi:10.1038/nbt.2842

Santamaría, J., Marí-Beffa, M., & Becerra, J. (1992). Interactions of the lepidotrichial matrix components during tail fin regeneration in teleosts. *Differentiation,49*(3), 143-150. doi:10.1111/j.1432-0436.1992.tb00662.x

Santos-Ruiz, L., Santamaría, J. A., Ruiz-Sánchez, J., & Becerra, J. (2002). Cell proliferation during blastema formation in the regenerating teleost fin. *Developmental Dynamics,223*(2), 262-272. doi:10.1002/dvdy.10055

Schneider, I., & Shubin, N. H. (2013). The origin of the tetrapod limb: From expeditions to enhancers. *Trends in Genetics,29*(7), 419-426. doi:10.1016/j.tig.2013.01.012

Schulte, C. J., Allen, C., England, S. J., Juárez-Morales, J. L., & Lewis, K. E. (2011). *Evx1* is required for joint formation in zebrafish fin dermoskeleton. *Developmental Dynamics*, *240*(5), 1240–1248. Doi:10.1002/dvdy.22534

Schuster, K., & Ghysen, A. (2013). Labeling Defined Cells or Subsets of Cells in Zebrafish by Kaede Photoconversion. *Cold Spring Harbor Protocols*, *2013*(11), pdb.prot078626-pdb.prot078626. doi: 10.1101/pdb.prot078626

Sims, K., Eble, D. M., & Iovine, M. K. (2009). *Connexin43* regulates joint location in zebrafish

fins. *Developmental Biology*, *327*(2), 410–418. Doi: 10.1016/j.ydbio.2008.12.027

Singh, S. P., Holdway, J. E., & Poss, K. D. (2012). Regeneration of Amputated Zebrafish Fin Rays from De Novo Osteoblasts. *Developmental Cell*, *22*(4), 879–886. doi: 10.1016/j.devcel.2012.03.006

Siomava, N., & Diogo, R. (2017). Comparative anatomy of zebrafish paired and median fin muscles: basis for functional, developmental, and macroevolutionary studies. *Journal Of Anatomy*, *232*(2), 186-199. doi: 10.1111/joa.12728

Smith, A., Avaron, F., Guay, D., Padhi, B. K., & Akimenko, M. A. (2006). Inhibition of BMP signaling during zebrafish fin regeneration disrupts fin growth and scleroblast differentiation and function. *Developmental Biology*, *299*(2), 438–454. doi:10.1016/j.ydbio.2006.08.016

Smith, C., & Osborn, A. (2009). Advantages and limitations of quantitative PCR (Q-PCR)-based approaches in microbial ecology. *FEMS Microbiology Ecology*, *67*(1), 6-20. doi: 10.1111/j.1574-6941.2008.00629.x

Sontheimer, E. J., & Barrangou, R. (2015). The Bacterial Origins of the CRISPR Genome-Editing Revolution. *Human Gene Therapy,26*(7), 413-424. doi:10.1089/hum.2015.091

Sordino, P., Hoeven, F. V., & Duboule, D. (1995). *Hox* gene expression in teleost fins and the origin of vertebrate digits. *Nature,375*(6533), 678-681. doi:10.1038/375678a0

St-Jacques B, Hammerschmidt M, McMahon AP. *Indian hedgehog* signaling regulates proliferation and differentiation of chondrocytes and is essential for bone formation. Genes Dev. 1999 Aug 15;13(16):2072-86. doi: 10.1101/gad.13.16.2072. Erratum in: Genes Dev 1999 Oct 1;13(19):2617. PMID: 10465785; PMCID: PMC316949.

Stewart, S., Gomez, A. W., Armstrong, B. E., Henner, A., & Stankunas, K. (2014). Sequential and

opposing activities of Wnt and BMP coordinate zebrafish bone regeneration. *Cell Reports*, *6*(3), 482–498. doi:10.1016/j.celrep.2014.01.010

Summersgill, J. T., Schupp, L. G., & Raff, M. J. (1982). Comparative penetration of metronidazole, clindamycin, chloramphenicol, cefoxitin, ticarcillin, and moxalactam into bone. *Antimicrobial Agents and Chemotherapy*, *21*(4), 601–603. Doi:10.1128/AAC.21.4.601.

Ton, Q. V., & Iovine, M. K. (2013). Identification of an *evx1*-dependent joint-formation pathway during fin regeneration. *PLOS ONE*, *8*(11). Doi:10.1371/journal.pone.0081240

Tu, S., & Johnson, S. L. (2011). Fate restriction in the growing and regenerating zebrafish fin. *Developmental Cell*, *20*(5), 725–732. doi:10.1016/j.devcel.2011.04.013

Vortkamp A, Pathi S, Peretti GM, Caruso EM, Zaleske DJ, Tabin CJ. Recapitulation of signals regulating embryonic bone formation during postnatal growth and in fracture repair. Mech Dev. 1998 Feb;71(1-2):65-76. doi: 10.1016/s0925-4773(97)00203-7. PMID: 9507067.

Wehner, D., & Weidinger, G. (2015). Signaling networks organizing regenerative growth of the zebrafish fin. *Trends in Genetics, 31*(6), 336-343.

Wehner, D., Cizelsky, W., Vasudevaro, M., Özhan, G., Haase, C., Kagermeier-Schenk, B., Weidinger, G. (2014). Wnt/catenin signaling defines organizing centers that orchestrate growth and differentiation of the regenerating zebrafish caudal fin. *Cell Reports*, *6*(3), 467–481. doi: 10.1016/j.celrep.2013.12.036

Welten, M. C. M., de Haan, S. B., van den Boogert, N., Noordermeer, J. N., Lamers, G. E. M., Spaink, H. P., Meijer, A. H. and Verbeek, F. J. (2006). ZebraFISH: fluorescent *in situ*

hybridization protocol and three-dimensional imaging of gene expression patterns. *Zebrafish*, 465–476.

Westerfield, M. (2007). *The Zebrafish Book: A Guide for the Laboratory Use of Zebrafish (Danio Rerio)*.

White, D. T., & Mumm, J. S. (2013). The nitroreductase system of inducible targeted ablation facilitates cell-specific regenerative studies in zebrafish. *Methods*, *62*(3), 232–240. Doi:10.1016/j.ymeth.2013.03.017

Wiley, E., Fuiten, A., Doosey, M., Lohman, B., Merkes, C., & Azuma, M. (2015). The Caudal Skeleton of the Zebrafish, *Danio rerio*, from a Phylogenetic Perspective: A Polyural Interpretation of Homologous Structures. *Copeia*, *103*(4), 740-750. doi: 10.1643/cg-14-105

Wood A, Thorogood P. An analysis of in vivo cell migration during teleost fin morphogenesis. J Cell Sci. 1984 Mar; 66:205-22. PMID: 6746756.

Wood, A. (1982). Early pectoral fin development and morphogenesis of the apical ectodermal ridge in the killifish, Aphyosemion scheeli. *The Anatomical Record,204*(4), 349-356. doi:10.1002/ar.1092040408

Yoshida, K., Kawakami, K., Abe, G., & Tamura, K. (2020). Zebrafish can regenerate endoskeleton in larval pectoral fin but the regenerative ability declines. *Developmental Biology*, *463*(2), 110-123. doi: 10.1016/j.ydbio.2020.04.010

Yoshinari, N., Ishida, T., Kudo, A., & Kawakami, A. (2009). Gene expression and functional analysis of zebrafish larval fin fold regeneration. *Developmental Biology, 325*(1), 71-81.

Zenno, S., Koike, H., Tanokura, M., & Saigo, K. (1996). Gene cloning, purification, and characterization of NfsB, a minor oxygen-insensitive nitroreductase from Escherichia coli, similar in biochemical properties to FRase I, the major flavin reductase in Vibrio fischeri. *Journal of Biochemistry*, *120*(4), 736–44. https://doi.org/10.1093/oxfordjournals.jbchem.a021473

Zhang, J., Wagh, P., Guay, D., Sanchez-Pulido, L., Padhi, B. K., Korzh, V. (2010). Loss of fish actinotrichia proteins and the fin-to-limb transition. *Nature, 466*(7303), 234-237.